ABSTRACT

Title of Document: A GENERIC RELIABILITY ANALYSIS AND
                         DESIGN FRAMEWORK WITH RANDOM
                         PARAMETER, FIELD, AND PROCESS
                         VARIABLES

                         Zhimin Xi, Doctor of Philosophy, 2010

Directed By: Professor Byeng D. Youn, Department of
                         Mechanical Engineering

This dissertation aims at developing a generic reliability analysis and design framework that enables reliability prediction and design improvement with random parameter, field, and process variables. The capability of this framework is further improved by predicting and managing reliability even with a dearth of data that can be used to characterize random variables. To accomplish the research goal, three research thrusts are set forth. First, advanced techniques are developed to characterize the random field or process. The fundamental idea of these techniques is to model the random field or process with a set of important field signatures and random variables. These techniques enable the use of random parameter, field, and process variables for reliability analysis and design even with a dearth of data. Second, a generic reliability analysis framework is proposed to accurately assess system reliability in the presence of random parameter, field, and process variables. An advanced probability analysis technique, the Eigenvector Dimension Reduction (EDR) method, is developed by

integrating the Dimension Reduction (DR) method with three proposed improvements: 1) an eigenvector sampling approach to obtain statistically independent samples over a random space; 2) a Stepwise Moving Least Square (SMLS) method to accurately approximate system responses over a random space; and 3) a Probability Density Function (PDF) generation method to accurately approximate the PDF of system responses for reliability analysis. Third, a generic Reliability-Based Design Optimization (RBDO) framework is developed to solve engineering design problems with random parameter, field, and process variables. This design framework incorporates the EDR method into RBDO. To illustrate the effectiveness of the developed framework, many numerical and engineering examples are employed to conduct the reliability analysis and RBDO with random parameter, field, and process variables. This dissertation demonstrates that the developed framework is very accurate and efficient for the reliability analysis and RBDO of engineering products and processes.

A GENERIC RELIABILITY ANALYSIS AND DESIGN FRAMEWORK WITH
RANDOM PARAMETER, FIELD, AND PROCESS VARIABLES

By

Zhimin Xi

Dissertation submitted to the Faculty of the Graduate School of the
University of Maryland, College Park, in partial fulfillment
of the requirements for the degree of
Doctor of Philosophy
2010

Advisory Committee:
Professor Byeng D. Youn, Chair
Professor Shapour Azarm
Professor Mohammad Modarres
Professor Teng Li
Professor Martin Peckerar

Acknowledgements

First of all, I would like to thank my advisor, Dr. Byeng D. Youn, for his gracious guidance, support, and encouragement throughout my study for pursuing the Ph.D. degree in University of Maryland.

I also would like to thank Dr. Shapour Azarm, Dr. Mohammad Modarres, Dr. Teng Li, and Dr. Martin Peckerar for serving on my committee and their time, effort, and valuable comments for improving my dissertation.

I also want to thank Ms. Artemis Kloess and Dr. John Cafeo for their support and help during my summer internship in General Motors. I appreciate Dr. Sangbum Kim in LG Electronics for providing the example of the refrigerator assembly model, and Dr. Jooho Choi for providing the example of the layered bonding plate model. Special thanks go to my colleagues and friends, Mr. Pingfeng Wang, Mr. Chao Hu, Ms. Lulu Wang, Dr. Soobum Lee, and Mr. Byungchang Jung, for all the collaborations, discussions, encouragements, and help when I was in need.

Finally, my grateful thanks go to my parents for their continuous support during my study, to my wife, Xiaoxia Lai, whose love and understanding always help me carry on during difficult times in my life. To my lovely son, Noah Z. Xi, and daughter, Emma Z. Xi, you are the greatest gift I ever had in my life. Daddy loves you!

Table of Contents

iv

List of Tables

List of Figures

Nomenclature

A

AD   Anderson-Darling

C

CDF   Cumulative Distribution Function

D

DPM   Design Potential Method

DPP   Design Potential Point

DR   Dimension Reduction

E

EDR   Eigenvector Dimension Reduction

F

FDM   Finite Difference Method

FE   Finite Element

FEA   Finite Element Analysis

FORM   First-Order Reliability Method

K

KKT   Karush-Kuhn-Tucker

| K-L | Karhunen-Loeve |
| K-S | Kolmogorov-Smirnov |

M

MARS	Multivariate Adaptive Regression Splines
MCMC	Markov Chain Monte Carlo
MCS	Monte Carlo Simulation
MEMS	Micro-Electro-Mechanical Systems
MLE	Maximum Likelihood Estimation
MLS	Moving Least Squares
MPP	Most Probable Point

P

PCE	Polynomial Chaos Expansion
PDF	Probability Density Function
PMA	Performance Measurement Approach
POD	Proper Orthogonal Decomposition
PoFs	Physics-of-Failures
PRSM	Polynomial Response Surface Models

R

| RBDO | Reliability-Based Design Optimization |
| RBF | Radial Basis Functions |

RDO	Robust Design Optimization
RIA	Reliability Index Approach
RPA	Random Parameter Approach

S

SMLS	Stepwise Moving Least Square
SORA	Sequential Optimization and Reliability Assessment
SORFS	Sequential Optimization with Reliability-based Factors of Safety
SORM	Second-Order Reliability Method
SQP	Sequential Quadratic Programming
SVR	Support Vector Regression

θ	continuous random field
$\tilde{\theta}$	approximate random field
μ	mean of the random field
ν	variation of the random field
ϕ	signature of the random field
α	coefficient of the signature
n	number of measurement points
m	number of sampled snapshots
Σ	covariance matrix
I	integral operator
λ	eigenvalue

ρ	normalized eigenvalue
ε	posteriori normalized error
ε_c	threshold error value
v	random field variable
q	number of nodes
H_i	the i-th polynomial shape function
C	cumulative distribution function of the Copula
c	probability density function of the Copula
Q	number of test Copulas
D	bivariate data
τ	Kendall's tau
u	random variable in standard uniform or normal space
$T_k(\bullet)$	Rosenblatt transformation with the k-th transformation sequence
$Y_{T,k}$	nonlinear response through the k-th transformation
$S_{j,k}$	degree of deviation for the k-th transformation sequence
Y	system response
Y_a	additive decomposition
$L(\bullet)$	likelihood function
$\mathbf{d}$	design vector
$\mathbf{x}$	random vector
$\boldsymbol{\delta}$	distribution parameter vector
β_t	target reliability
β_1	square of skewness

β_2	kurtosis
σ	standard deviation
NP	number of probabilistic constraints
ND	number of design variables
N	number of random variables
$f_X(x)$	probability density function
$F_X(x)$	cumulative distribution function
E	expectation operator

Chapter 1: Introduction

1.1 Background and motivation

A random field/process is a generalization of a stochastic field, of which randomness can be characterized as a function of spatial/time variables. For the sake of convenience, random field is used throughout the dissertation to represent both random field and random process. So far, little effort has been made to consider the random field in most engineered system design [Choi et al. 2006; Missoum 2008; Chen et al. 2010]. That is mainly because of little or no effective approach for random field characterization, misconception of minor influence of the random field on system responses, or both. Hence, the Random Parameter Approach (RPA) has been popular in probability analysis and design for engineering products and processes. The RPA parameterizes manufacturing and operation variability while simplifying or ignoring the spatial variability. For instance, one thickness random parameter is used for modeling thickness variability although it has spatial variability over an entire plate. However, it has been widely acknowledged [Rajaee et al. 1994; Tamura et al. 1999; Berkooz et al. 1996; Fukunaga 1990; Missoum 2008; and Yin et al. 2009] that consideration of the random field is quite significant to variability in system responses, especially, geometry-sensitive failures (e.g., buckling) and small-scale applications, in which tolerance control is more challenging. Ignorance of the random field in engineering design may lead to an unreliable and risk design. Examples of the random field can be often found as a geometry, material, and process variation in Micro-Electro-Mechanical Systems (MEMS), mechanical, and electronics products.

Figure 1-1 presents two examples of the random field in an MEMS bi-stable mechanism and a mechanical assembly process.

(a)   (b)
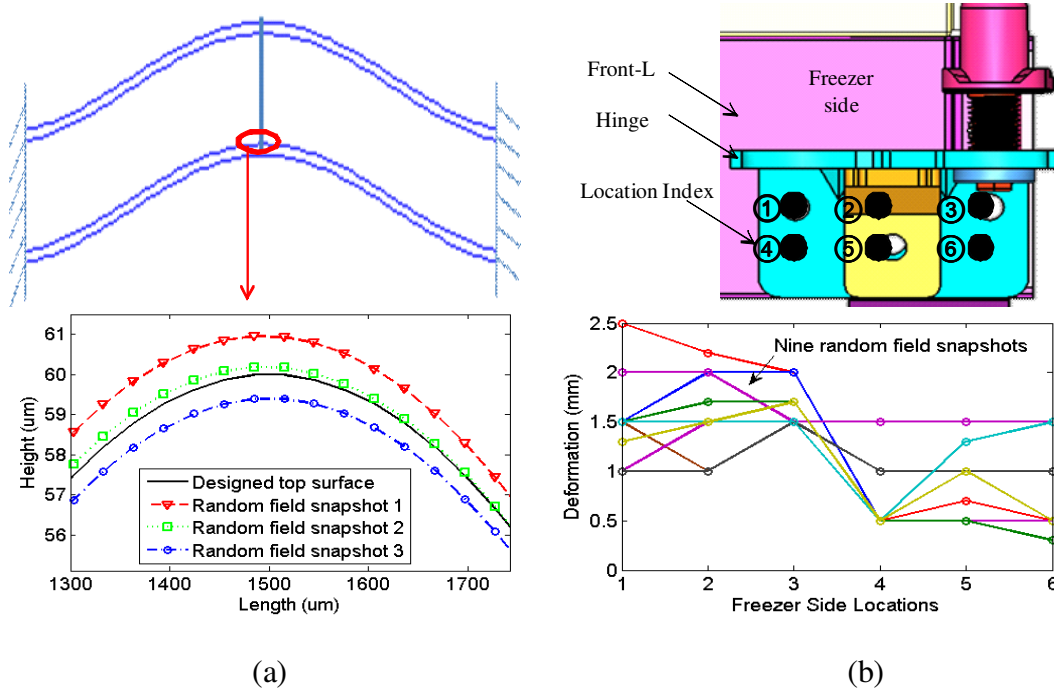
Figure 1-1: Geometrical random field in (a) a MEMS bi-stable mechanism; and (b) hinge installation in a refrigerator assembly process

The use of random field for reliability analysis and design is challenging due to four primary reasons. First, characterization of the random field in engineered systems could be prohibitively complicated and expensive. Massive multi-dimensional random field data must be accurately measured and systematically stored. Second, there is no generic framework to take into account both random parameter and field variables for reliability analysis and design. Third, statistical dependence in random field increases technical difficulty for reliability analysis and design. Fourth, the amount of data to characterize the random field is often lacking in most engineering problems. The objective of this dissertation is to understand and

2

manage the effect of the random field on system responses, reliabilities, and designs of engineered systems. In this dissertation, three technical concerns are addressed: 1) effective random field characterization with both sufficient and insufficient number of data; 2) reliability analysis for engineering problems with both random parameter and field variables; and 3) reliability-based design optimization for engineering problems with both random parameter and field variables.

1.2 Research scopes and objectives

The goal of the research is to develop a generic reliability analysis and design framework, which enables the use of both random parameter and field variables even with the dearth of corresponding data as shown in Fig. 1-2. First of all, statistical input data of the engineered system are classified into random parameter data and random field data. The random field data indicate that the randomness can be characterized as a function of spatial variables, such as the wind field loading applied to the wind turbine generator, or the thermal field loading applied to mechatronic products. The random parameter data denote that the randomness is independent on the spatial variables. Then, the random parameter variables are characterized from the available random parameter data and their statistical properties are represented by the Probability Density Functions (PDFs). Furthermore, the random field variables are defined from the random field characterization approach and their statistical properties are also represented by the PDFs. Next, the statistical dependency of the random parameter and field variables has to be considered for accurate prediction of engineered system performances. Then, reliability analysis is conducted to identify the reliability of engineered system performances with both random parameter and

field variables. Finally, Reliability-Based Design Optimization (RBDO) is performed to improve the reliability of engineered system performances considering both random parameter and field variables. This research development could bring a great impact to many engineering design problems where the random field is the inherent property for the loading conditions, material properties and manufacturing tolerance. To achieve this research goal, this dissertation sets three research objectives.

```
┌─────────────────────────────────────────────────────────────────────┐
│                                Data                                   │
└─────────────────────────────────────────────────────────────────────┘
        │                                       │
        ▼                                       ▼
┌──────────────────────────┐     ┌──────────────────────────────────────┐
│  Random Parameter Data   │     │          Random Field Data           │
└──────────────────────────┘     └──────────────────────────────────────┘
        │                             │                      │
        │                             ▼                      ▼
        │                   ┌───────────────────┐  ┌──────────────────────┐
        │                   │ Sufficient Field  │  │ Insufficient Field   │
        │                   │      Data         │  │       Data           │
        │                   └───────────────────┘  └──────────────────────┘
        │                             │                      │
        │                             ▼                      ▼
        │                   ┌──────────────────────────────────────────┐
        │                   │      Random Field Characterization        │
        │                   └──────────────────────────────────────────┘
        ▼                                       ▼
┌──────────────────────────┐     ┌──────────────────────────────────────┐
│ Random Parameter Variables│    │        Random Field Variables        │
└──────────────────────────┘     └──────────────────────────────────────┘
        │                                       │
        ▼                                       ▼
┌─────────────────────────────────────────────────────────────────────┐
│                        Statistical Dependency                         │
└─────────────────────────────────────────────────────────────────────┘
                                    │
                                    ▼
┌─────────────────────────────────────────────────────────────────────┐
│     Reliability Analysis with Both Random Parameter and Field Variables│
└─────────────────────────────────────────────────────────────────────┘
                                    │
                                    ▼
┌─────────────────────────────────────────────────────────────────────┐
│Reliability-Based Design Optimization with Both Random Parameter and Field Variables│
└─────────────────────────────────────────────────────────────────────┘
```

Figure 1-2: A generic reliability analysis and design framework with a set of random parameter and field variables

The first research objective is to develop advanced techniques for random field characterization. The fundamental idea of the techniques is to model the random field in terms of a set of important field signatures. These techniques enable the use of both random parameter and field variables even with the dearth of corresponding data. This research objective is achieved through the accomplishment of following

techniques: 1) projection of the random field onto a set of important field signatures for the random field characterization with the minimum number of random field variables; 2) a Bayesian approach with Bayesian Copula dependence modeling to characterize the random field with the lack of field data sets; and 3) Rosenblatt transformation with an optimal transformation sequence for the transformation of statistically dependent random field variables into statistically independent random field variables;

The second research objective is to propose a generic reliability analysis framework, which assesses system reliability accurately in the presence of both random field and parameter variables. This technique is developed based upon the Dimension Reduction (DR) method [Rabitz and Alis 1999; Rahman and Xu 2004]. This research objective is achieved through the accomplishment of following techniques: 1) an eigenvector sampling to obtain statistically independent samples over a random space; 2) a Stepwise Moving Least Square (SMLS) method to accurately approximate system responses over a random space; and 3) a Probability Density Function (PDF) generation method to accurately approximate PDFs of system responses for reliability analysis.

The third research objective is to structure a generic framework for Reliability-Based Design Optimization (RBDO) that can solve an engineering design problem with both random parameter and field variables to achieve target reliability. This research objective is achieved through the accomplishment of following techniques: 1) sensitivity analysis to calculate sensitivity of controllable random parameters; and 2) sensitivity analysis to calculate sensitivity of controllable means of the random field.

1.3 Dissertation overview

The rest of the dissertation is organized as follows. Chapter 2 provides an overview of random field characterization, reliability analysis and Reliability-Based Design Optimization (RBDO). Chapter 3 aims at developing advanced techniques for random field characterization in order to model any geometric and non-geometric random fields in engineered systems whether or not the random field can be realized with either sufficient or insufficient field data. Chapter 4 develops a generic reliability analysis framework that requires no derivative information of system responses while taking into account statistical dependence among random variables. The Eigenvector Dimension Reduction (EDR) method is proposed for the generic reliability analysis framework. Chapter 5 proposes a generic RBDO framework that can deal with both random parameter and field variables. Chapter 6 concludes the dissertation with a discussion on potential future research directions.

1.4 Summary of contributions

The significant contributions of this dissertation are as follows.

1) An effective random field characterization approach capable of projecting the random field onto a set of important field signatures (or random field variables).

2) Rosenblatt transformation with an optimal transformation sequence to transform statistically dependent random variables into statistically independent random variables.

3) A Bayesian approach with Copula dependence models to characterize the random field with the lack of field data sets.

4) A generic reliability analysis framework to assess system reliability accurately in the presence of both random field and parameter variables.

5) A generic Reliability-Based Design Optimization (RBDO) framework to solve engineering design problems with both random parameter and field variables.

The items indicated above present a generic reliability analysis and design framework, which enables the use of both random parameter and field variables even with the dearth of corresponding data.

Chapter 2: Literature Review

2.1 Random field characterization

In the area of the stochastic finite element methods, a random field is the mathematical theory to represent and analyze uncertainties in the mechanical properties of a continuous media. A random field $\theta\,(x,\,t)$ can be defined as a collection of infinitely many random variables denoted by a continuous parameter x. This means that for a given x_i, $\theta\,(x_i,\,t)$ is a random variable. Conversely, for a given outcome t_i, $\theta\,(x,\,t_i)$ is a realization of the random field. A discretization procedure of the random field is the approximation of $\theta\,(\cdot)$ by $\tilde{\theta}\,(\cdot)$ defined by means of a finite set of random variables $\{x_i,\,i=1,\,2,\,\ldots,\,n\}$.

In the 1990s, the random field had already gained its popularity in applications of civil engineering [Yamazaki and Shinozuka 1990; Liu and Der Kiureghian 1991; Ghanem and Spanos 1991; Liu and Liu 1993; Zhang and Ellingwood 1994; Sudret and Der Kiureghian 2000]. It had also been considered in many different disciplines, including fluid dynamics [Rajaee et al. 1994], wind pressure field [Tamura et al. 1999], coherent structures [Berkooz et al. 1996], and pattern recognition [Fukunaga 1990]. Numerous techniques to characterize a discrete random field (or scanned digital data) had been developed. The methods include the midpoint method [Der Kiureghian and Ke 1988], spatial averaging method [Vanmarcke and Grigoriu 1983], shape function method [Liu et al. 1986], and Karhunen-Loeve (K-L) decomposition or Proper Orthogonal Decomposition (POD) method [Turk and Pentland 1991].

2.1.1 The midpoint method

This method was first introduced by Der Kiureghian and Ke to approximate the random field in each discrete element by a single random variable $\theta(x_i, t)$. Its value is defined as the field value at the centroid of this element. The approximate random field is then defined by the random vector $\tilde{\theta} = [\theta(x_1, t), \theta(x_2, t), \ldots, \theta(x_n, t)]$ in an entire field domain, where n is the number of elements in the field domain. Its mean $\mathbf{\mu}$ and covariance matrix $\mathbf{\Sigma}$ are evaluated at the element centroids. Each realization of $\tilde{\theta}(\bullet)$ is a piecewise constant with the discontinuities being localized at the element boundaries.

2.1.2 The spatial averaging method

The spatial average method was proposed by Vanmarcke and Grigoriu. Provided a mesh of the structure is available, it defines the approximate random field in each element as a constant being computed as the average of the original field over the element. The approximate random field is then defined by the random vector $\tilde{\theta} = [\theta(x_1, t), \theta(x_2, t), \ldots, \theta(x_n, t)]$ in an entire field domain, where n is the number of elements in the field domain. The mean and covariance matrix of $\tilde{\theta}$ are computed from the mean and covariance function of $\theta(\bullet)$ as integrals over the element domain.

2.1.3 The shape function method

Liu et al. first proposed this method, which approximates $\theta(\bullet)$ in each element using the nodal value x_i and shape functions as follows:

$$\tilde{\theta}(x) = \sum_{i=1}^{q} H_i(x)\theta(x_i) \tag{2.1}$$

where q is the number of nodes, x_i is the coordinate of the i-th node and H_i is the polynomial shape function associated with the element. The approximate random field $\tilde{\theta}(\bullet)$ is obtained from $[\theta(x_1), \theta(x_2), \ldots, \theta(x_N)]$, where $\{x_i, i = 1, 2, \ldots, N\}$ is the set of the nodal coordinates of the mesh. Each realization of the approximate random field $\tilde{\theta}(x, t_0)$ is a continuous function, which is an advantage over the previous two methods.

2.1.4 K-L decomposition (or POD) method

A random field $\theta(x,t)$ can be decomposed into the mean $\mu(x)$ and variation parts $v(x,t)$. At time t_k, the random field of a sampled snapshot (or the kth snapshot) is observed as

$$\theta(x,t_k) = \mu(x) + v(x,t_k) \tag{2.2}$$

The purpose of the K-L decomposition (or POD) method is to find the most important signature $\phi(x)$ of an ensemble of the random field variation $v(x,t)$ over the entire sampled time (or entire sampled snapshots). This turns out to be an optimization problem expressed as:

$$\textit{Maximize} \quad y = \left(\phi(x) \bullet v_\infty\right)^2 \tag{2.3}$$

where v_∞ stands for the ensemble of the field variation $v(x,t)$ and the operator $\bullet$ indicates an inner product. By definition of the inner product, the objective function y can be further expressed as

$$
\begin{aligned}
y = (\phi(x) \bullet v_\infty)^2 &= \int_\Omega \phi(x) v_\infty(x) dx \int_\Omega \phi(x') v_\infty(x') dx' \\
&= \int_\Omega \left\{ \int_\Omega v_\infty(x) v_\infty(x') \phi(x) dx \right\} \phi(x') dx' \\
&= \int_\Omega \left\{ \int_\Omega K(x,x') \phi(x) dx \right\} \phi(x') dx'
\end{aligned}
\tag{2.4}
$$

where $K(x,x') = V_\infty(x)V_\infty(x')$ and x' is the dummy variable. Define a positive-definite integral operator as

$$I = \int_\Omega K(x,x')(\cdot)dx \qquad (2.5)$$

Then the objective function can be simplified as

$$y = (\phi(x) \bullet V_\infty)^2 = \int_\Omega (I\phi)(\phi)dx' = (I\phi \bullet \phi) \qquad (2.6)$$

To maximize the objective function, $I\phi$ should have the same direction with the vector ϕ. Thus, the maximum objective function can be obtained when

$$I\phi = \lambda\phi \qquad (2.7)$$

From Eq.(2.7), $\phi(x)$ is the signature of the operator I and λ is the corresponding eigenvalue. Thus, the field variation $V(x,t)$ can be decomposed as

$$V(x,t) = \sum_{i=1}^\infty \alpha_i(t) \frac{\phi_i(x)}{\|\phi_i(x)\|} \qquad (2.8)$$

where $\alpha_i(t)$ is the coefficient of the corresponding signature. Its value can be achieved by the projection of the field variation $V(x,t)$ on the corresponding unit signatures and stated as

$$\alpha_i(t) = V(x,t) \bullet \frac{\phi_i(x)}{\|\phi_i(x)\|} \qquad (2.9)$$

Therefore, the random field can be decomposed into Eq. (2.10) using the K-L (or POD) approach

$$\theta(x,t) = \mu(x) + \sum_{i=1}^\infty \alpha_i(t) \frac{\phi_i(x)}{\|\phi_i(x)\|} \qquad (2.10)$$

2.1.4.1 Discrete representation of a random field

In engineering applications, it is more practical to represent a random field in a discrete manner than in a continuous way because a finite amount of field data is given at discrete field locations. Each snapshot is assumed to have a finite amount of measurement points (n) and the physical quantity at the measurement points has variability over a finite amount of sampled snapshots (m). The data sets characterizing the random field could be relevant to geometries, material properties, and loads. Thus an $m \times n$ matrix ($\boldsymbol{\theta}$) representing the discrete random field can be constructed as [Missoum 2008]

$$\boldsymbol{\theta} = \begin{bmatrix} \theta_{11} & \theta_{12} & \cdots & \theta_{1n} \\ \theta_{21} & \theta_{22} & \cdots & \theta_{2n} \\ \vdots & \vdots & \ddots & \vdots \\ \theta_{m1} & \theta_{m2} & \cdots & \theta_{mn} \end{bmatrix}$$

where θ_{ij} indicates the measured data at the j-th measurement point of the i-th sampled snapshot. Such representation works for multi-dimensional problems. Regardless of the dimension of the random field, the scanned multi-dimensional data are listed in a one-dimensional array from θ_{i1} to θ_{in} for the i-th sampled snapshot. The mean of the random field is estimated as

$$\boldsymbol{\mu} = \left[\bar{\theta}_{\bullet 1}, \bar{\theta}_{\bullet 2}, \cdots, \bar{\theta}_{\bullet n} \right]$$

where $\bar{\theta}_{\bullet j}$ stands for the average of the jth measured data over the samples. Hence the variation part is expressed as

$$\boldsymbol{\nu} = \begin{bmatrix} \theta_{11} - \bar{\theta}_{\bullet 1} & \theta_{12} - \bar{\theta}_{\bullet 2} & \cdots & \theta_{1n} - \bar{\theta}_{\bullet n} \\ \theta_{21} - \bar{\theta}_{\bullet 1} & \theta_{22} - \bar{\theta}_{\bullet 2} & \cdots & \theta_{2n} - \bar{\theta}_{\bullet n} \\ \vdots & \vdots & \ddots & \vdots \\ \theta_{m1} - \bar{\theta}_{\bullet 1} & \theta_{m2} - \bar{\theta}_{\bullet 2} & \cdots & \theta_{mn} - \bar{\theta}_{\bullet n} \end{bmatrix}$$

The signature ϕ can then be obtained by solving an eigen-problem as

$$\Sigma \phi = \lambda \phi \qquad (2.11)$$

where λ is the eigenvalue and Σ ($m \times m$) is a covariance matrix and defined as

$$\Sigma = vv^T \qquad (2.12)$$

2.1.5 Discussion

So far, little effort has been made to consider the random field in engineered system design. Most researches in the random field characterization focus on how to represent the random field effectively, either in a discrete or continuous domain. The techniques for random field characterization have been applied for modeling the random field in physical quantities, such as material properties and spatial variation in geometry shape and size. Furthermore, should the random field realizations (or snapshots) be sufficiently given, techniques addressed above can precisely model the random field.

This random field study has widely perceived limitations including: 1) an effective approach to characterize the random field for reliability analysis and Reliability-Based Design Optimization (RBDO) is lacking; 2) statistical dependence in random field characterization has not been considered for reliability analysis and RBDO; and 3) existing techniques for random field characterization demand a large number of field realizations (e.g., snapshots), which may become impractical in many engineering applications.

2.2 Reliability analysis

Reliability analysis is of critical importance to predict the chances of physics-of-failures (PoFs) in various engineering applications. However, a common challenge in

reliability analysis is a multi-dimensional integration to assess the probability of failure (e.g., failures due to fatigue, corrosion, and injury metrics) in various engineering applications (e.g., vehicle, airplane, and electronics). It is almost impossible to conduct analytical multi-dimensional integration or direct numerical integration for reliability analysis in large-scale engineering applications. Other than this approach, existing reliability analysis methods can be categorized into the four groups as: 1) sampling method; 2) expansion method; 3) the Most Probable Point (MPP)-based method; and 4) stochastic response surface method.

2.2.1 The sampling method

The sampling method is the most comprehensive but expensive method to use for estimating statistical moments, reliability, and quality of system responses. Monte Carlo Simulation (MCS) [Varghese et al. 1996; Lin et al. 1997] is the most widely used sampling method but demands thousands of computational analyses (e.g., Finite Element Analysis (FEA), crash analysis, *etc*.). To relieve the computational burden, other sampling methods have been developed, such as quasi-MCS [Niederreiter and Spanier 2000; Sobol 1998], importance (adaptive) sampling [Engelund and Rackwitz 1993; Melchers 1989; Bucher 1988; Wu 1994], directional sampling [Bjerager 1988], *etc*. Nevertheless, sampling methods are considerably expensive. Thus, it is often used for verification of reliability analysis when alternative methods are employed.

2.2.2 The expansion method

The idea of the expansion method is to estimate statistical moments of system responses with a small perturbation to simulate input uncertainty. This expansion method includes Taylor expansion, perturbation method [Kleiber and Hien 1992;

Rahman and Rao 2001], Neumann expansion method [Yamazaki and Shinozuka 1988], *etc*. Taylor expansion and perturbation methods require high-order partial sensitivities to maintain good accuracy. The Neumann expansion method employs Neumann series expansion of the inverse of random matrices, which requires an enormous amount of computational effort. In summary, all expansion methods could become computationally inefficient or inaccurate when the number or the degree of input uncertainty is high. Moreover, since it requires high-order partial sensitivities of system responses, it may not be practical for large-scale engineering applications.

2.2.3 The MPP-based method

The MPP-based method has been widely used to perform reliability analysis. Rotationally invariant reliability index is introduced through a nonhomogeneous transformation [Hasofer and Lind 1974]. Reliability analysis can be conducted in two different ways: response-level (G-level) [Hasofer and Lind 1974] and probability-level (P-level) [Youn et al. 2004; Du and Chen 2004]. It has been found that the P-level method is more efficient and stable than the G-level method [Youn et al. 2004]. However, the MPP-based method requires the first-order sensitivities of system responses. Moreover, it could generate relatively large error due to some nonlinearity of the system response and is not suitable for multiple MPP problems.

2.2.4 The stochastic response surface method

There currently exist a number of stochastic response surface methods, such as Polynomial Response Surface Models (PRSM) [Myers and Montgomery 1995], Multivariate Adaptive Regression Splines (MARS) [Friedman 1991], Radial Basis Functions (RBF) [Dyn et al. 1986], kriging [Cressie 1988], neural networks [Haykin

1999], Support Vector Regression (SVR) [Clarke et al. 2005], Polynomial Chaos Expansion (PCE) [Ghanem and Spanos 1991; Xiu and Karniadakis 2003], and Dimension Reduction (DR) [Rabitz and Alis 1999; Rahman and Xu 2004]. Each method has its associated fitting approach. For example, PRSM are usually fitted with the (moving) least square method [Myers and Montgomery 1995]. The kriging is fitted with the search for the best linear unbiased predictor [Cressie 1988; Simpson et al. 2001]. All of these techniques are capable of the function approximation, but they vary in their accuracy, robustness, computational efficiency, and transparency. PRSM is not suitable for high dimensional problems because of a curse of dimensionality [Youn et al. 2008]. MARS constructs response surface from a set of coefficients and basis functions from the regression data, which makes it suitable for problems with high input dimensions [Friedman 1991]. However, it normally cannot produce accurate results for nonlinear problems [Wang and Shan 2007]. RBF is useful for multivariate scattered data interpolation [Dyn et al. 1986; Fang and Horstemeyer 2006]. However, it is unable to interpolate large sets of data in an efficient and numerically stable way and maintain a good level of accuracy at the same time [Mullur and Messac 2005]. In general the Kriging can produce accurate results for nonlinear problems but difficult to obtain and use because a global optimization process is applied to identify the maximum likelihood estimators [Wang and Shan 2007]. Although neural networks are able to well approximate very complex models, they have the two disadvantages: 1) being a "black box" approach, and 2) having a computationally expensive training process [Jin et al. 2001; Haykin 1999]. It is well known that the accuracy of SVR depends on a good setting of meta-parameters and

the kernel parameters where optimal parameter selection is complicated [Clarke et al. 2005]. Although the PCE method is considered to be accurate, the primary drawback of the PCE method is the curse of dimensionality, which substantially increases the computational cost with the increase of the number of random variables [Hu and Youn 2009]. In the univariate DR method [Rahman and Xu 2004], it uses an additive decomposition of the responses that simplifies one multi-dimensional integration to multiple one-dimensional integrations. Generally, it can provide accurate lower moment of system responses such as mean. However, it may produce a relatively large error for the second-order or higher moments of nonlinear system responses. In the general DR method [Xu and Rahman 2004], the theoretical error of the univariate DR method can be reduced by considering multi-dimensional integrations. However, the computation effort is increased exponentially. Therefore, it is hard to afford a general DR calculation in most engineering applications.

2.2.5 Discussion

In the last decade, a considerable advance has been made in the area of reliability analysis. Many advanced methods for reliability analysis have been focused on the enhancement of numerical efficiency, accuracy and stability. Despite these advances, statistical dependence has little been considered in reliability analysis and design. This is mainly because of the misconception of minor influence of the statistical dependence on system responses and the lack of an effective tool to model the statistical dependence and perform reliability analysis.

2.3 Reliability-Based Design Optimization (RBDO)

RBDO is the technique used for engineering design when uncertainty is being considered. In general, the RBDO can be formulated as

$$\text{minimize } y(\mathbf{x};\mathbf{d})$$
$$\text{subject to } P(G_i(\mathbf{x};\mathbf{d}) \leq 0) = F_{G_i}(0) \geq \Phi(\beta_{t_i}), \quad i = 1, \cdots, NP$$
$$\mathbf{d}^{\mathbf{L}} \leq \mathbf{d} \leq \mathbf{d}^{\mathbf{U}}, \quad \mathbf{d} \in R^{ND} \text{ and } \mathbf{x} \in R^N$$

where $y(\mathbf{x}; \mathbf{d})$ is the objective function, $\mathbf{d} = \boldsymbol{\mu}(\mathbf{x})$ is the design vector, $\mathbf{x}$ is the random vector, β_{ti} is the prescribed target reliability, NP, ND, and N are the number of probabilistic constraints, design variables, and random variables, respectively. The probabilistic constraint, $F_{Gi}(0)$, is expressed as

$$F_{G_i}(0) = \int \cdots \int_{G_i(\mathbf{X}) \leq 0} f_{\mathbf{X}}(\mathbf{x}) d\mathbf{x} \tag{2.13}$$

RBDO is composed of two sub-problems, reliability analysis and design optimization. Reliability analysis evaluates probabilistic constraints at a given design. Design optimization seeks for an optimal design subject to the probabilistic constraints. Many efforts have been made to enhance the numerical accuracy, efficiency and stability of the RBDO through the development of three RBDO approaches: a nested double-loop, decoupled double-loop, and single-loop approach.

2.3.1 Nested double-loop RBDO approach

The efficiency of this type of method is usually low since it employs nested optimization loops. The inner loop is the assessment of probabilistic constraints, which involves an iterative procedure using either Reliability Index Approach (RIA) [Tu et al. 1999] or Performance Measurement Approach (PMA) [Youn et al. 2003]. The outer loop controls the design search process, which calls the inner loop

repeatedly for sensitivity or function assessments.

2.3.2 Decoupled double-loop RBDO approach

To improve the efficiency of the double-loop RBDO, some methods decouple the nested optimization loops. With the decoupling strategies, the reliability analysis loop and optimization loop are in the same design cycle sequentially instead of being nested. In general, the decoupled double-loop RBDO reduces the computational effort compared to the nested double-loop RBDO.

Du and Chen developed a decoupled double-loop RBDO termed Sequential Optimization and Reliability Assessment (SORA) [Du and Chen 2004]. The key concept of the SORA method is to shift the boundaries of violated constraints to the feasible direction based on the reliability information obtained in the previous cycle. The reliability analysis is performed using the MPP based method after the deterministic optimization to verify the constraint feasibility. Hence, the design is improved from cycle to cycle and the computation efficiency is improved by decoupling the reliability analysis from the optimization loop. By building a relation between the safety factor and the reliability of a system, researchers developed Sequential Optimization with Reliability-based Factors of Safety (SORFS) methods [Qu and Haftka 2004; Wu et al. 2001; Ba-abbad et al. 2006]. This type of methods decouples the reliability analysis from the design optimization using the safety factor to replace the probabilistic constraints with deterministic constraints. Tu et al. developed the Design Potential Method (DPM), where the search direction for optimization is determined at the so called Design Potential Point (DPP) [Tu et al. 2001], which is defined as the design point derived from the MPP using either RIA or

19

PMA. The DPM improves the efficiency of RBDO by taking advantage of the important design information unveiled in the reliability analysis. Zou and Mahadevan decoupled the optimization and reliability analysis by approximating the probabilistic constraints using the first-order Taylor series expansion [Zou and Mahadevan 2006].

2.3.3 Single-loop RBDO approach

The single-loop RBDO was proposed to enhance numerical efficiency in the RBDO process by eliminating numerical iterations in the reliability analysis [Thanedar and Kodiyalam 1992; Chen and Hasselman 1997; Wang and Kodiyalam 2002; Shan and Wang 2008]. Two different approaches were made: using the mean value first-order reliability method [Thanedar and Kodiyalam 1992; Shan and Wang 2008] or using the steepest ascent direction obtained at the previous design [Chen and Hasselman 1997; Wang and Kodiyalam 2002]. Thus, the single-loop structure benefits the RBDO by improving numerical efficiency. However, it is well known that single-loop RBDO using a mean value method shows numerical inaccuracy or instability because of inaccurate estimation of probabilistic constraints in the RBDO process. The single-loop RBDO using the steepest ascent direction improves numerical accuracy of evaluating probabilistic constraints. However, it has been found [Chen and Hasselman 1997] that this method could be numerically unstable and/or inaccurate because it does not satisfy Karush-Kuhn-Tucker (KKT) necessary condition.

2.3.4 Discussion

Nested double-loop methods are structured with the inner loop for the reliability analysis and the outer loop for the design optimization. As a result, these methods are

computationally expensive for most engineering design problems. Later, decoupled double-loop and single-loop methods have been developed to address the computational challenges aforementioned. Despite the extensive effort made in the RBDO methods, the numerical efficiency, accuracy, and stability is still of great concern.

Chapter 3: Random Field Characterization in Engineered Systems

This chapter aims at developing advanced techniques for random field characterization in order to model any geometric or non-geometric random fields in engineered systems whether or not the random field can be realized with either sufficient or insufficient field data (or snapshots).

3.1 Introduction

Manufacturing variability (geometries and material properties) over samples and stochastic nature in loads have been modeled using spatially independent random parameter variables [Zou et al. 2002; Penmetsa and Grandhi 2002; Maute and Frangopol 2003; Qu and Haftka 2004; Du and Chen 2005; Youn et al. 2004a; Youn et al. 2004b; Youn et al. 2005; Smith and Mahadevan 2005; Yin and Chen 2006]. Although these literatures have provided a great foundation to integrate probability analysis to engineering system design, their works lack practical consideration of spatial variability over samples (or the random field).

In many engineering applications the manufacturing and load variability is a function of spatial variables (x, y, and z) and temporal variable (t). The random field is thus coined to reflect spatial and temporal variability. For instance, the thickness of a metal sheet has variation over space and samples (or sampled time). This notion of the random field can also be observed in material properties (e.g., an elastic modulus) and loading conditions. In the 1990s, the random field had already gained its popularity in applications of civil engineering [Yamazaki and Shinozuka 1990; Liu and Der Kiureghian 1991; Ghanem and Spanos 1991; Liu and Liu 1993; Zhang and

22

Ellingwood 1994; Sudret and Der Kiureghian 2000]. It had also been considered in many different disciplines, including fluid dynamics [Rajaee et al. 1994], wind pressure fields [Tamura et al. 1999], coherent structures [Berkooz et al. 1996], and pattern recognition [Fukunaga 1990]. Numerous techniques have been developed to represent a discrete or continuous random field. Methods include the midpoint method [Der Kiureghian and Ke 1988], spatial averaging method [Vanmarcke and Grigoriu 1983], shape function method [Liu et al. 1986], and Proper Orthogonal Decomposition (POD) method [Turk and Pentland 1991]. However, little effort has been made to consider the random field in probability analysis and design [Choi et al. 2006; Missoum 2008; Chen et al. 2010]. The major reason lies in the fact that spatial variability has been conceived to negligibly affect system responses. However, our study showed that spatial variability may influence variability in system responses significantly, especially in geometry-sensitive failures (e.g., buckling, fillet failures) and small-scale applications in which tolerance control is more challenging.

This research was initially inspired by a random field paper [Missoum 2008] that originally applied the idea of the POD to engineering design problems. The POD method has been employed to extract the important signatures of the random field observed in an engineering product or process. Our preliminary study found that the parametric representation of the random field in Missoum's work is not directly related to the available random field data and the coefficients of the signatures are statistically uncorrelated but dependent in most cases. Furthermore, existing techniques for random field characterization demand a large number of random field realizations (e.g., snapshots), which may become impractical in many engineering

applications. This chapter thus proposes a generic and robust random field characterization method, which can characterize any geometric or non-geometric random fields in engineered systems whether or not the random field can be realized with either sufficient or insufficient field data while accounting for the statistical dependence among the coefficients for probability analysis and design. The proposed approach has three technical contributions. The first contribution is to develop a generic approximation scheme of random field as a function of the most important field signatures while preserving prescribed approximation accuracy. The coefficients of the signatures can be modeled as random field variables and their statistical properties are identified using the Chi-Square goodness-of-fit test. Second, a Bayesian approach with Bayesian Copula dependence modeling to characterize the random field with the lack of field data sets. Third, the Rosenblatt transformation is employed to transform the statistically dependent random field variables into statistically independent random field variables. The number of the transformation sequences exponentially increases as the number of random field variables becomes large. It was found that improper selection of a transformation sequence among many may introduce high nonlinearity into system responses, which may result in inaccuracy in probability analysis and design. Hence, this chapter proposes a novel procedure of determining an optimal sequence of the Rosenblatt transformation that introduces the least degree of nonlinearity into the system response. The proposed random field characterization can be integrated with any advanced probability analysis method, such as the Dimension Reduction (DR) method [Rabitz et al. 1999; Rabitz and Alis 1999; Xu and Rahman, 2004], Eigenvector Dimension Reduction

(EDR) method [Youn et al. 2008], Polynomial Chaos Expansion (PCE) method [Lee and Chen 2009; Hu and Youn 2009], etc. Three structural problems including a Micro-Electro-Mechanical Systems (MEMS) bistable mechanism, one refrigerator assembly problem, and one heat generation problem of the Lithium-ion battery are used to demonstrate the effectiveness of the proposed approach in Section 3.5.

3.2 Random field characterization with sufficient data

This section characterizes the random field with sufficient data. In Section 3.2.1, an adaptive loop is proposed to select the most important signatures for representing a random field. In Section 3.2.2, a unique approach for modeling the random field variable is proposed for probability analysis and design. Statistical properties of the random field variable are discussed in Section 3.2.3.

3.2.1 Important signatures for representing a random field

Theoretically, an infinite number of signatures are required to represent the random field exactly using the Proper Orthogonal Decomposition (POD) method. Practically, only a few important signatures may be vital to approximate the random field accurately. Hence, instead of using all signatures, a small number of important signatures (r) are selected to approximate the random field as shown in Eq. (3.1).

$$\theta(x,t) \approx \tilde{\theta}(x,t) = \mu(x) + \sum_{i=1}^{r} \alpha_i(t) \frac{\phi_i(x)}{\|\phi_i(x)\|} \tag{3.1}$$

where $\tilde{\theta}(x,t)$ is an approximate random field with r number of important signatures.

The importance of the signature is indicated by the magnitude of the eigenvalue as shown in Eq. (2.11). The larger eigenvalue indicates the greater importance of the

corresponding signature in approximating the random field. Therefore, the eigenvalue can be ranked based on the magnitude of the normalized eigenvalue (ρ_i) defined as

$$\rho_i = \frac{\lambda_i}{\lambda_1}, \quad 0 \le \rho_i \le 1 \quad \text{for } i = 1, \cdots, m \tag{3.2}$$

where λ_1 is the largest eigenvalue and m is the total number of eigenvalues.

It could be subjective to determine the number (r) based on the magnitude of the normalized eigenvalue. Therefore, a posteriori normalized error ε is defined to adaptively determine the minimal number of the most important signatures, which preserves a prescribed accuracy in approximating the random field. The normalized error is defined as

$$\varepsilon = \frac{1}{mn} \frac{\sum_{i=1}^{m} \sum_{j=1}^{n} \left| \theta_{ij} - \tilde{\theta}_{ij} \right|}{\mu_{\max} - \mu_{\min}} \tag{3.3}$$

where m is the number of the sampled snapshots; n is the number of the measurement points at each snapshot; $\tilde{\theta}_{ij}$ is the approximate random field data at the j-th measurement point of the i-th sampled snapshot with k ($\le r$) number of important signatures; θ_{ij} is the actual random field data; $\mu_{\max}$ and $\mu_{\min}$ are the maximum and minimum values of the mean of the random field, respectively. The normalized error indicates an average error between the actual and approximate random fields at all measurement points. A flowchart for adaptively selecting the number of the most important signatures is shown in Fig. 3-1. Once the random field data sets ($\theta_{m \times n}$) are obtained, the total m number of the signatures can be ranked based on Eq. (3.2). The approximate random field is gradually refined by adding one more signature in each iteration until the normalized error in Eq. (3.3) is smaller than a threshold error value

ε_c which is generally set to 0.1%. The threshold value must be small enough to ensure high accuracy of the random field modeling while using the minimal number of the important signatures. Otherwise, the statistical uncertainty in the random field modeling may be comparable to the physical uncertainty or even dominate in probability analysis.
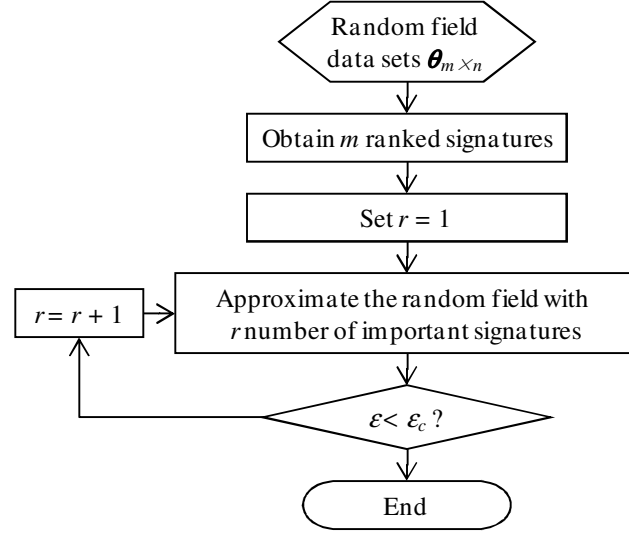
Figure 3-1: Flowchart for determining the number of the important signatures

3.2.2 Modeling random field variables

The random field variables will be used to characterize a random field observed in an engineering product or process. In Eq.(3.1), $\alpha_i(t)$ represents a coefficient dataset of the i-th signature obtained from all sampled snapshots (t=1,…,m). V_i is thus defined as a random field variable that statistically models the coefficient dataset of the i-th signature. By replacing $\alpha_i(t)$ with the random field variable (V_i), Eq. (3.1) can be rewritten as

$$\tilde{\theta}(x,t) = \mu(x) + \sum_{i=1}^{r} V_i \frac{\phi_i(x)}{\|\phi_i(x)\|} \tag{3.4}$$

The formulation of the random field variable (V_i) is unique compared with the previous study [Missoum, 2008] where a weight function was multiplied by a user-selected coefficient, say $\alpha_i(1)$, for the parametric representation of a random field. The weight function was used to modify the contribution of each random field signature. However, it may fail to represent the actual random field since this parametric representation is not directly related to the available random field data. The random field variable (V_i) contains the variability over the sampled snapshots that are obtained during the sampled time (t). Once the statistical properties of V_i are characterized, the original random field can be approximated by Eq. (3.4). Therefore, the random system response in the presence of the random field can be effectively analyzed using any probability analysis method.

Accuracy in modeling the random field variable V_i depends upon the number of sampled snapshots. This section employs a large amount of sampled snapshots and, thereafter, considers aleatory uncertainty[1] only. For epistemic uncertainty[2] with the lack of sampled snapshots, Bayesian statistics [Wang et.al 2009] can be integrated to the proposed framework in Section 3.3. This study uses a large amount of input random data for the construction of aleatory uncertainty. The statistical properties of the random field variable V_i can be characterized with the following three steps as:

Step 1: Obtain optimum distribution parameters for candidate distributions using the maximum likelihood method. It can be formulated as

$$\text{maximize} \quad L(V_i \mid \boldsymbol{\delta}) = \sum_{l=1}^{m} log_{10}[f(v_{il} \mid \boldsymbol{\delta})]$$

---

[1] Aleatory uncertainty is defined as objective and irreducible uncertainty with sufficient information on the random variable.
[2] Epistemic uncertainty can be classified as subjective and reducible uncertainty due to the lack of knowledge on the random variable.

where $\boldsymbol{\delta}$ is the unknown distribution parameter vector; v_{il} is a realization of V_i from the l-th snapshot; $L(\bullet)$ is the likelihood function; m is the number of snapshots; and f is the Probability Density Function (PDF) of V_i for the given $\boldsymbol{\delta}$.

Step 2: Perform quantitative hypothesis tests for the candidate distribution types with the optimum distribution parameters obtained in Step 1. Among the Chi-Square goodness-of-fit test, Kolmogorov-Smirnov (K-S) test, and Anderson-Darling (AD) test, the Chi-Square goodness-of-fit test is selected in this study due to its good performance for both continuous and discrete distributions given a large amount of data.

Step 3: Select the distribution type with the maximum p-value as the optimal distribution type for V_i.

3.2.3 Statistical properties of random field variables

When multiple random field variables are needed to accurately approximate the random field, statistical correlation and statistical dependence of the random field variables becomes one of the greatest concerns in probability analysis. Using Eqs. (2.9), (2.12), and (3.4), the inner product of any two random field variables can be expressed as

$$V_i V_j = \frac{\lambda_i \phi_i(x) \bullet \phi_j(x)}{\|\phi_i(x)\| \|\phi_j(x)\|} \tag{3.5}$$

Since two signatures ($\phi_i(x)$ and $\phi_j(x)$) are orthogonal, $E(V_i V_j)$ becomes zero. Furthermore, the expected value (or mean) of every random field variable is zero because the mean of the variation in Eq. (2.9) is zero. Thus, V_i and V_j must be statistically uncorrelated, that is

$$E\left[(V_i - \mu_i)(V_j - \mu_j)\right] = E(V_i V_j) - E(V_i)E(V_j) = 0$$

However, they may not be statistically independent because of $f_{V_i V_j}(v_i, v_j) \neq f_{V_i}(v_i) f_{V_j}(v_j)$. If the random field variables are statistically independent, they are statistically uncorrelated. But the converse is not true. A complicated random field tends to require a large number of random field variables. Such a problem poses a great challenge in handling statistical dependence of the random field variables since little effort has been devoted to handling probability analysis for system responses with statistically dependent random variables. This problem will be resolved in Section 3.4 in this chapter.

3.3 Random field characterization with insufficient data

This section characterizes the random field with insufficient data. Insufficient data refers to a small amount of samples for a random field from which statistical distributions of random field variables cannot be modeled precisely. Efron [Efron 1982] suggested that to achieve a reasonable result, at least 100 samples are needed to use bootstrapping resampling method for modeling a random variable. Picheny et al. [Picheny et al. 2010] considered 20 to 1000 samples as limited samples when modeling random variables. In Section 3.3.1, a Bayesian updating approach using the Markov Chain Monte Carlo (MCMC) method is proposed to update the random field. In Section 3.3.2, a Bayesian Copula dependence modeling approach is proposed to model the statistical dependence among random field realizations at different measurement locations. Hence, Monte Carlo Simulation (MCS) can be employed to generate sufficient random field snapshots based on the dependence modeling.

3.3.1 Random field updating using the MCMC method

Let $\theta(x, t)$ be a random field of interest. Every realization (or snapshot) of the random field consists of n measurement points such that $\theta(x, t) \approx \boldsymbol{\theta} = [\theta(x_1, t), \ldots, \theta(x_n, t)]$, where $x_1, \ldots, x_n$ are known measurement locations. Assume the random field realizations at n measurement points are independent. Thus, the random field $\boldsymbol{\theta}$ is represented by n independent random variables. Let the random field $\boldsymbol{\theta}$ follows an n-dimensional joint Probability Density Function (PDF) $f_{\boldsymbol{\Theta}}(\boldsymbol{\theta} \mid \boldsymbol{\delta})$, where $\boldsymbol{\delta}$ is the independent unknown distribution parameter vector. According to the Bayesian point of view, $\boldsymbol{\delta}$ is interpreted as a realization of a random vector $\boldsymbol{\Delta}$ with an n-dimensional joint PDF $f_{\boldsymbol{\Delta}}(\boldsymbol{\delta})$. The density function expresses what one thinks about the occurring frequency of $\boldsymbol{\Delta}$ before any future observation of $\boldsymbol{\theta}$ is taken, that is, a prior distribution. Based on the Bayes' theorem, the posterior distribution of $\boldsymbol{\Delta}$ given a new observation $\boldsymbol{\theta}$ can be expressed as

$$f_{\boldsymbol{\Delta} \mid \boldsymbol{\Theta}}(\boldsymbol{\delta} \mid \boldsymbol{\theta}) = \frac{f_{\boldsymbol{\Theta}, \boldsymbol{\Delta}}(\boldsymbol{\theta}, \boldsymbol{\delta})}{f_{\boldsymbol{\Theta}}(\boldsymbol{\theta})} = \frac{f_{\boldsymbol{\Theta} \mid \boldsymbol{\Delta}}(\boldsymbol{\theta} \mid \boldsymbol{\delta}) \cdot f_{\boldsymbol{\Delta}}(\boldsymbol{\delta})}{f_{\boldsymbol{\Theta}}(\boldsymbol{\theta})} \tag{3.6}$$

The Bayesian approach is used for updating information about the parameter vector $\boldsymbol{\delta}$. First, a prior distribution of $\boldsymbol{\Delta}$ must be assigned before any future observation of $\boldsymbol{\theta}$ is taken. Then, the prior distribution of $\boldsymbol{\Delta}$ is updated to the posterior distribution as the data for $\boldsymbol{\theta}$ is obtained. This process can be repeated with evolution of data sets by setting the posterior distribution to a new prior distribution.

It is extremely difficult to compute the exact analytical form of the posterior distribution for the parameter vector $\boldsymbol{\delta}$ since the normalization factor (the denominator in Eq. (3.6)) requires complicated and multi-dimensional integration. Although it is

hard to obtain the posterior distribution directly, it is feasible to draw relevant samples. MCMC method provides a mechanism to draw samples from the complicated posterior distribution. This study uses the Metropolis-Hastings algorithm for MCMC method [Berg 2004].

3.3.2 Random field dependence modeling using the Bayesian Copula

Copulas are multivariate distributions modeling the dependence structure among random variables, irrespective of their marginal distributions. The choice of the best multivariate distribution can be done in two steps: 1) choose the optimal marginal distribution; and 2) choose the optimal Copula. The optimal marginal distribution is obtained from the n-dimensional joint PDF $f_{\Theta}(\theta \mid \delta)$ after the updating of parameter vector δ in Eq. (3.6). In this section, a Bayesian Copula approach [Huard et al. 2006] combined with a neighboring search algorithm are employed to choose the optimal Copula for the dependence modeling of the random field realizations at different measurement locations.

A Copula is a joint distribution function of standard uniform random variables [Sklar 1959]. According to Sklar's theorem, there exists an n-dimensional Copula C such that for all x in real random space

$$F(x_1, \ldots, x_n) = C(F_1(x_1), \ldots, F_n(x_n)) \tag{3.7}$$

where F is an n-dimensional distribution function with marginal functions $F_1, \ldots, F_n$. Most Copulas deal with bivariate data due to the lack of practical n-dimensional generalization of the correlation parameter [Roser 1999; Huard et al. 2006]. For multivariate data, the usual approach is to analyze the data pair by pair using two-dimensional Copulas. The most commonly employed methods to select the best

Copula are based on a likelihood approach [Fermanian 2005; Chen and Fan 2005; Panchenko 2005], which relies on the estimation of an optimal parameter set. Strictly speaking, comparisons are made among Copulas with given parameters. The Bayesian Copula approach selects the best Copula independent of the parameter estimation.

According to Huard et al, a set of hypotheses are first made as follows:

H_l : The data come from Copula C_l, $l = 1, \ldots, Q$

The objective is to find the Copula with the highest $Pr(H_l \mid D)$ from a finite set of Copulas (C_Q), where D represents bivariate data in standard uniform space. Based on the Bayes' theorem, the probability that data come from the Copula C_l is expressed as

$$Pr\left(H_l \mid D\right) = \frac{Pr\left(D \mid H_l\right)Pr(H_l)}{Pr(D)} = \int_{-1}^{1} \frac{Pr\left(D \mid H_l, \tau\right)Pr(H_l \mid \tau)Pr(\tau)d\tau}{Pr(D)} \qquad (3.8)$$

where τ is the Kendall's tau, which is a non-parametric measure of the statistical dependence associated to Copulas. Kendall's tau (τ) belongs to the set of each Copula and the outcome is equally likely. All Copulas are equally probable with respect to a given τ which reflects no preference over the Copulas. The likelihood $Pr(D \mid H_l, \tau)$ depends upon the τ and can be calculated from the Copula PDF as

$$Pr\left(D \mid H_l, \tau\right) = \prod_{i=1}^{m} c_l\left(u_{1i}, u_{2i} \mid \tau\right) \qquad (3.9)$$

where c_l ($\bullet$) is the PDF of the l-th Copula; m is the total number of data (or snapshots); u_{1i} and u_{2i} are the i-th realizations of the statistically dependent bivariate variables. The normalization of $Pr(D)$ can be computed using the sum rule [Jaynes and Bretthorst 2003].

To improve the accuracy of the statistical dependence modeling among the

random field realizations at different measurement locations, a neighboring search algorithm is proposed to control the range of the statistical dependence. For the realizations at a given measurement location, the statistical dependence modeling is only performed for the neighbors of that location. The neighbors are defined according to an assigned Euclidean distance.

3.4 Statistically dependent random field variables

To handle the statistical dependence of the random field variables for probability analysis of system responses, the statistically dependent random field variables need to be transformed into statistically independent random field variables. Thus, any advanced probability analysis method can be integrated with the proposed random field approach for probability analysis and design. In Section 3.4.1, the Rosenblatt transformation is employed to transform the statistically dependent random field variables into statistically independent random field variables. The number of the transformation sequences exponentially increases as the number of random field variables becomes large. It was found that improper selection of a transformation sequence among many may introduce high nonlinearity into system responses, which may result in inaccuracy in probability analysis and design. Section 3.4.2 thus proposes a novel procedure of determining an optimal sequence of the Rosenblatt transformation that introduces the least degree of nonlinearity to the system response.

3.4.1 Incorporation of the Rosenblatt transformation

In many advanced probability analysis methods, only a few simulations or function evaluations at a set of samples of the input random variables are required for probability analysis if the input random variables are statistically independent. For

example, the Eigenvector Dimension Reduction (EDR) method demands either $2N+1$ or $4N+1$ samples for probability analysis where N is the number of the input random variables. In the Polynomial Chaos Expansion (PCE) method, the evaluation of the PCE coefficients requires the response values at the predefined Gaussian quadrature points [Le Maître et al. 2002], the collocation points specified by the Smolyak algorithm [Gerstner and Griebel 1998] or the univariate and bivariate sample points [Hu and Youn 2009]. Hence, probability analysis of the system response can be carried out using one of the advanced probability analysis methods if the system response can be evaluated at the required samples in the transformed standard normal space (or U-space). In this section, the objective is to determine the samples in the statistically dependent random space (or V-space) for probability analysis. The samples in V-space can be obtained through the inverse Rosenblatt transformation from those in U-space. The overall procedure is detailed as follows:

Step 1: Obtain the required sample points $(u_1^{(j)}, \ldots, u_N^{(j)})$ for $j = 1, \ldots, M$ in U-space for a given probability analysis method, where M is the total number of the sample points.

Step 2: Transform the sample points from U-space to V-space using the inverse Rosenblatt transformation as

$$\begin{cases} v_1^{(j)} = F_{V_1}^{-1}\left[\Phi\left(u_1^{(j)}\right)\right] \\ v_2^{(j)} = F_{V_2|V_1}^{-1}\left[\Phi\left(u_2^{(j)}\right)\right] \\ \vdots \\ v_N^{(j)} = F_{V_N|V_1,V_2,\ldots,V_{N-1}}^{-1}\left[\Phi\left(u_N^{(j)}\right)\right] \end{cases} \tag{3.10}$$

where $(v_1^{(j)}, \ldots, v_N^{(j)})$ denotes the j-th transformed sample point in V-space, $F^{-1}(\bullet)$ is the inverse joint Cumulative Distribution Function (CDF) of the random variable in V-space. It is noted that the choice of a transformation sequence significantly affects the nonlinearity of the system response and will be discussed in the subsequent section.

Step 3: Obtain the system response values at the transformed sample points: $Y(v_1^{(j)}, \ldots, v_N^{(j)})$, for $j = 1, \ldots, M$ and perform probability analysis.

Step 2 is further elaborated with a two-dimensional problem. Let $(u_1, u_2) = (-3, 0)$ be one of the required samples in U-space. An empirical CDF of v_1 can be obtained using the dataset for v_1. The first component value $c_1 (= v_1)$ of the sample in V-space can be set to $F_{V_1}^{-1}(\Phi(u_1 = -3))$. Given the identified first component value $v_1 = c_1$ an empirical conditional CDF of v_2 can be constructed using the statistically dependent dataset. The second component value $c_2 (= v_2)$ of the sample in V-space can then be set to $F_{V_2|V_1}^{-1}(\Phi(u_2 = 0))$. This process can be continued to determine other samples in V-space using the available statistically dependent data.

3.4.2 Determination of an optimal transformation sequence

The number of the transformation sequences exponentially increases as the number of random field variables becomes large. It was found that improper selection of a transformation sequence among many may introduce high nonlinearity into system responses, which may result in inaccuracy in probability analysis and design. Hence, it is critical to determine an optimal sequence of the Rosenblatt transformation that introduces the least degree of nonlinearity into the system response.

A linear response function is employed to study the nonlinearity introduced by different transformation sequences as shown in Eq. (3.11).

$$Y_T = \sum_{i=1}^{N} v_i \qquad (3.11)$$

where N is the total number of random variables; v_i is the i-th random variable. The linear response function becomes nonlinear after the Rosenblatt transformation and is expressed as

$$Y_{T,k} = f\left(u_1, u_2, \cdots, u_N\right) \quad \text{where} \quad \mathbf{u} = T_k(\mathbf{v}) \qquad (3.12)$$

where $T_k(\bullet)$ indicates the Rosenblatt transformation with the k-th transformation sequence; $Y_{T,k}$ stands for the nonlinear response obtained through the k-th transformation; and $k = 1, \cdots, N!$. It is apparent that the best sequence must have the least degree of nonlinearity in the system response. Hence, the nonlinearity of $Y_{T,k}$ needs to be quantified for all possible sequences. The degree of nonlinearity in Eq. (3.12) introduced by a particular transformation sequence can be obtained by measuring the degree of deviation from a linear response $Y_L = \sum_i u_i$. The degree of deviation of $Y_{T,k}(\bullet)$ from the j-th linear response ($\hat{Y}_j$) through the k-th transformation sequence can be defined as

$$S_{j,k} = \sum_{l=1}^{Q} \left[Y_{T,k}(0,...,0,u_{j,l},0,...,0) - \hat{Y}_{j,l} \right]^2 \quad \text{where} \quad \hat{Y}_{j,l} = u_{j,l} \qquad (3.13)$$

where Q is the number of discrete data points along the j-th random variable u_j. Repeating this for N random variables, the total degree of deviation can be calculated as $\sum_j S_{j,k}$ for the k-th transformation sequence. The sequence with the minimum total degree of deviation will be defined as the optimal sequence of the Rosenblatt

transformation. For a small number of random variables (say $N<10$), the best sequence can be determined by finding the minimum total degree of deviation in all possible sequences. For a large number of random variables (say $N>10$), a genetic algorithm can be employed to effectively determine the best sequence with the minimum total degree of deviation. An optimization problem can be formulated as

$$Minimize : \sum_{j=1}^{N} S_{j,k}$$
$$S.T. \qquad k \in \{1, \cdots, N!\}$$

3.5 Examples and results

Examples are presented in this section to demonstrate the proposed random field characterization with both sufficient and insufficient data.

3.5.1 Examples with sufficient data

Three structural examples including a Micro-Electro-Mechanical Systems (MEMS) bistable mechanism are used to demonstrate the effectiveness of the proposed approach with sufficient data.

3.5.1.1 Beam example

A cantilever beam is one of the most commonly used structures in engineering applications, which has spatial variability to some degree. This variability may influence variability in beam responses. The top and bottom surfaces of the beam were modeled to have a symmetric random field about the mid-surface. A mathematical expression of the random field in the top surface is formulated as

$$h(x) = 0.1\sin\left(K\pi x / 2\right) \tag{3.14}$$

where $K \sim Normal$ $(2, 0.02^2)$ and $0 \leq x \leq 10$ [*mm*]. The beam height is 2*mm* at *x*=0. One thousand sampled snapshots were artificially created by generating 1000 random *K* values from the prescribed normal distribution. One hundred measurement points are evenly distributed along the length of the beam.

Step 1: Determination of the important signatures

First, an *m*×*n* matrix (**θ**) representing the random field was created to obtain the field signatures. Using the posteriori normalized error in Eq. (3.3), the two most important signatures were selected to approximate the random field as shown in Fig. 3-2. The normalized error of the approximate random field is less than 0.1% with these two signatures. Thus, the random field can be approximated as

$$\tilde{h}(x) = \mu(x) + \sum_{i=1}^{2} V_i \frac{\phi_i(x)}{\|\phi_i(x)\|} \tag{3.15}$$
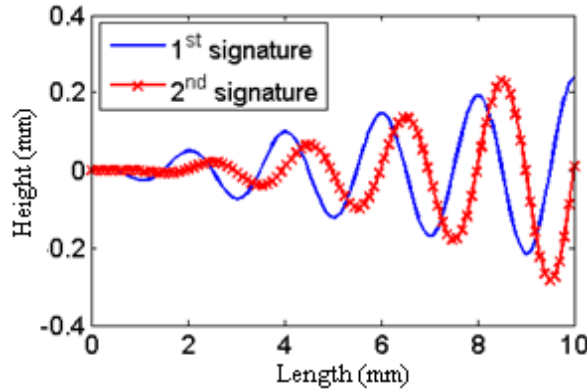
Figure 3-2: The first two normalized signatures

Figure 3-3 shows the 1-st random field realizations in the region of $8 \leq x \leq 10$ [*mm*], which confirms the accuracy of approximate random fields with the two most important signatures. The figure contains one true and two approximate realizations

of the random field. The approximate realizations were built using one and two of the most important signatures. The use of the most important signature produced a normalized error of 0.44% in approximating the random realization. The inclusion of the second most important signature decreased the error to 0.03%. Two random field variables (V_1 and V_2) were thus used to describe the random field.
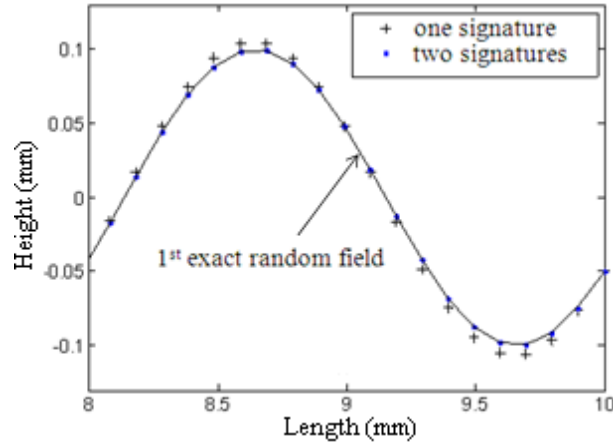
Figure 3-3: Comparison of the exact and approximate random fields

(the 1-st random field realization)

Step2: Modeling random field variables and statistical dependence

One thousand random samples of two random field variables (V_1 and V_2) were obtained from one thousand sampled snapshots and the histograms of two random field variables are shown in Fig. 3-4 (a) and (b). The Maximum Likelihood Estimation (MLE) and Chi-Square goodness-of-fit test were used to find the distributions and statistical parameters of two random field variables. They were modeled as

$$V_1 \sim Normal(0, 0.1192^2) \quad \text{and} \quad V_2 \sim Beta(0, 0.0181, -0.1560, 0.0126)$$

The Probability Density Function (PDF) and normalized histograms were compared in the figures. As explained in Section 3.2.3, no statistical correlation exists between V_1 and V_2. However, their statistical dependence was clearly observed by plotting one thousand samples of V_1 and V_2, as shown in Fig. 3-4 (c). In this special case, V_2 is a function of V_1. For a given V_1 value, the corresponding V_2 value was obtained using the moving least square method. Therefore, Eq. (3.15) can be reformulated to resolve the difficulty of the statistical dependence.

$$\tilde{h}(x) = \mu(x) + V_1\phi_1(x) + f(V_1)\phi_2(x) \tag{3.16}$$
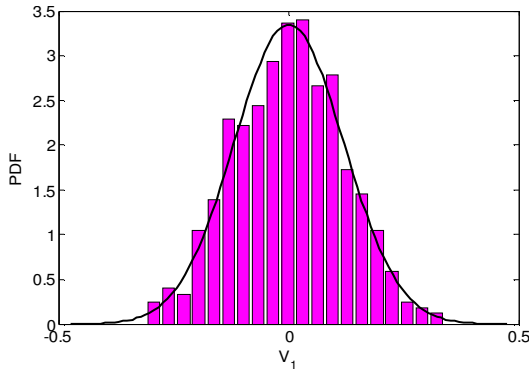
(a) Histogram and distribution for V_1 (b) Histogram and distribution for V_2
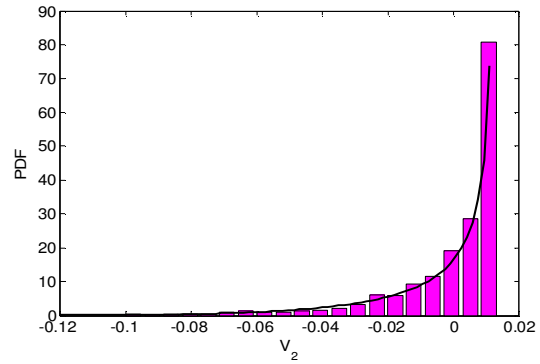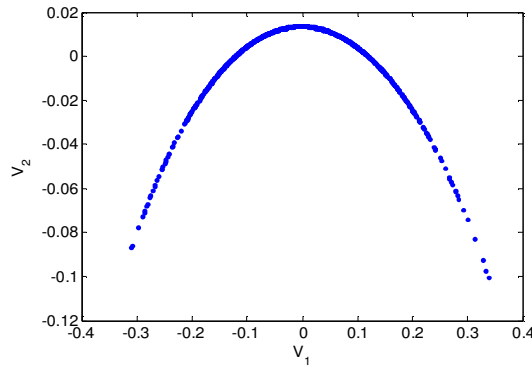
(c) Random realizations of V_1 and V_2

Figure 3-4: Statistical properties of V_1 and V_2

Comparison between the proposed approach and Missoum's approach

The proposed approach for the random field characterization is directly related to the available random field data. In Missoum's approach, a weight function was multiplied by a user-selected coefficient, say $\alpha_i(1)$, for the parametric representation of a random field. The weight function was used to modify the contribution of each random field signature. This approach may fail to represent the actual random field since it is not directly related to the available random field data. As a demonstration, the weight function is assumed to follow the uniform distribution and multiplied by a user-selected coefficient $\alpha_i(1)$ in Missoum's approach. Figure 3-5 shows the comparison between two approaches for the parametric representation of a random field. Black solid curves represent the contour of the true random field. Red solid dots indicate the random field contour from the proposed approach. Blue dotted lines stand for the contour from Missoum's approach. The proposed approach is more accurate than the Missoum's approach for representing the actual random field as shown in Fig. 3-5.
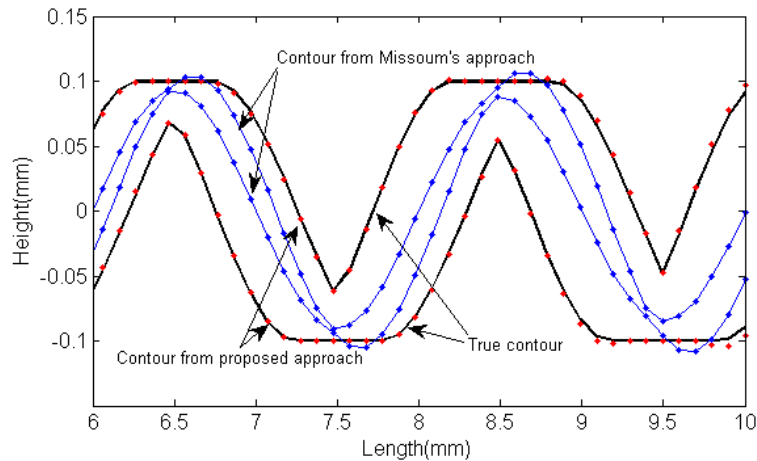
Figure 3-5: Comparison between the proposed approach and Missoum's approach

3.5.1.2 MEMS bistable mechanism

A MEMS device was used for the second example because spatial variability may influence variability in MEMS device responses significantly. A bistable mechanism is able to remain in stable equilibrium in two distinct positions. MEMS bistable mechanisms are useful as micro valves [Golly et al. 1996], micro relays [Qiu et al. 2003], fiber optical switches [Hoffmann et al. 1999], etc. In a micro scale, a monolithic bistable mechanism is necessary to avoid friction, backlash, and wear at joints. One feasible monolithic MEMS bistable mechanism [Qiu et al. 2004] was recently developed by rigidly coupling two curved beams together at their midpoints as shown in Fig. 3-6. Figure 3-7 shows the relationship between a typical force and displacement curve for such a bistable mechanism when the force is applied downwards at the center of the upper beam. There are three equilibriums during this process. S_1 and S_3 are the stable equilibriums and S_2 is the unstable one. If the force is released before passing the unstable equilibrium S_2, the structure returns to the stable equilibrium S_1. Otherwise, it moves to the second stable equilibrium S_3. Three system responses, the maximum force, minimum force, and distance from the state S_1 to S_2, are normally important for different applications.
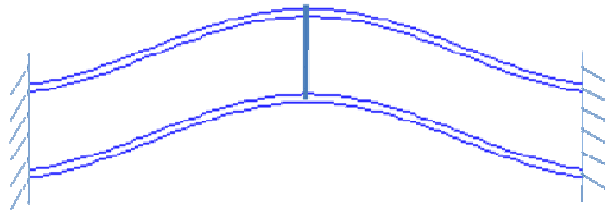
Figure 3-6: Bistable mechanism
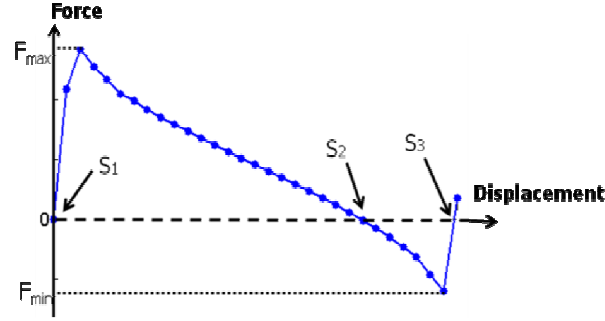
Figure 3-7: Force displacement curve

The two curved beams were designed to have uniformly distributed thickness and the top surface of the beam can be modeled as

$$w(x) = \frac{h}{2}\left[1 - \cos\left(\frac{2\pi x}{l}\right)\right] \tag{3.17}$$

where $h/2$ is the apex of the curved beam, and l is the length. The bottom surface of the beam is described as $w(x) - t$, where t is the thickness of the beam. In the application of such a MEMS bistable mechanism, the thickness commonly lies in the range of a few micro-meters, so it is extremely difficult to fabricate a uniformly thick beam. Random field may affect the reliability of the MEMS device significantly since the device responses are considerably affected by the spatial variability of the thickness.

A mathematical expression for the random field in the top surface is formulated as

$$w'(x) = \frac{h}{2}\left[k_1 - \cos\left(\frac{k_2\pi x}{l}\right)\right] \tag{3.18}$$

where $k_1 \sim Normal(1, 0.01^2)$ and $k_2 \sim Normal(2, 0.01^2)$. Figure 3-8 displays the top (w^+), bottom (w^-), and a realization of the randomly field for the top surface (w'). This example employs a moderate degree of random field, compared to the previous

44

example. Two beams in the bistable mechanism are assumed to share the same random field. One thousand sampled snapshots were used for characterizing the random field and each snapshot has one hundred measurement points evenly distributed along the length of the beam.
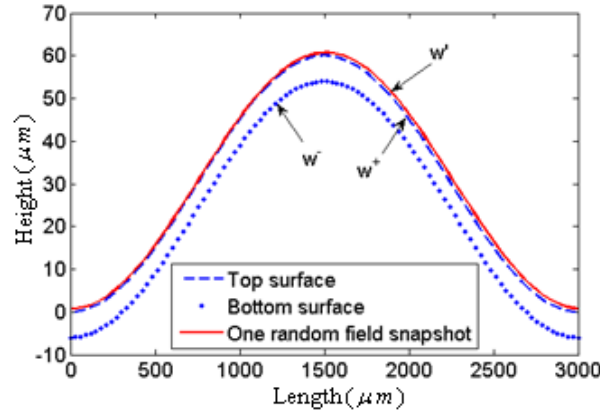
Figure 3-8: Creation of the random field for one beam

Step 1: Determination of the important signatures

An $m{\times}n$ matrix ($\boldsymbol{\theta}$) representing the random field was created to obtain the important field signatures. Using the posteriori normalized error in Eq. (3.3), the two most important signatures were selected to approximate the random field as shown in Fig. 3-9. The criterion for the normalized field characterization error is set to 0.1%. The random field in the top surface of the beam can be approximated as

$$\tilde{w}'(x) = \mu(x) + \sum_{i=1}^{2} V_i \phi_i(x) \tag{3.19}$$

Figure 3-10 shows the 1-st random field realizations in the region of $1000 \leq x \leq 2000$ [μm], which confirms the accuracy of approximate random fields with the two most important signatures. The figure contains one true and two approximate

45

realizations of the random field. The approximate realizations were built using one and two of the most important signatures. The use of the most important signature led to a normalized error of 0.29% in approximating the random realization, whereas the inclusion of the second most important signature decreased the error to 0.01%. Two random field variables (V_1 and V_2) can be thus used to describe the random field.
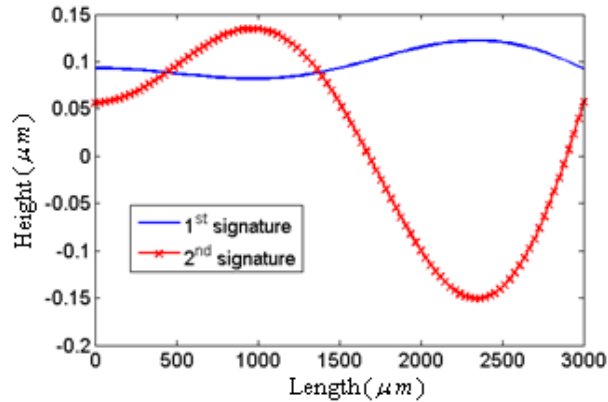
Figure 3-9: The first two normalized signatures
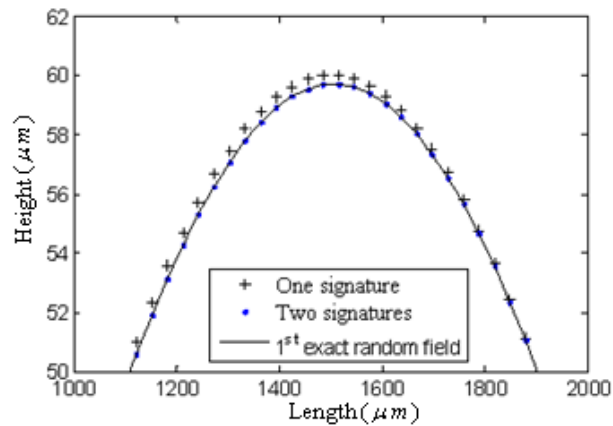
Figure 3-10: Comparison of exact and approximate random fields

(the 1-st random field realization)

Step2: Modeling random field variables and statistical dependence

One thousand random values for two random field variables (V_1 and V_2) can be generated from one thousand sampled snapshots and the histograms of two random field variables are shown in Fig. 3-11 (a) and (b). The MLE and Chi-Squae goodness-of-fit test were used to find the distributions and statistical parameters of two random field variables. Two random field variables were modeled as

$$V_1 \sim Normal(0, 4.00^2) \quad \text{and} \quad V_2 \sim Normal(0, 2.56^2)$$

The PDF and normalized histograms were compared in the figures. Unlike the 1-st example, it is found that V_1 and V_2 are statistically independent as shown in Fig. 3-11 (c).
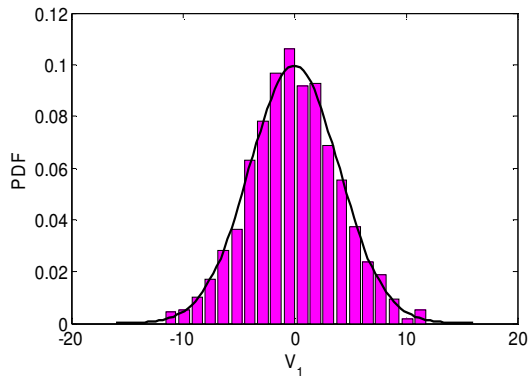
(a) Histogram and distribution for V_1 (b) Histogram and distribution for V_2
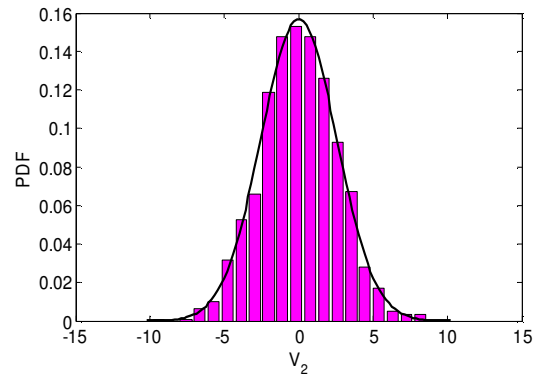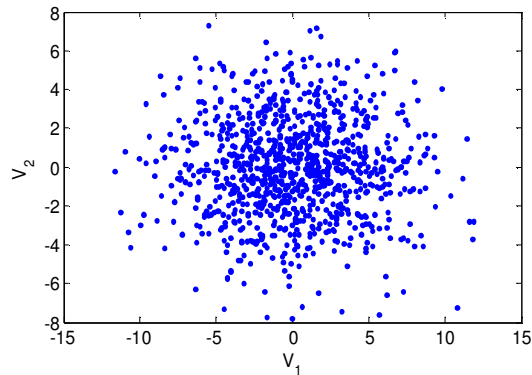
(c) Random realizations of V_1 and V_2

Figure 3-11: Statistical properties of V_1 and V_2

3.5.1.3 Beam example with a complex random field

This example employed the same cantilever beam used in Section 3.5.1.1 with different spatial variability. The top and bottom surfaces of the beam were modeled to have a symmetric random field about the mid-surface. A mathematical expression for the random field in the top surface is formulated as

$$Y = 0.1 \sum_{i=1}^{5} \left[\sin\left(\frac{K_i \pi x}{i} \right) + \sin\left(\frac{K_i \pi (L - x)}{i} \right) \right] \qquad (3.20)$$

where $K_i \sim Normal(2, 0.02^2)$; L (= 10 mm) is the length; the beam height is 2 mm at x= 0. One thousand snapshots of the random field can be constructed by generating one thousand random values of K_i. Figure 3-12 shows the 1-st, 501-st and 1000-th random field snapshots. Figure 3-13 shows the normalized error history as more significant signatures are adaptively included. The eight most important signatures are required to attain the prescribed accuracy in approximating the random field.
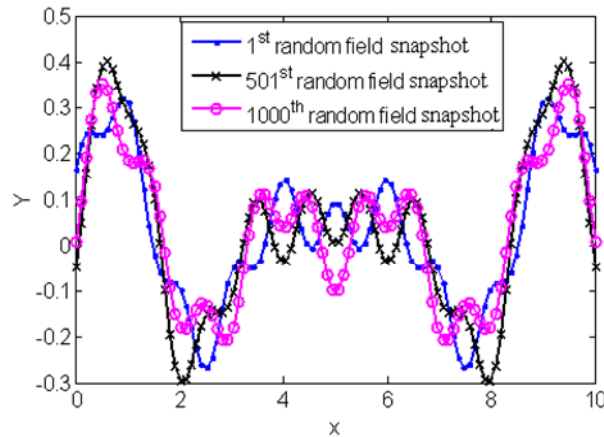
Figure 3-12: Three random field snapshots

48
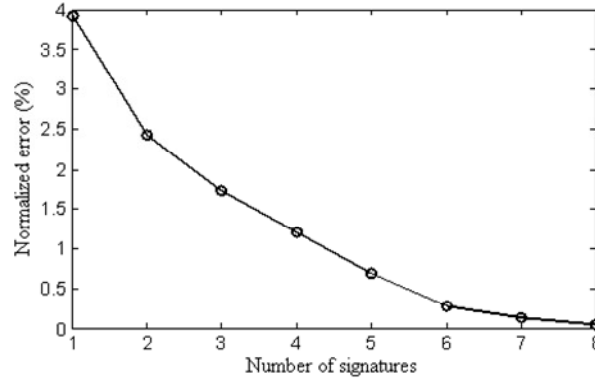
Figure 3-13: History of the normalized error

Figure 3-14 displays three approximate random fields (with one, four, and eight signatures) for the 501-st and 1000-th random field snapshot. It is apparent that the use of the eight most important signatures represents the true random field very accurately. Statistical dependences were observed for the eight random field variables. Among all statistical dependences, three statistical dependences between V_1, V_4, and V_8 are shown in Fig. 3-15.
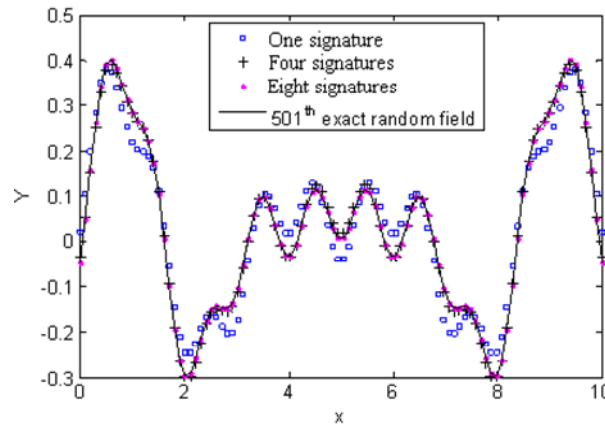
(a)
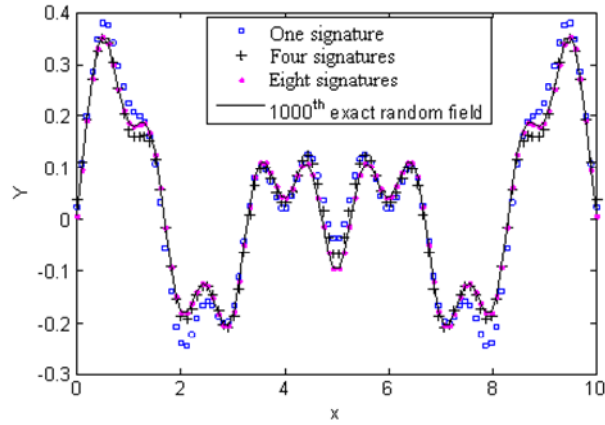
(b)

Figure 3-14: Approximation of the random field with different number of signatures
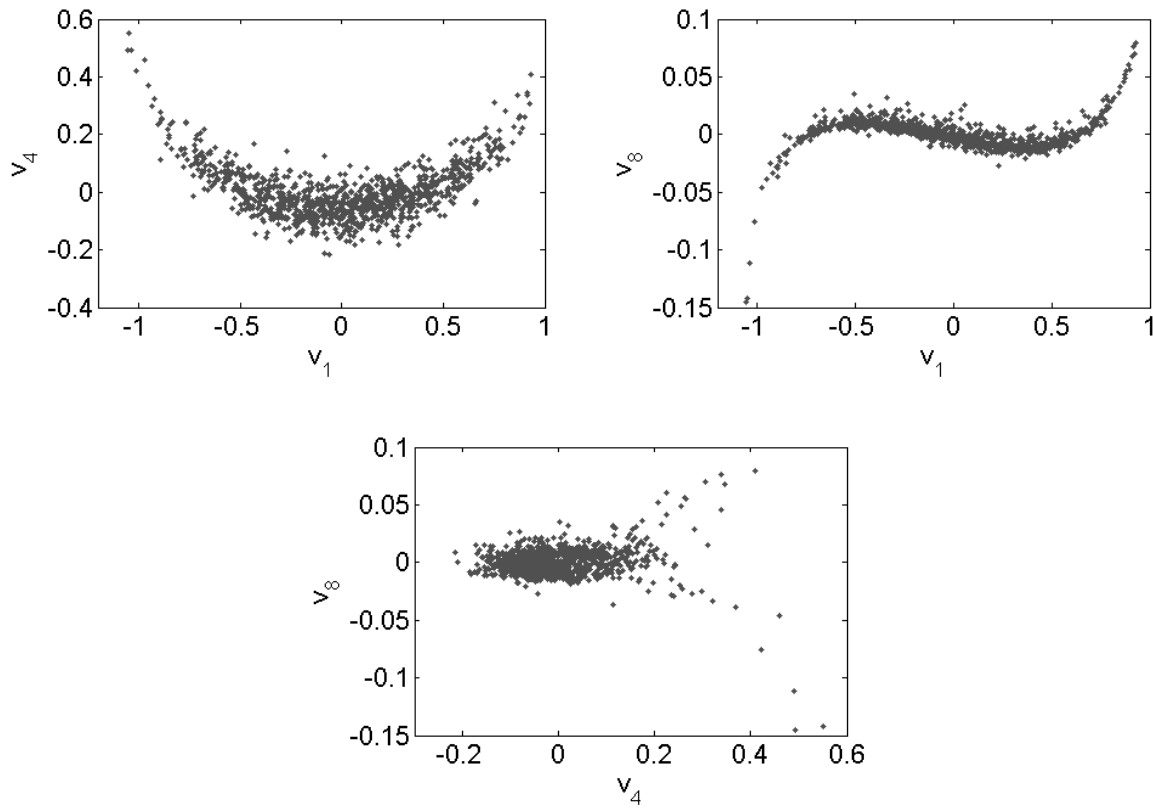
Figure 3-15: Statistical dependence of random field variables

3.5.2 Examples with insufficient data

Three examples including a structural problem, a refrigerator assembly problem, and a heat generation problem of the Lithium-ion battery are used to demonstrate the effectiveness of the proposed approach with insufficient data.

3.5.2.1 Beam example with a complex random field

This example employed the same cantilever beam used in Section 3.5.1.3. Five snapshots of the random field were constructed by generating five random values of K_i in Eq. (3.20). Figure 3-16 shows five known random field snapshots. Each snapshot consists of 100 measurement locations over the length of the beam.
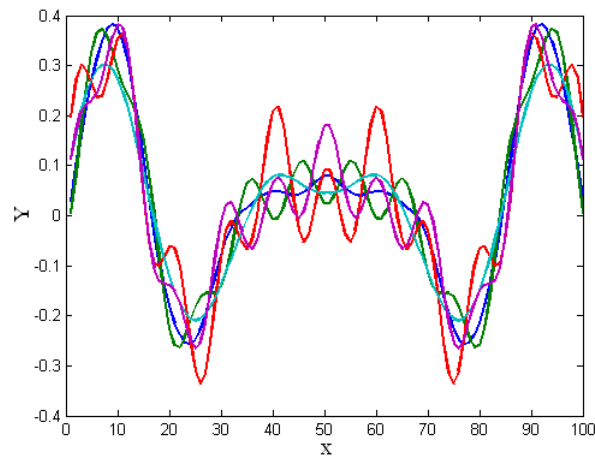
Figure 3-16: Five random field snapshots

Step 1: Random field updating using the Markov Chain Monte Carlo (MCMC) method

Assume five random field realizations at 100 measurement points are independent. Thus, the random field θ is represented by 100 independent random variables. Let the random field θ follows a 100-dimensional joint Gaussian PDF with the known standard deviation (=0.1) vector and unknown mean vector (μ). Assume

51

the mean vector ($\boldsymbol{\mu}$) follows a prior joint Gaussian PDF with the known mean (=0) and standard deviation (=0.1) vector. Based on the Bayes' theorem, the posterior distribution of the unknown mean vector ($\boldsymbol{\mu}$) given a new observation $\boldsymbol{\theta}$ can be expressed as

$$f_{\mathbf{M|\Theta}}(\boldsymbol{\mu} \mid \boldsymbol{\theta}) = \frac{f_{\boldsymbol{\Theta},\mathbf{M}}(\boldsymbol{\theta},\boldsymbol{\mu})}{f_{\boldsymbol{\Theta}}(\boldsymbol{\theta})} = \frac{f_{\boldsymbol{\Theta}|\mathbf{M}}(\boldsymbol{\theta}|\boldsymbol{\mu}) \cdot f_{\mathbf{M}}(\boldsymbol{\mu})}{f_{\boldsymbol{\Theta}}(\boldsymbol{\theta})} \qquad (3.21)$$

MCMC method with the Metropolis-Hastings algorithm was employed to draw samples from the posterior distribution of the mean vector ($\boldsymbol{\mu}$). Monte Carlo Simulation (MCS) was then used to draw 1000 snapshots of the random field $\boldsymbol{\theta}$ as shown in Fig. 3-17. It is observed that the contour of the random field well matches the five snapshots. However, the random field realizations may not be realistic as shown in Fig. 3-18 because the statistical dependence is not considered in this step.
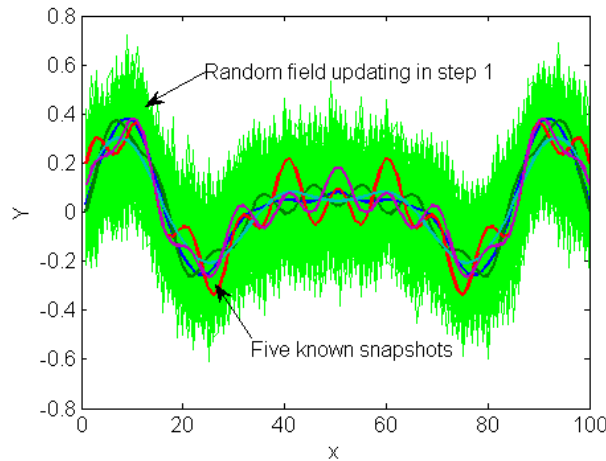
Figure 3-17: Random field updating using the MCMC method
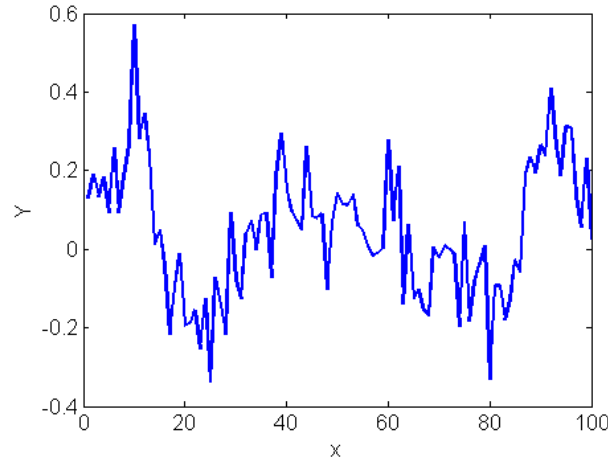
Figure 3-18: One random field realization after the random field updating

Step 2: Random field dependence modeling using the Bayesian Copula

Five procedures were conducted for the dependence modeling in this step. First, the random field realizations at each measurement location were transformed into a standard uniform space based on its marginal distribution obtained in step 1. Second, a neighboring search algorithm was employed to find the neighbors of each measurement location. In this one-dimensional example, the Euclidean distance was defined as 1 *mm*. Third, Bayesian Copula dependence modeling was performed at each measurement location with its neighbors. Four types of Copula, such as Clayton, Gaussian, Frank, and Gumbel, were employed in this study. Forth, MCS was employed to generate sufficient random field snapshots in the standard uniform space according to the dependence modeling. Fifth, the random field snapshots in the standard uniform space were transformed back to the original random space. Figure 3-19 shows the statistical dependence modeling between the random field realizations at the 1-st and 2-nd location where Gaussian Copula was selected. The contour of the modeled random field covers the actual random field as shown in Fig. 3-20. It

53

indicates that the modeled random field contains the conservativeness due to the lack

of data. Furthermore, the random field realizations become more realistic as shown in

Fig. 3-21 because the statistical dependence is considered in this step.
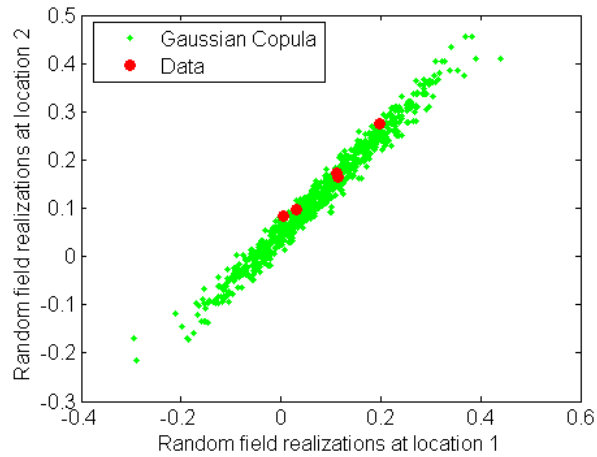
Figure 3-19: Random field dependence modeling using the Gaussian Copula
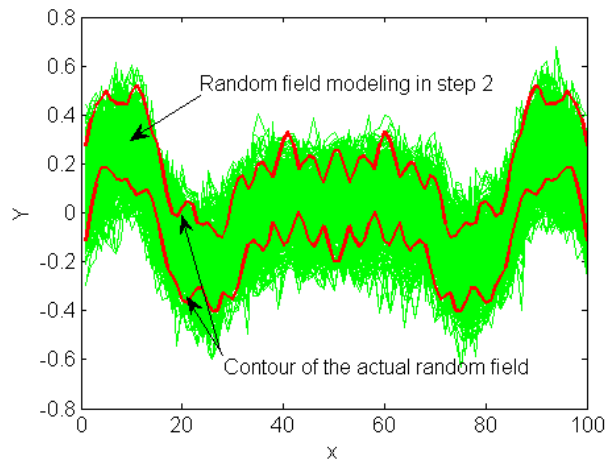
Figure 3-20: Random field modeling in step 2
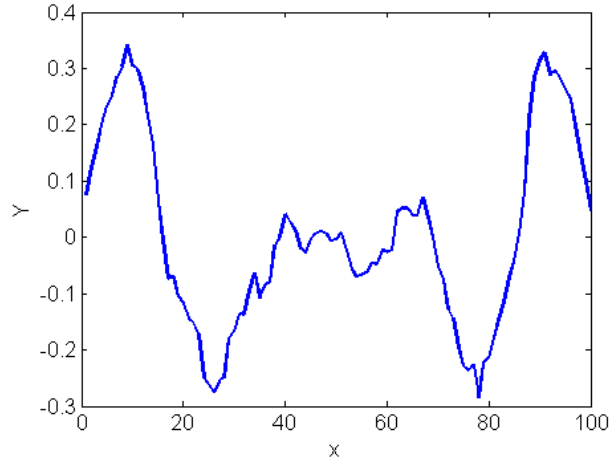
Figure 3-21: One random field realization after the dependence modeling

3.5.2.2 Door misalignment of a two-door refrigerator

As shown in Fig. 3-22, the door misalignment of a two-door refrigerator can be realized as a result of three assembly processes. The objective of this study is to statistically predict the door misalignment by sequentially analyzing field and parameter variability in three assembly processes as:

1) Insertion of the front-L to the inner case in both freezer and refrigerator sides;

2) Foaming process to increase the stiffness of the refrigerator main frame;

3) Hinge installation to the front-L.
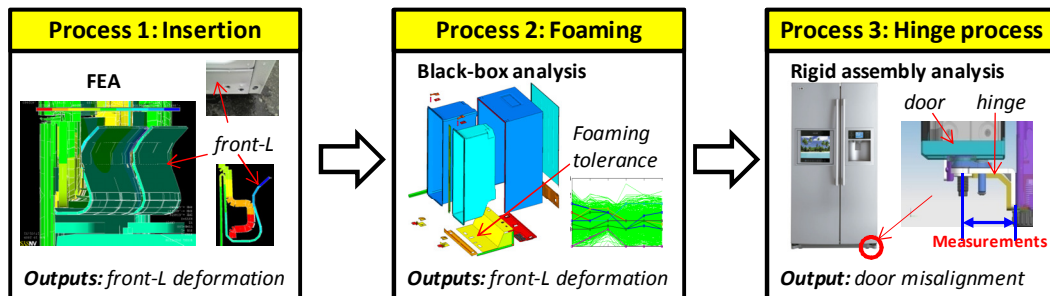
Figure 3-22: Door misalignment prediction of a two-door refrigerator

Figure 3-23 shows relevant parts (front-L, inner case, hinge, and freezer and refrigerator sides) in the assembly process. In these processes, the deformation of the front-L was represented by the random field since the deformation is not uniformly distributed over the front-L. In this example, the objective is to characterize the front-L deformation after the foaming process. The front-L deformation was modeled as two random fields based on insufficient field deformation data for both freezer and refrigerator sides. Figure 3-24 presents nine known random field snapshots where each snapshot consists of six measurement locations.
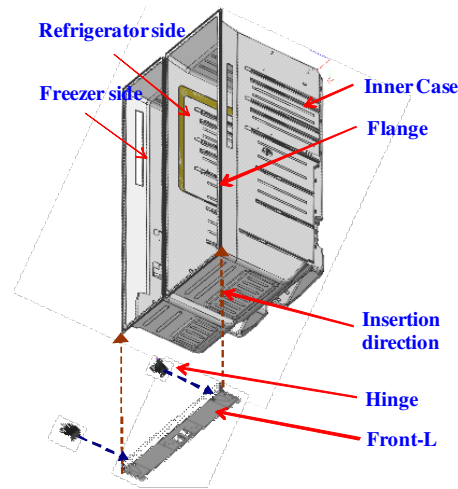
Figure 3-23: Main parts in a two-door refrigerator assembly process

Step 1: Random field updating using the MCMC method

Assume nine random field realizations at six measurement points are independent. Thus, the random field θ is represented by six independent random variables. Let the random field θ follows a six-dimensional joint Gaussian PDF with the known standard deviation (=0.3) vector and unknown mean vector (μ). Assume

the mean vector (μ) follows a prior joint Gaussian PDF with the known mean (=1) and standard deviation (=0.3) vector.

(a)   (b)

(c)
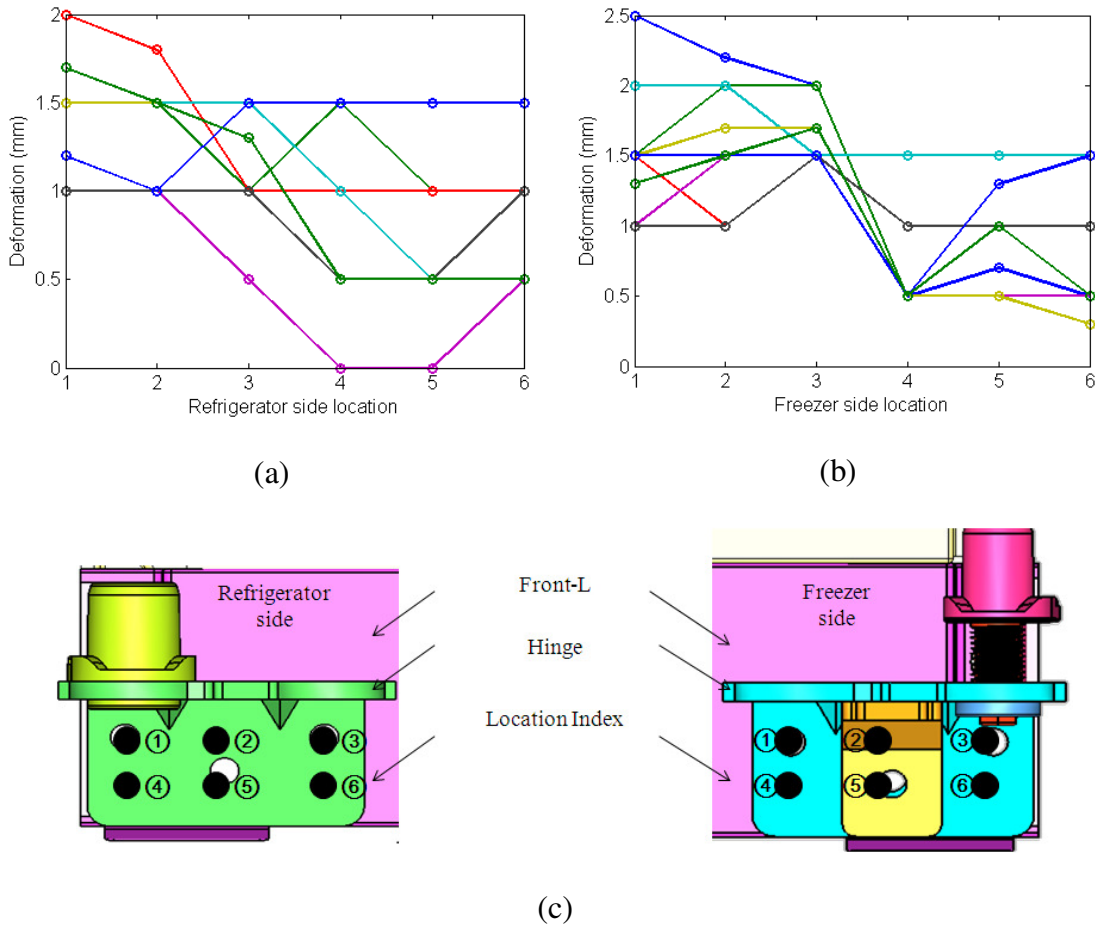
Figure 3-24: Random field snapshots of both freezer and refrigerator sides

MCMC method with the Metropolis-Hastings algorithm was employed to draw samples from the posterior distribution of the mean vector (μ). MCS was then used to draw 1000 snapshots of the random field θ as shown in Fig. 3-25. It is observed that the contour of the random field well matches the nine snapshots. However, random field realizations may not be realistic because the statistical dependence is not considered in this step.
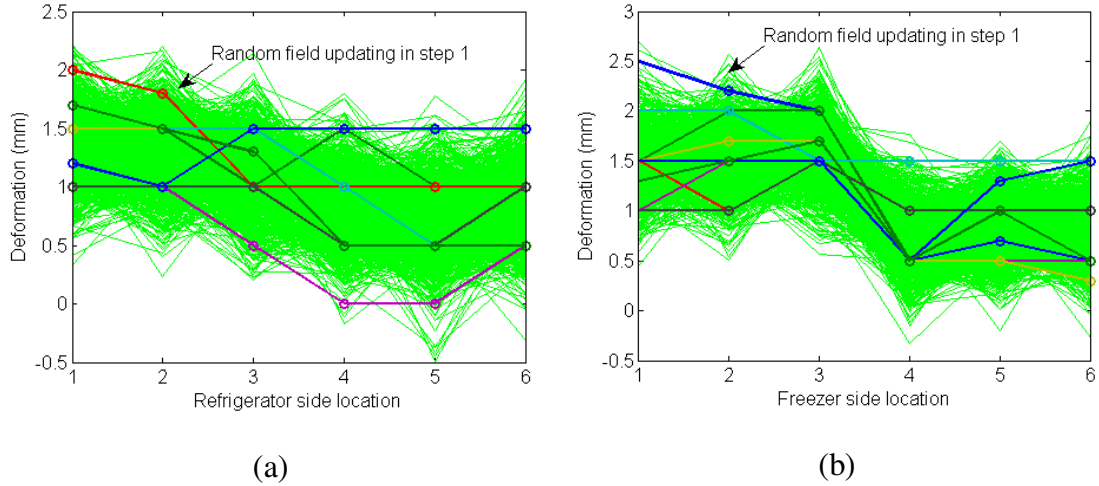
Figure 3-25: Random field updating using the MCMC method

Step 2: Random field dependence modeling using the Bayesian Copula

Five procedures were conducted for the dependence modeling in this step. First, random field realizations at each measurement location were transformed into a standard uniform space based on its marginal distribution obtained in step 1. Second, a neighboring search algorithm was employed to find neighbors of each measurement location as shown in Table 3-1. Third, Bayesian Copula dependence modeling was performed at each measurement location with its neighbors. Four types of Copula, such as Clayton, Gaussian, Frank, and Gumbel, were employed in this study. Forth, MCS was employed to generate sufficient random field snapshots in the standard uniform space according to the dependence modeling. Fifth, the random field snapshots in the standard uniform space were transformed back to the original random space. Figure 3-26 shows the statistical dependence modeling between the random field realizations at the 1-st and 2-nd location, and the 3-rd and 4-th location. The statistical dependence is observed between the 1-st and 2-nd location because

58

they are close to each other in the geometrical space, whereas this is not applicable for the 3-rd and 4-th location. Figure 3-27 presents 1000 snapshots of the random field θ after the statistical dependence modeling.

Table 3-1: Neighbor list at each measurement location

Location	Neighbors
1	2, 4
2	1, 3, 5
3	2, 6
4	1, 5
5	2, 4, 6
6	3, 5

(a)   (b)
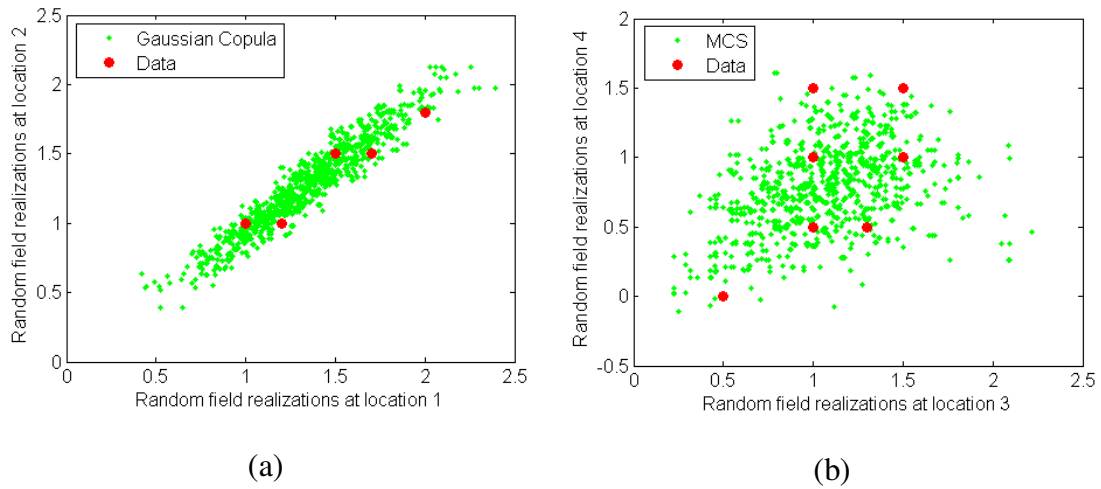
Figure 3-26: Random field dependence modeling using the Copula

59
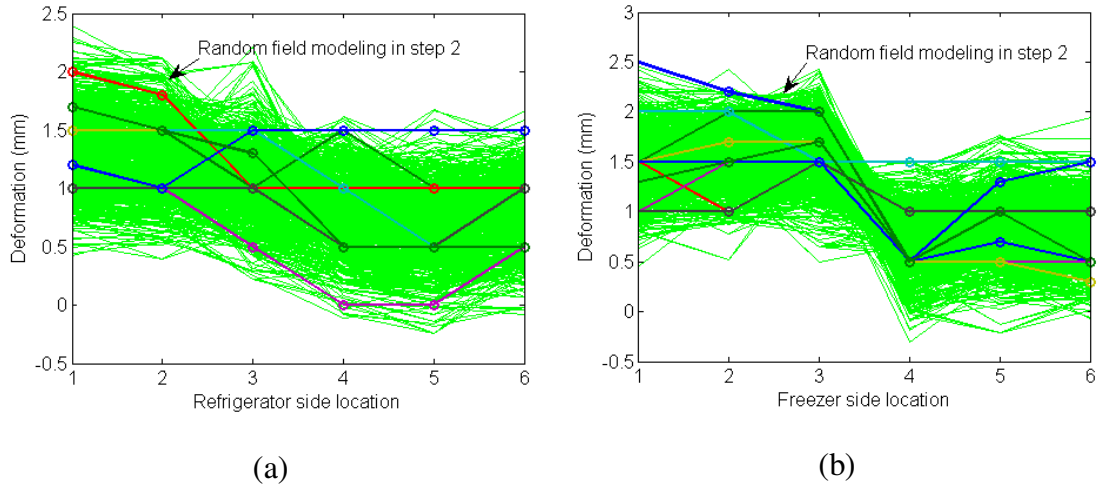
Figure 3-27: Random field modeling in step 2

3.5.2.3 Heat generation rate of Lithium-ion batteries

Lithium-ion batteries are growing in popularity for many engineering applications with several advantages such as high energy density, little memory effect, and low self-discharge. The main disadvantage is the rare, but highly risky failure mode such as fire and explosions. In most cases, thermal runaway is the initiating failure mechanism where increased temperature causes some chemical reactions, which in turn further increase the temperature and cause more the reactions. Hence, thermal management of the Lithium-ion battery has become critical for the system design. When the Lithium-ion battery is charged or discharged at various operating conditions, heat is generated because of the inherent electrical, thermodynamic, and electrochemical impedances. Accurate characterization of the heat generation rate of the Lithium-ion battery is one of the cornerstones to build an effective thermal management platform for the system design. However, the heat generation rate is heavily uncertain over the time at a given charge or discharge rate.

60

Figure 3-28 shows ten heat generation curves obtained from ten Lithium-ion cells at a 0.5C (1.15A) discharge rate where each curve consists of 64 measurement time.
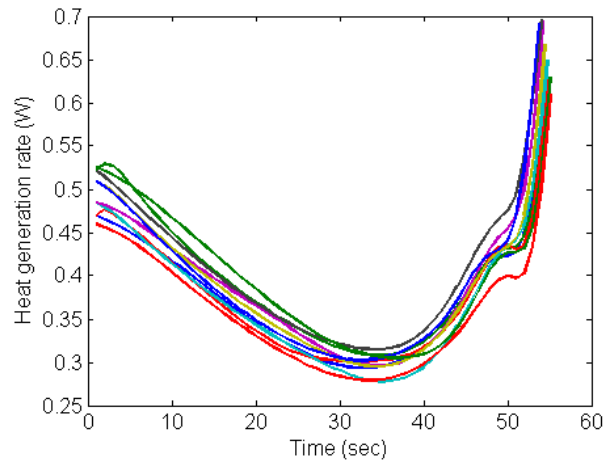
Figure 3-28: Ten curves of the heat generation rate

Step 1: Random process updating using the MCMC method

Assume ten random process realizations at 64 measurement time are independent. Thus, the random process θ is represented by 64 independent random variables. Let the random process θ follows a 64-dimensional joint Gaussian PDF with the known standard deviation (=0.02) vector and unknown mean vector (μ). Assume the mean vector (μ) follows a prior joint Gaussian PDF with the known mean (=0.5) and standard deviation (=0.02) vector.

MCMC method with the Metropolis-Hastings algorithm was employed to draw samples from the posterior distribution of the mean vector (μ). MCS was then used to draw 1000 snapshots of the random process θ as shown in Fig. 3-29. It is observed that the contour of the random process well matches the ten snapshots. However, the

61

random process realizations may not be realistic as shown in Fig. 3-30 because the statistical dependence is not considered in this step.
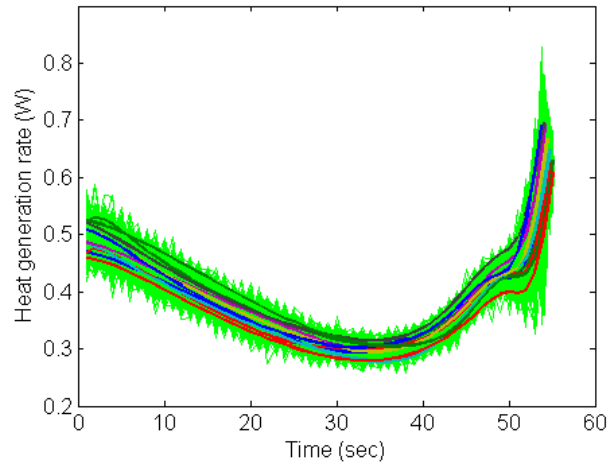
Figure 3-29: Random process updating using the MCMC method
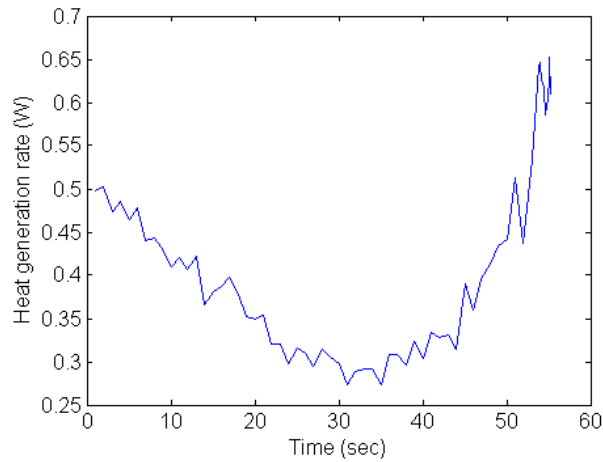
Figure 3-30: One random process realization after the random process updating

Step 2: Random process dependence modeling using the Bayesian Copula

Five procedures were conducted for the dependence modeling in this step. First, the random process realizations at each measurement time were transformed into a standard uniform space based on its marginal distribution obtained in step 1. Second,

a neighboring search algorithm was employed to find the neighbors of each measurement time. In this example, the realizations of the heat generate rate at the (k+1)-th time step is only depends upon the realizations at the *k*-th time step. Third, Bayesian Copula dependence modeling was sequentially performed at each measurement time. Four types of Copula, such as Clayton, Gaussian, Frank, and Gumbel, were employed in this study. Forth, MCS was employed to generate sufficient random process snapshots in the standard uniform space according to the dependence modeling. Fifth, the random process snapshots in the standard uniform space were transformed back to the original random space. Figure 3-31 presents 1000 snapshots of the random process θ after the statistical dependence modeling. The random process realizations become more realistic as shown in Fig. 3-32 because the statistical dependence is considered in this step.
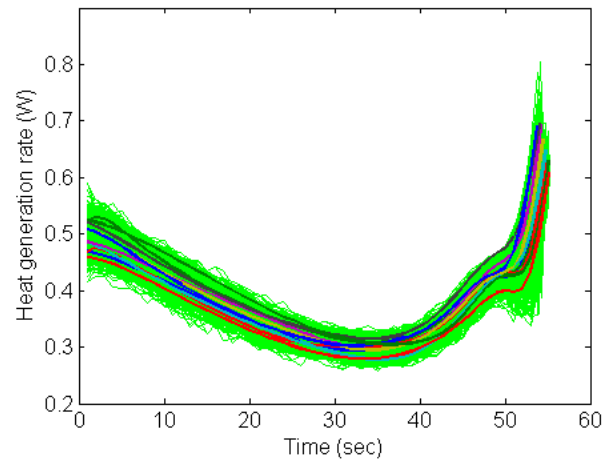
Figure 3-31: Random process modeling in step 2
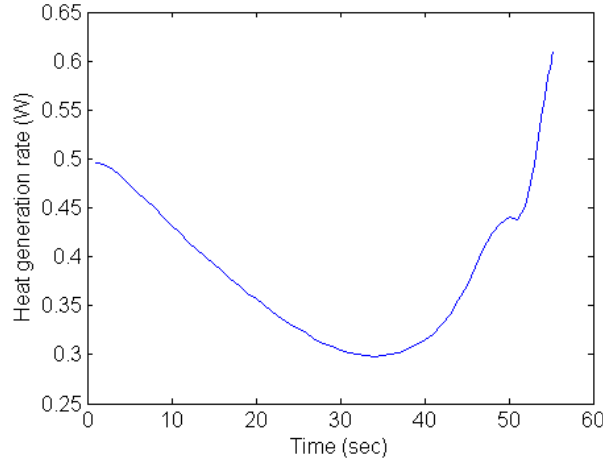
Figure 3-32: One random process realization after the dependence modeling

3.6 Summary

So far, spatial variability (or the random field) has been generally overlooked in most engineering probability analysis and design. The reason could be in part a lack of an effective approach for random field characterization in probability analysis and design, misconception of minor influence of the random field on the system response, or both. Hence, the random parameter approach (RPA) has been popular in engineering probability analysis and design by simply modeling manufacturing variability without its spatial randomness.

This chapter proposed a generic and robust random field characterization method, which can characterize any geometric or non-geometric random fields in engineered systems whether or not the random field can be realized with either sufficient or insufficient field data while accounting for the statistical dependence among the random field variables for probability analysis and design. The proposed approach has three technical contributions. The first contribution is the development of a

64

generic approximation scheme of the random field as a function of the most important field signatures while preserving prescribed approximation accuracy. The coefficients of the signatures can be modeled as random field variables and their statistical properties are identified using the Chi-Square goodness-of-fit test. Second, a Bayesian approach with Bayesian Copula dependence modeling is designed to characterize the random field with the lack of field data sets. Third, the Rosenblatt transformation is employed to transform the statistically dependent random field variables into statistically independent random field variables. The number of the transformation sequences exponentially increases as the number of random field variables becomes large. It was found that improper selection of a transformation sequence among many may introduce high nonlinearity into system responses, which may result in inaccuracy in probability analysis and design. Hence, this chapter proposed a novel procedure of determining an optimal sequence of the Rosenblatt transformation that introduces the least degree of nonlinearity into the system response. The proposed random field characterization can be integrated with any advanced probability analysis method, such as the Dimension Reduction (DR) method, Eigenvector Dimension Reduction (EDR) method, Polynomial Chaos Expansion (PCE) method, etc. Three structural problems including a Micro-Electro-Mechanical Systems (MEMS) bistable mechanism, one refrigerator assembly problem, and one heat generation problem of the Lithium-ion battery were used to demonstrate the effectiveness of the proposed approach. The results show that the proposed random field approach is very accurate and efficient. Moreover, it is shown that the statistical dependence in random field characterization cannot be neglected.

Chapter 4: Reliability Analysis with Both Random Parameter and Field Variables

This chapter develops a generic reliability analysis framework that requires no derivative information of system responses while taking into account both random parameter and field variables. The Eigenvector Dimension Reduction (EDR) method is proposed for the generic reliability analysis framework.

4.1 Introduction

A high-fidelity modeling has come true as computational mechanics has been sophisticated. Thus, probability analysis is of critical importance to understand random nature of physics in various engineering applications. However, a common challenge in probability analysis is a multi-dimensional integration to quantify probabilistic nature of system responses (e.g., fatigue life, corrosion, injury metrics) in various engineering applications (e.g., vehicle, airplane, electronics). Neither analytical multi-dimensional integration nor direct numerical integration is possible for large-scale engineering applications. Other than those approaches, existing approximate methods for probability analysis can be categorized into four groups: 1) sampling method; 2) expansion method; 3) the Most Probable Point (MPP)-based method; and 4) stochastic response surface method.

Recently, the Dimension Reduction (DR) method [Rabitz and Alis 1999; Rahman and Xu 2004; Xu and Rahman 2004] has been proposed and is known to be a sensitivity-free method. In the univariate DR method [Rahman and Xu 2004], it uses an additive decomposition of the responses that simplifies one multi-dimensional integration to multiple one-dimensional integrations. Generally, it can provide

accurate lower moment of system responses such as mean. However, it may produce a relatively large error for the second-order or higher moments of nonlinear system responses. Otherwise, it could be expensive with large number of numerical integration points. In the general DR method [Xu and Rahman 2004], the theoretical error of univariate DR method can be reduced by considering multi-dimensional integrations. However, the computation effort is increased exponentially. Therefore, it is hard to afford a general DR calculation in most engineering applications.

This chapter proposes the Eigenvector Dimension Reduction (EDR) method, which is an enhancement of the univariate DR method. It has three technical elements: 1) eigenvector sampling; 2) one-dimensional response approximations; and 3) a stabilized Pearson system. The $2N$+1 and $4N$+1 eigenvector sampling schemes are proposed in the EDR method to resolve correlated and asymmetric random input variables while maintaining high accuracy and efficiency for sensitivity-free probability analysis. The Stepwise Moving Least Squares (SMLS) method is proposed for response approximation. The SMLS method integrates a Moving Least Squares (MLS) method [Youn and Choi 2004b] with a stepwise regression scheme [Myers and Montgomery 1995]. The one-dimensional response approximation allows the increase of integration points without demanding additional computation. Therefore, the EDR method improves numerical accuracy in calculating the statistical moments with no extra expense other than the eigenvector samples. The stabilized Pearson system is proposed to predict the probability density function (PDF) of the responses while eliminating singular behavior of the original Pearson system.

In this chapter, the univariate DR method is first reviewed. The EDR method is then developed based on the univariate DR method with three new technical components in Section 4.2. Numerous examples demonstrate that the EDR method makes considerable improvements from the perspective of accuracy, efficiency, and stability compared with the univariate DR method and some traditional probability analysis methods in Section 4.3.

4.2 Eigenvector Dimension Reduction (EDR) method

The univariate Dimension Reduction (DR) method is enhanced by incorporating three technical components: 1) eigenvector sampling; 2) the Stepwise Moving Least Squares (SMLS) method for efficient and accurate numerical integration; and 3) a stabilized Pearson system for Probability Density Function (PDF) generation. Although the univariate DR method gives reasonably good results for probability analysis, the EDR method attempts to resolve the disadvantages of the DR method addressed in Section 4.1.

4.2.1 Univariate DR method

4.2.1.1 DR method using additive decomposition

In general, statistical moments of system responses (e.g., fatigue life, corrosion, injury metrics), $Y(\mathbf{X})$, can be calculated as

$$E\left\{Y^m(\mathbf{X})\right\} = \int_{-\infty}^{+\infty} \cdots \int_{-\infty}^{+\infty} Y^m(\mathbf{x}) \cdot f_{\mathbf{X}}(\mathbf{x}) \cdot d\mathbf{x}, \quad m = 0, 1, 2, \cdots \qquad (4.1)$$

In Eq. (4.1), a major challenge is a multi-dimensional integration over the entire random input ($\mathbf{X}$) domain. To resolve this difficulty, the univariate DR method uses an additive decomposition that converts a multi-dimensional integration in Eq. (4.1)

into multiple one-dimensional integrations. The additive decomposition, Y_a, is defined as

$$Y(X_1,...,X_N) \cong Y_a(X_1,...,X_N) = \sum_{j=1}^{N} Y(\mu_1,...,X_j,...,\mu_N) - (N-1)Y(\mu_1,...,\mu_N) \quad (4.2)$$

To validate the use of the additive decomposition, the error incurred due to its use in determining the statistical moments must be small. To accomplish this, the Taylor series expansion of the actual function, $Y(\mathbf{x})$, in Eq. (4.3) is compared to the expansion of the additive decomposition, $Y_a(\mathbf{x})$, in Eq. (4.4).

$$I[Y(\mathbf{x})] = I[Y(\mathbf{0})] + \frac{1}{2!}\sum_{i=1}^{N} \frac{\partial^2 Y}{\partial x_i^2}(\mathbf{0})I\left[x_i^2\right] + \frac{1}{4!}\sum_{i=1}^{N} \frac{\partial^4 Y}{\partial x_i^4}(\mathbf{0})I\left[x_i^4\right] +$$
$$\frac{1}{2!2!}\sum_{i<j} \frac{\partial^4 Y}{\partial x_i^2 \partial x_j^2}(\mathbf{0})I\left[x_i^2 x_j^2\right] + \cdots \quad (4.3)$$

$$I[Y_a(\mathbf{x})] = I[Y(\mathbf{0})] + \frac{1}{2!}\sum_{i=1}^{N} \frac{\partial^2 Y}{\partial x_i^2}(\mathbf{0})I\left[x_i^2\right] + \frac{1}{4!}\sum_{i=1}^{N} \frac{\partial^4 Y}{\partial x_i^4}(\mathbf{0})I\left[x_i^4\right] +$$
$$\frac{1}{6!}\sum_{i=1}^{N} \frac{\partial^6 Y}{\partial x_i^6}(\mathbf{0})I\left[x_i^6\right] \cdots \quad (4.4)$$

It can be seen in Eq. (4.5) that the largest error occurs at the fourth even-order term, producing negligible error. In fact, the error produced by the additive decomposition is less than that of a second-order Taylor expansion method for probability analysis [Rahman and Xu 2004]. The accuracy in the use of the additive decomposition is partly because the integration is being performed over a symmetric domain. This results in all of the odd-order terms in the integration to be zero.

$$I[Y(x)] - I[Y_a(x)] = \frac{1}{2!2!}\sum_{i<j} \frac{\partial^2 Y}{\partial x_i^2 \partial x_j^2} + \cdots \quad (4.5)$$

In aid of the additive decomposition, probability analysis of system responses becomes much simpler. For reliability and quality assessment, the *m*-th statistical moments for the responses are considered in Eq. (4.6) as

$$
\begin{aligned}
& E\left[Y^m(\mathbf{X})\right] \\
& \cong E\left[Y_a^m(\mathbf{X})\right] = E\left\{\left[\sum_{j=1}^{N} Y(\mu_1,...,X_j,...,\mu_N) - (N-1)\cdot Y(\mu_1,...,\mu_N)\right]^m\right\} \quad (4.6) \\
& = \int_{-\infty}^{\infty}\left[\sum_{j=1}^{N} Y(\mu_1,...,X_j,...,\mu_N) - (N-1)\cdot Y(\mu_1,...,\mu_N)\right]^m \cdot f_{X_j}(x_j)\cdot dx_j
\end{aligned}
$$

Using a binomial formula, Eq. (4.6) can be evaluated by executing one-dimensional integration recursively. In other words, uncertainty of system responses can be evaluated through multiple one-dimensional numerical integrations. So the challenge of the problem still remains how to carry out one dimensional integration effectively. Using numerical integration, one-dimensional integration will be performed with integration weights $w_{j,i}$ and points $x_{j,i}$ using Eq. (4.7).

$$
E\left[\sum_{j=1}^{N} Y^m(\mu_1,...,X_j,...,\mu_N)\right] \cong \sum_{j=1}^{N}\sum_{i=1}^{n} w_{j,i}Y^m(\mu_1,...,x_{j,i},...,\mu_N) \quad (4.7)
$$

The number of integration points determines computational efficiency of the univariate DR method. In general, the univariate DR method uses $(n-1)\times N+1$ integration points where N is the number of input random parameters and n is the integration points along each random variable. It is suggested in the proposed EDR method that n must be maintained at 3 or, at most, 5, for large-scale engineering design problems.

4.2.1.2 One-dimensional numerical integration in the DR method

The DR method suggests the use of a moment-based quadrature rule to perform the one-dimensional numerical integration in Eq. (4.6). Integration points and weights can be obtained by solving a linear system equation that requires the statistical information of the input parameters. The linear relationship is made between low- and high-order moments of the random input variables, as shown in Eq. (4.8).

$$
\begin{bmatrix}
\mu_{j,n-1} & -\mu_{j,n-2} & \mu_{j,n-3} & \cdots & (-1)^{n-1}\mu_{j,0} \\
\mu_{j,n} & -\mu_{j,n-1} & \mu_{j,n-2} & \cdots & (-1)^{n-1}\mu_{j,1} \\
\mu_{j,n+1} & -\mu_{j,n} & \mu_{j,n-1} & \cdots & (-1)^{n-1}\mu_{j,2} \\
\vdots & \vdots & \vdots & \vdots & \vdots \\
\mu_{j,2n-2} & -\mu_{j,2n-3} & \mu_{j,2n-4} & \cdots & (-1)^{n-1}\mu_{j,n-1}
\end{bmatrix}
\begin{bmatrix}
r_{j,1} \\ r_{j,2} \\ r_{j,3} \\ \vdots \\ r_{j,n}
\end{bmatrix}
=
\begin{bmatrix}
\mu_{j,n} \\ \mu_{j,n+1} \\ \mu_{j,n+2} \\ \vdots \\ \mu_{j,2n-1}
\end{bmatrix}
\tag{4.8}
$$

Here, $\mu_{j,n}$ represents the n-th raw moment considering the j-th input variable and r is a moment vector. The solution of Eq. (4.8) can be manipulated to produce the resulting integration points and the weights.

4.2.1.3 Remarks on the DR method

A different statistical moment formula from Eq. (4.6) was developed in the DR paper [Xu and Rahman 2004] by replacing Y^m with Z, expressed as

$$
\begin{aligned}
E_Z\left[Y^m(X)\right] &= E[Z] \\
&= E_Z\left[\sum_{j=1}^{N} Z(\mu_1,...,X_j,...,\mu_N) - (N-1)\cdot Z(\mu_1,...,\mu_N)\right] \\
&= E_Z\left[\sum_{j=1}^{N} Y^m(\mu_1,...,X_j,...,\mu_N) - (N-1)\cdot Y^m(\mu_1,...,\mu_N)\right]
\end{aligned}
\tag{4.9}
$$

Thus, it may eliminate a complicated process using a binomial formula. But it is found that this formula could lead to larger error due to the replacement of the power

term before the additive decomposition. For example, when $m = 2$, Eq. (4.6) gives the following formula as

$$E\left[Y^2(X)\right] = E\left[\sum_{j=1}^{N} Y^2(\mu_1, ..., X_j, ..., \mu_N)\right] + (N-1)^2 Y^2(\mu_1, ..., \mu_N)$$
$$-2(N-1)Y(\mu_1, ..., \mu_N)E\left[\sum_{j=1}^{N} Y(\mu_1, ..., X_j, ..., \mu_N)\right] \tag{4.10}$$

However, Eq. (4.9) proposed for simplicity gives the different formula as

$$E_Z\left[Y^2(X)\right] = E_Z\left[\sum_{j=1}^{N} Y^2(\mu_1, ..., X_j, ..., \mu_N)\right] - (N-1) \cdot Y^2(\mu_1, ..., \mu_N) \tag{4.11}$$

A distinctive difference is found between two formulae as

$$E\left[Y^2(X)\right] - E_Z\left[Y^2(X)\right] = (N^2 - N)Y^2(\mu_1, ..., \mu_N)$$
$$-2(N-1)Y(\mu_1, ..., \mu_N)E\left[\sum_{j=1}^{N} Y(\mu_1, ..., X_j, ..., \mu_N)\right] \tag{4.12}$$

where the difference is an additional error induced by the different formulation in the reference [Xu and Rahman 2004].

4.2.2 Eigenvector sampling

With the additively decomposed function in Eq. (4.2), the challenge of probability analysis still remains how to carry out one dimensional integration efficiently and accurately. Accuracy for probability analysis can be increased as the number of integration points increases in recursive one-dimensional integration. However, the increase of integration points makes probability analysis prohibitively expensive for large-scale applications. To achieve both accuracy and efficiency in probability analysis, an eigenvector sampling scheme selects sample points along the eigenvectors of the covariance matrix (Σ) of the system input random parameters (X),

and then one dimensional response surface (Section 4.2.3) will be created using the response values at the samples. The primary reason to choose samples along the eigenvectors is because the eigenvectors and eigenvalues contain information for statistical correlation and variation.

The eigenvector sampling scheme assist finding the samples using the eigenvectors and eigenvalues of the covariance of the system input random parameters. For efficiency, the EDR method employs either two ($n=2$) or four ($n=4$) samples along each eigenvector excluding the sample at the design point, depending on nonlinearity of the system responses. For N number of random variables, the EDR method demands $2N+1$ or $4N+1$ samples. To obtain the eigenvectors and eigenvalues, an eigenvalue problem for the covariance of the system input random parameters $\mathbf{X}$ can be formulated as

$$\mathbf{\Sigma X} = \lambda \mathbf{X} \tag{4.13}$$

where $\mathbf{X}$ and λ are eigenvectors and eigenvalues of the covariance matrix, $\mathbf{\Sigma}$. The covariance matrix with the N random input variables is defined as

$$\mathbf{\Sigma} = \begin{bmatrix} \Sigma_{11} & \Sigma_{12} & \Sigma_{13} & \cdots & \Sigma_{1N} \\ \Sigma_{21} & \Sigma_{22} & \Sigma_{23} & \cdots & \Sigma_{2N} \\ \Sigma_{31} & \Sigma_{32} & \Sigma_{33} & \cdots & \Sigma_{3N} \\ \vdots & \vdots & \vdots & \ddots & \vdots \\ \Sigma_{N1} & \Sigma_{N2} & \Sigma_{N3} & \cdots & \Sigma_{NN} \end{bmatrix} = \begin{bmatrix} \sigma_1^2 & \Sigma_{12} & \Sigma_{13} & \cdots & \Sigma_{1N} \\ \Sigma_{21} & \sigma_2^2 & \Sigma_{23} & \cdots & \Sigma_{2N} \\ \Sigma_{31} & \Sigma_{32} & \sigma_3^2 & \cdots & \Sigma_{3N} \\ \vdots & \vdots & \vdots & \ddots & \vdots \\ \Sigma_{N1} & \Sigma_{N2} & \Sigma_{N3} & \cdots & \sigma_N^2 \end{bmatrix}$$

where the covariance between the input variables X_i and X_j can be defined as

$$\mathrm{Cov}(X_i, X_j) = \Sigma_{ij} = \mathrm{E}[(X_i - \mu_i)(X_j - \mu_j)]$$

and μ_i and μ_j are the means of X_i and X_j. According to the definition, the covariance is symmetric with $\Sigma_{ij} = \Sigma_{ji}$ and σ_i^2 is the variance of any random variable X_i.

Depending on the random properties of system inputs, four different types of the random properties can be defined as: (a) uncorrelated and symmetric, (b) correlated and symmetric, (c) uncorrelated and asymmetric, and (d) correlated and asymmetric. The 2N+1 eigenvector sampling scheme is first considered here. For any circumstance, the 2N+1 eigenvector samples will be found at

$$^1\mathbf{V}_i = \boldsymbol{\mu} - k\sqrt{\lambda_i}\mathbf{X}_i' \text{ and } ^2\mathbf{V}_i = \boldsymbol{\mu} + k\sqrt{\lambda_i}\mathbf{X}_i' \qquad (4.14)$$

where $\mathbf{X}_i'$ and λ_i are the i-th eigenvector and eigenvalue, and k determines a sample location along the eigenvectors. The locations of the eigenvector samples dictate accuracy of one-dimensional response approximations. Subsequently, accuracies of one-dimensional response approximations determine accuracy of one-dimensional numerical integrations and, eventually, probability analysis in the EDR method.

If the k is too large, accuracy of one-dimensional response approximations will be degraded on the inner side of two eigenvector samples $^1\mathbf{V}_i$ and $^2\mathbf{V}_i$; on the other hand, if k is too small, accuracy of the response approximations will be descended on the outer side of eigenvector samples because of an extrapolation. Since the response approximation is involved, it is nearly impossible to determine the optimum location (k) of the eigenvector samples with a reasonable justification. Thus, a parametric study is performed by using a set of mathematical examples and two facts are observed: (1) the accuracy of the EDR appears to be the best with k = [2.5 ~ 3.5]; (2) the accuracy is nearly insensitive with any k value in the range. So, this study uses k=3 for eigenvector sampling. For the different types of the system input random properties, the eigenvector samples are found as follows:

a. Uncorrelated and symmetric

If all random variables are statistically uncorrelated, all off-diagonal terms in the covariance matrix become zero. In this case, the eigenvectors are simply the original random variable axes. The eigenvector samples are obtained along the original random vectors at $^1\mathbf{V}_i = \boldsymbol{\mu} - 3\sqrt{\lambda_i}\mathbf{X}_i' = \boldsymbol{\mu} - 3\sigma_i\mathbf{X}_i'$ and $^2\mathbf{V}_i = \boldsymbol{\mu} + 3\sqrt{\lambda_i}\mathbf{X}_i' = \boldsymbol{\mu} + 3\sigma_i\mathbf{X}_i'$, where $\mathbf{X}_i'$ is the i-th eigenvector where all elements are zero except the i-th element is one.

b. Correlated and symmetric

If some random variables are statistically correlated, the eigenvector samples are obtained at $^1\mathbf{V}_i = \boldsymbol{\mu} - 3\sqrt{\lambda_i}\mathbf{X}_i'$ and $^2\mathbf{V}_i = \boldsymbol{\mu} + 3\sqrt{\lambda_i}\mathbf{X}_i'$ along the eigenvectors of the eigenvalue problem in Eq. (4.13).

c. Uncorrelated and asymmetric

If all random variables are statistically uncorrelated but asymmetrically distributed, the eigenvectors are still same as the original random variable axes. To facilitate the eigenvector sampling for asymmetrically distributed random input parameters, the random parameters are transformed into a standard-normally distributed random parameter (U), such as T: $\mathbf{X}_i \rightarrow \mathbf{U}_i$ []. The eigenvector samples are similarly obtained along the eigenvectors in the transformed space at $^1\mathbf{U}_i = -3\mathbf{U}_i'$ and $^2\mathbf{U}_i = +3\mathbf{U}_i'$, where $\mathbf{U}_i'$ is the i-th eigenvector where all elements are zero except the i-th element is one. Then, two eigenvector samples $^1\mathbf{V}_i$ and $^2\mathbf{V}_i$ will be found from $^1\mathbf{U}_i$ and $^2\mathbf{U}_i$ through the inverse transformation, T^{-1}.

d. Correlated and asymmetric

If some random variables are both correlated and with asymmetric distributions, the eigenvectors of the covariance matrix of the system input random parameters must be first obtained, as illustrated in the part b. For the random variables with correlated and asymmetric distributions, the eigenvector samples will be chosen along the eigenvectors through the transformation given in the part c.

The $2N+1$ eigenvector samples are illustrated for the four different cases shown in Fig. 4-1 and the samples are used for constructing one-dimensional response approximation using the SMLS method in the following section. To enhance numerical accuracy in probability analysis, the $4N+1$ eigenvector samples will be selected with two extra samples located at $^{3}\mathbf{V}_{i} = \boldsymbol{\mu} - 1.5\sqrt{\lambda_{i}}\mathbf{X}_{i}^{'}$ and $^{4}\mathbf{V}_{i} = \boldsymbol{\mu} + 1.5\sqrt{\lambda_{i}}\mathbf{X}_{i}^{'}$.

4.2.3 SMLS for numerical integration

The moving least square (MLS) method is improved by a stepwise selection of basis functions, referred to as the SMLS method. The optimal set of basis terms is adaptively chosen to maximize numerical accuracy by screening the importance of basis terms. This technique is exploited for approximating the additively decomposed one-dimensional integrand in Eq. (4.6). The idea of a stepwise selection of basis functions comes from the stepwise regression method [Myers and Montgomery 1995]. The SMLS method for one-dimensional response approximation proceeds in the following steps:
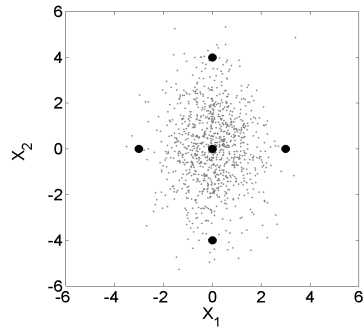
(a) uncorrelated and symmetric
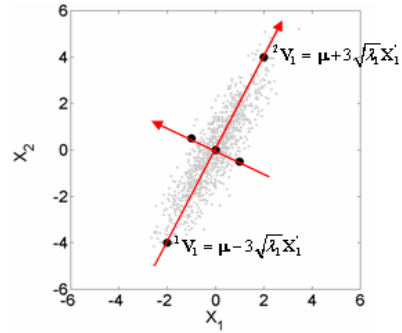
(b) correlated and symmetric
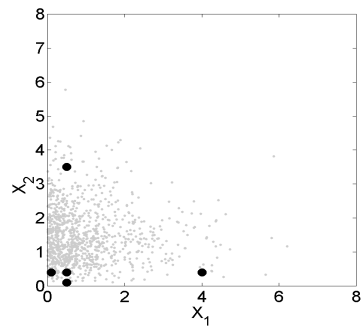
(c) uncorrelated and asymmetric
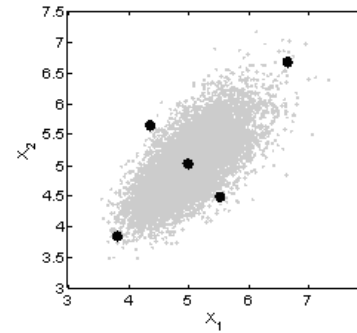
(d) correlated and asymmetric

Figure 4-1: Eigenvector samples for EDR method

STEP 1. Define a pool of basis elements and forced basis elements out of the pool. Set the total number of basis elements, nb, and sub-domain counter, m=0.

STEP 2. Define the m-th sub-domain surrounded by nb neighboring samples.

STEP 3. Find nt training points in all sub-domains, where training points are defined in the middle of every two samples.

STEP 4.   Approximate responses at training points using the MLS method as

$$\hat{\mathbf{Y}}(\mathbf{d}) = \mathbf{h}^T(\mathbf{d})\mathbf{M}^{-1}(\mathbf{d})\mathbf{B}(\mathbf{d})\mathbf{Y}, \text{ where } \mathbf{M} = \mathbf{H}^T\mathbf{W}(\mathbf{d})\mathbf{H}, \ \mathbf{B} = \mathbf{H}^T\mathbf{W}(\mathbf{d}),$$

where $\mathbf{W}$ is the weight matrix and $\mathbf{H}$ is the basis matrix.

STEP 5.   Filter the basis elements adaptively in the m-th subdomains by ranking the magnitudes of the coefficients. The basis element with the maximum coefficient will be selected and add to the forced basis elements as the current basis elements. This process will be repeated until the total number of required basis elements (nb) is reached.

STEP 6.   Set $m = m + 1$ and go to STEP 2 if $m \leq ns$ where ns is the total number of subdomains. Otherwise go to STEP 7.

STEP 7.   Construct one-dimensional response surface using sample responses.

Example of SMLS Method

Since the objective is to approximate one-dimensional response accurately, a highly nonlinear one-dimensional response example is used to show accuracy of the SMLS. For the purpose of the EDR method, the response would be treated as the integrand used in the EDR method. The exact response is explicitly expressed as

$$Y(X) = X^2(2 + \sin(2X))/4, \quad 1 \leq X \leq 7 \tag{4.15}$$

Six subdomains (m=6) are defined and six training points ($nt = 6$) are used. Seven basis terms ($nb = 7$) are used where two (1 and X) are the forced basis terms. Including the forced basis terms, the pool of basis terms are {1, X, X^2, X^3, X^4, X^5, X^6, X^7, $\sin X$, $\cos X$, $\exp(X)$}. In addition to the ordinary polynomial basis, the sinusoidal

and exponential basis terms are used because they are good for nonlinear representation. For example, at $X = 4$ the selected basis terms are [1, X, sin$X$, cos$X$, X^2, X^3, X^4] with the corresponding coefficients [-124.2285, 617.9624, -151.2387, -97.4442, -382.9456, 74.3153, -4.4639]. As shown in Fig. 4-2, the SMLS method approximates the response very accurately in aid of the adaptive selection of basis elements in different subdomains. In Table 4-1, the normalized error is measured as

$$e = \frac{1}{nt} \sum_{i=1}^{nt} \left(\frac{(\hat{y}_i - y_i^t)^2}{(y_i^t)^2} \right) \qquad (4.16)$$

where the total trial points, $nt = 61$. $\hat{y}_i$ and y_i^t are approximate and true responses, respectively, at the i-th trial points.
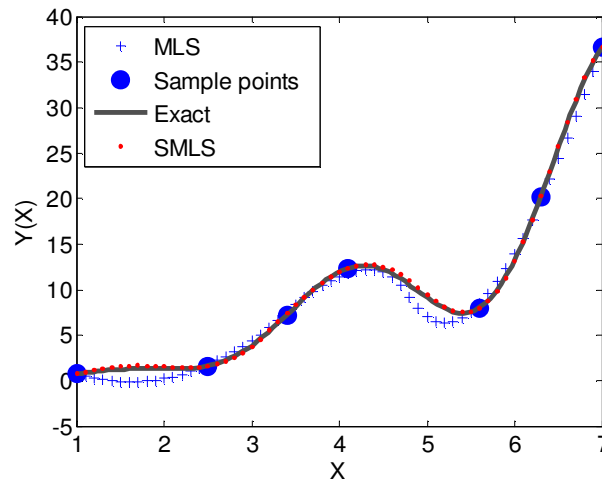
Figure 4-2: Response approximation using SMLS method

Table 4-1: Normalized Errors of the MLS and SMLS.

Method	MLS	SMLS
Normalized error	3.2200	0.0130

In general, for numerical calculation of statistical moments, the integration domain is relatively small because the contribution of PDF is negligible for $X < \mu - 6\sigma$ and $X > \mu + 6\sigma$. For some bounded random distributions, such as uniform and beta distributions, the integration domain will be limited from lower to upper bounds. Therefore, although probability analysis is applied for nonlinear system responses, they are less nonlinear in a local region than those in a global region. Thus, the SMLS method can approximate system responses very accurately in the integration domain. The SMLS method allows the increase in the number of numerical integration points without requiring actual simulations (or experiments) for system response evaluations. Responses at all integration points are approximately obtained from approximated one-dimensional responses, $\hat{Y}(x_{j,i})$, instead of system responses, $Y(x_{j,i})$ through actual system evaluations, as shown in Eq. (4.17).

$$
\begin{aligned}
E\left[\sum_{j=1}^{N} Y(\mu_1,...,X_j,...,\mu_N) \right] &\cong \sum_{j=1}^{N} \sum_{i=1}^{n} w_{j,i} Y(\mu_1,...,x_{j,i},...,\mu_N) \\
&\cong \sum_{j=1}^{N} \sum_{i=1}^{n} w_{j,i} \hat{Y}(\mu_1,...,x_{j,i},...,\mu_N)
\end{aligned}
\tag{4.17}
$$

Thus, a large number ($n = 20 \sim 30$) of integration points can be used to increase numerical accuracy in assessing statistical moments of the responses without requiring actual system evaluations. So, numerical accuracy in estimating statistical moments is improved considerably while high efficiency is remained, since only $2N+1$ or $4N+1$ simulations or experiments are required.

a. Moment based quadrature rule [Rahman and Xu 2004]

In the DR method, a moment based quadrature rule was proposed for one-dimensional numerical integration due to its good accuracy and efficiency, compared

with other integration methods. However, it may still produce a relatively large error for the second order or higher moments of nonlinear responses as will be shown in the later examples. In the EDR method, however, since large amount of integration points could be employed without actual simulations (or experiments) for system response evaluations, accuracy of moment based quadrature rule could be improved substantially. Thus, moment based quadrature rule could still be used in the EDR method. However, moment based quadrature rule could have two problems as

1) The number of integration points should be predetermined. So it is hard to decide an optimal number of the points to maximize accuracy of the EDR method for probability analysis.

2) Larger amount of integration points could result in a singular moment matrix in Eq. (4.8). So it may fail to find the corresponding integration points. Specifically, a large number of integration points require the use of higher order statistical raw moments. As the order of the moments is increased, the matrix in Eq. (4.8) becomes singular due to the higher-order moments asymptotically approaching zero.

b. Adaptive Simpson rule [Yamazaki and Shinozuka 1988]

This study suggests an adaptive Simpson rule as an alternative integration method. It gives more freedom on selection of probability distribution types for system input random variables. Adaptive Simpson's rule uses an adaptive way to estimate the error from calculating a definite integral using Simpson's rule. If the error is larger than a user specified tolerance, the integration interval is divided into subintervals and Simpson's rule is applied to each subinterval. The adaptive Simpson

rule generally demands a large number of integration points to preserve good accuracy by specifying the tolerance. The SMLS method enables the increase in the number of integration points to as many as possible with no additional computation. Unlike the DR method, the EDR method has no restriction to choose numerical integration schemes, although this study uses the adaptive Simpson rule for the one-dimension integration.

4.2.4 A stabilized Pearson system

The Pearson system [Johnson et al. 1995] can be used to construct the PDF of a random response (y) based on its first four moments (mean, standard deviation, skewness and kurtosis). The detail expression of the PDF can be achieved by solving the differential equation as

$$\frac{1}{f(y)} \frac{df(y)}{dy} = -\frac{a+y}{c_0 + c_1 y + c_2 y^2} \tag{4.18}$$

where a, c_0, c_1 and c_2 are four coefficients determined by the first four moments of the random response (y) and expressed as

$$c_0 = (4\beta_2 - 3\beta_1)(10\beta_2 - 12\beta_1 - 18)^{-1} \mu_2$$
$$a = c_1 = \sqrt{\beta_1}(\beta_2 + 3)(10\beta_2 - 12\beta_1 - 18)^{-1}\sqrt{\mu_2}$$
$$c_2 = (2\beta_2 - 3\beta_1 - 6)(10\beta_2 - 12\beta_1 - 18)^{-1}$$

where β_1 is the square of skewness (x-axis in Fig. 4-3), β_2 is the kurtosis (y-axis in Fig. 4-3), and μ_2 is the variation. The mean value is always treated as zero in the Pearson system, and later it can be shifted to the true mean value once the differential equation is solved. Basically, the differential equation can be solved based on the different assumptions of the four coefficients a, c_0, c_1, and c_2. For example, if $c_1 = c_2 = 0$, this equation can be solved with a normal distribution, which corresponds to [0, 3]

point in Fig. 4-3, and the type 1 in Pearson system corresponds to both roots of $c_0 +$ $c_1 y + c_2 y^2$ being real. For more detail information, readers can refer to the reference [Johnson et al. 1995].

Generally, there are seven distribution types in the Pearson system based on the four coefficients, and among some types, subtypes are present. Normally, PDF can be successfully constructed based on the first four moments. However, the Pearson system can fail to construct the PDF, especially when the statistical moments in the Pearson curve fall into the region that several distribution types merge, as shown in Fig. 4-3. The horizontal axis is for the square of skewness (β_1) and vertical axis is for the kurtosis (β_2). The solid dots stand for the locations having an instability problem while constructing the PDF. The trouble lies at the calculation of coefficients of a specific distribution type, which results in a numerical instability.
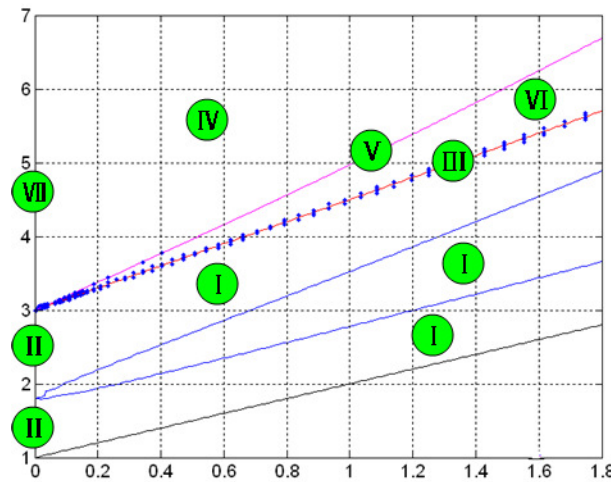
Figure 4-3: Pearson curve (*x*-axis is the square of skewness, β_1,

and *y*-axis is the kurtosis, β_2)

For the distributions (type II, III, V, VII) with an equality condition, it is rare that statistical moments meet the condition tightly. To resolve instability of the Pearson system, the condition is relaxed with a tolerance bound. In this study, 0.001 is used for the tolerance bound. For instance, the PDF should belong to type 6 based on the first four moments [−0.5491, 0.1085, −0.1573, 3.0464]. However, numerical singularity is met due to larger numbers of n_1=3273.5 and n_2= −3930.2 in type 6 as

$$f(y) = K(a_1 - y)^{n_1}(a_2 - y)^{n_2}, \qquad y < a_2$$

The Pearson system fails to calculate the coefficient, K, since $f(y)$ approaches $0 \cdot \infty$. By relaxing the tolerance bounds, type 3 can be selected, but the singularity problem still remains. Finally, a normal distribution is selected to approximate the PDF by increasing the tolerance value to 0.0118. However, as shown in Fig. 4-4, the Pearson system produces a noticeable error, compared to MCS with 1,000,000 samples.
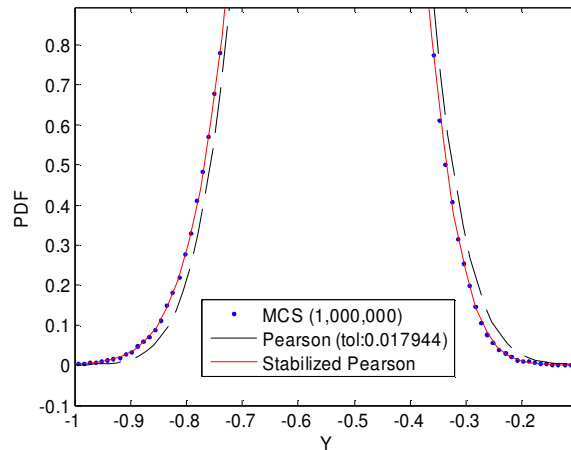
Figure 4-4: Comparison of PDF

In the EDR method, a stabilized Pearson system is proposed to avoid instability without relaxing tolerances. Two PDFs are generated by fixing the first three

84

statistical moments, and slightly increasing or decreasing the original kurtosis until two PDFs are successfully constructed. Then these two PDFs are used to approximate the PDF with original kurtosis. Suppose that the Pearson system fails to construct a PDF with the first four moments [m_1, m_2, m_3, m_4]. Detail procedures follow as

Step1: The first three moments are kept constant and gradually decrease the m_4 by a small decrement ($\Delta m_4 = 0.01$) until a PDF can be successfully constructed. $f_1(y)$ and $m_{4,1}$ are denoted as the PDF and the corresponding kurtosis value, respectively.

Step2: The first three moments are kept constant and gradually increase the m_4 by a small increment ($\Delta m_4 = 0.01$) until a PDF can be successfully constructed. $f_2(y)$ and $m_{4,2}$ are denoted as the PDF and the corresponding kurtosis value, respectively.

Step3: To build the PDF over the entire domain of the random response (y), the response domain is discretized as y_i, $i=1$ to l. At every value y_i, the PDF value, $f(y_i)$, is obtained using two hyper-PDFs $f_1(y_i)$ and $f_2(y_i)$, where they are obtained with the kurtosis $m_{4,1}$ and $m_{4,2}$, respectively. With two hyper-PDF values having the kurtosis $m_{4,1}$ and $m_{4,2}$, the PDF $f(y_i)$ with the actual kurtosis m_4 ($m_{4,1} < m_4 < m_{4,2}$) can be approximated using SMLS without a singularity. It is found that the PDF $f(y_i)$ is accurately generated because the amount of the kurtosis perturbation is relatively small.

The perturbation size ($\Delta m_4 = 0.01$) of a kurtosis is used to preserve a relatively small perturbation. Basically, the smaller the difference between $m_{4,1}$ and $m_{4,2}$, the more accurate the PDF approximation for the actual kurtosis m_4. Once the probability

distribution ($f(y)$) for system response is obtained, the distribution is explicitly given. So, reliability is computed through a numerical integration for

$$\text{Reliability} = \int_{-\infty}^{0} f(y)dy \qquad (4.19)$$

4.3 Examples and results

4.3.1 Probability analysis with random field variables

Random field approach is recommended if the randomness of statistical inputs for the engineered system can be characterized as a function of spatial variables. Three structural examples including a Micro-Electro-Mechanical Systems (MEMS) bistable mechanism are used to demonstrate the effectiveness of the proposed approach for probability analysis with random field variables.

4.3.1.1 Beam example

The same example in Section 3.5.1.1 is employed for probability analysis after the random field characterization. The cantilever beam is fixed at the right end and a concentrate force (100N) is applied at the left tip of the beam as shown in Fig. 4-5. The maximum beam deflection was considered as the system response. The beam deflection was calculated through a finite element (FE) analysis using OptiStruct in HyperMesh. Different FE models were created for different snapshots using HyperMorph in HyperMesh. Specifically, a FE basis model was first built based on the mean of the random field. HyperMorph was then used to define the perturbation vectors of the measurement points (or element nodes) based on the signatures of the random field. The signature coefficients were next defined as the perturbation coefficients of the perturbation vectors in HyperMorph. Hence, different FE models were constructed by providing the corresponding set of coefficients. The thickness of

the shell elements was set to 1 *mm*. Both probability analyses of the system response using the Random Field Approach (RFA) and Random Parameter Approach (RPA) were carried out for the purpose of comparison. For the RPA, the average height of the one hundred measurement points obtained in one sampled snapshot was treated as the uniform height over the entire beam length.
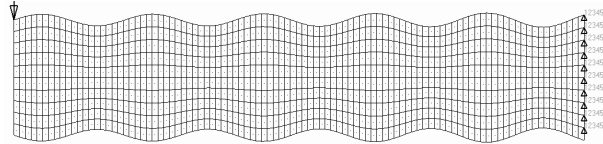
Figure 4-5: Simulation model of a cantilever beam with the random field

Probability analysis considering a random field

Probability analyses using MCS with one thousand samples were conducted using two different approaches: RFA and RPA. For RPA, the histogram of the beam height is shown in Fig. 4-6. The maximum beam deflection was considered as a system response and the histograms from two different approaches are shown in Fig. 4-7. The two approaches produced substantially different histograms because the beam with a uniform height in RPA is stiffer than the beam with a varying height in RFA. Because the RPA greatly underestimates the displacement by ignoring the spatial variation, it is very important to consider the RFA for probability analysis and design. The EDR method with $2N+1$ samples (3 analyses) was employed for RFA and the maximum beam deflection was statistically quantified in terms of the four statistical moments. Table 4-2 shows that the proposed RFA accurately estimates the four statistical moments compared with MCS. The $100(1-2\alpha)\%$ confidence intervals $[d_1, d_2]$ of the four statistical moments can be found by solving the equation of $F(m´|$

$m = d_1) = 1 - \alpha$ and $F(m' \mid m = d_2) = \alpha$, where m denotes the true statistical moment; m' is a consistent estimator of m; $F(m' \mid m)$ is the CDF of the estimator m' [Buckland 1984]. It was confirmed in Fig. 4-7 that the proposed RFA can accurately approximate the PDF of the maximum beam deflection.
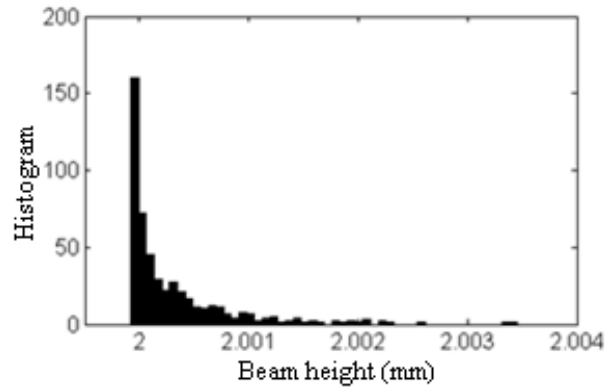
Figure 4-6: Histogram of the beam height for RPA
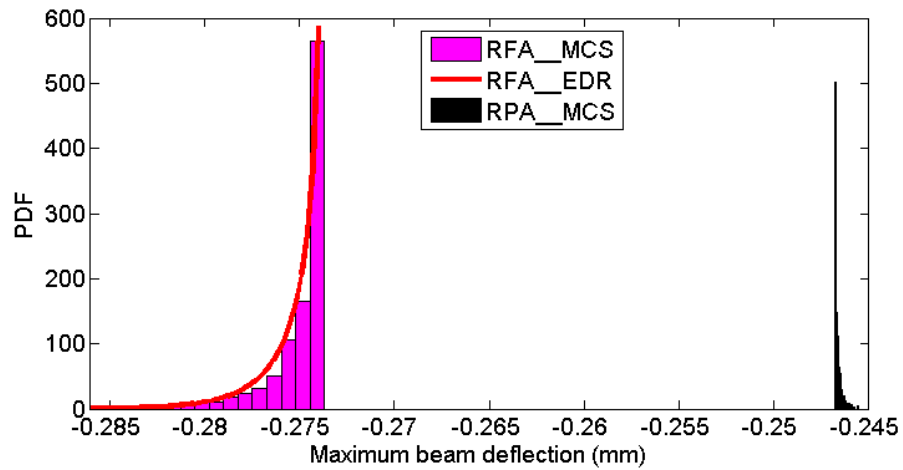
Figure 4-7: Histograms of the maximum beam deflection using RFA and RPA

Table 4-2: Statistical moments of Y using the proposed RFA and MCS

	Mean	Std	Skewness	Kurtosis	Fun. Eval.
MCS	-0.2749	0.0016	-2.4728	11.8629	1,000
RFA	-0.2749	0.0016	-2.3244	11.3535	3

4.3.1.2 MEMS bistable mechanism

The same example in Section 3.5.1.2 is employed for probability analysis after the random field characterization. The bistable mechanism was modeled with beam23 elements using 1,388 nodes and 4,148 DOFs, and the connection between two beams was modeled using a rigid element. ANSYS 10.0 was employed for the FE analysis. To achieve the force-displacement system response, nonlinear FE analyses were performed and each simulation takes about 40 seconds. The FE model information follows: the length l is 3mm; the thickness t is 6 μm; the apex value is 60 μm; the beam depth is 490 μm; Young's modulus is 169 Pa, and the gap between two beams is 90 μm.

Probability analysis considering a random field

Probability analyses using MCS with one thousand samples were conducted using two different approaches: RFA and RPA. For RPA, the histogram of variability in the beam thickness is shown in Fig. 4-8. The maximum and minimum forces, and unstable equilibrium distance were considered as system responses and the histograms from two different approaches are shown in Fig. 4-9. Even if this example engages the smaller degree of random field variability, both approaches produced substantially different histograms in three system responses. It was observed that RFA produced relatively narrower distributions for both maximum and minimum forces than RPA whereas RFA yielded wider unstable equilibrium distance than RPA. Smaller variation of the unstable equilibrium distance is better because it is robust to operate the MEMS device. Greater variability of the distance can be predicted when accounting for the random field, as shown in Fig. 4-9(c). In other words, it is
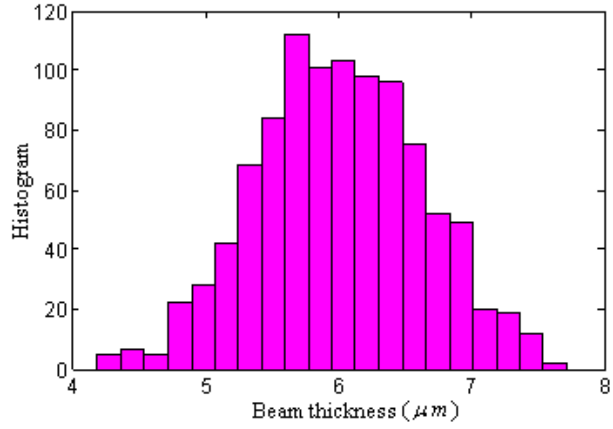
Figure 4-8: Histogram of beam thickness for RPA
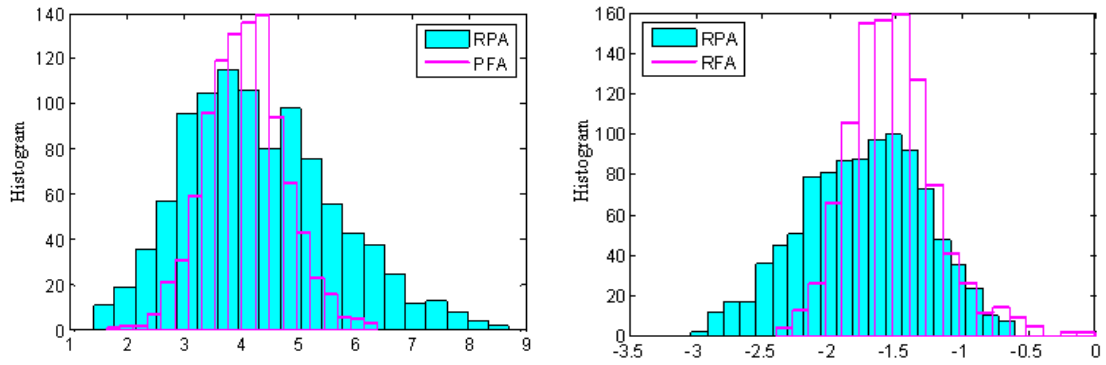
(a) Maximum force

(b)Minimum force
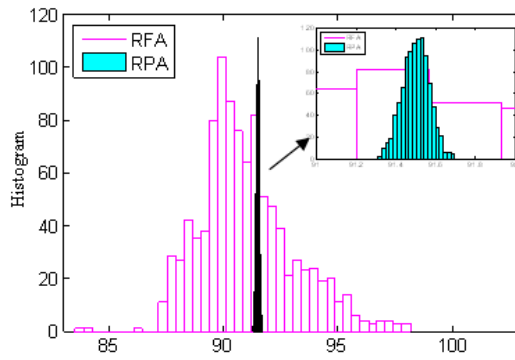
(c)Unstable equilibrium distance

Figure 4-9: Comparison of RFA and RPA

important to take into account the random field if exist. The EDR method with $2N+1$ samples (5 analyses) was employed to predict the random behavior of the system responses for RFA. Table 4-3 shows that the proposed RFA accurately estimates the four statistical moments. The accuracy comparison of the PDFs of the system responses is shown in Fig. 4-10.

Table 4-3: Statistical moments of Y using the proposed RFA and MCS

Response	Method	Mean	Std	Skewness	Kurtosis	Fun. Eval.
Maximum force	MCS	4.0986	0.6923	0.2367	3.2445	1,000
	RFA	4.1253	0.6561	0.3181	3.1545	5
Minimum force	MCS	-1.5221	0.3389	0.7759	5.6786	1,000
	RFA	-1.5617	0.3004	0.5695	5.5742	5
Unstable equilibrium	MCS	90.6885	1.6106	0.7327	5.1094	1,000
distance	RFA	91.3631	1.7723	0.5221	4.1532	5

4.3.1.3 Beam example with statistical dependence

The same example in Section 3.5.1.3 is employed for probability analysis after the random field characterization. A concentrate force ($100N$) is applied at the left tip of the beam. The system response is the maximum beam deflection. Statistical dependences were observed for eight random field variables. The optimal sequence was obtained as $[v_1, v_2, v_3, v_4, v_7, v_8, v_6, v_5]$, which presents the minimum total degree of deviation (= 0.0458) using the genetic algorithm provided in the Matlab software. Then the EDR method with a bivariate decomposition [Rabitz et al. 1999; Rabitz and Alis 1999; Xu and Rahman 2004] was used to predict the statistical properties of the maximum beam deflection for RFA. MCS with 1,000 samples was executed for a benchmarking solution. Table 4-4 shows that the proposed RFA accurately assesses

the four statistical moments compared with MCS. Figure 4-11 compares the PDFs from RFA using the EDR method and MCS. It was found that RPA produced the PDF of the maximum beam deflection which is significantly different from RFA. Figure 4-12 shows reliability errors using RFA with and without considering the statistical dependences between the eight random field variables and underscores the importance for the consideration of statistical dependence in probability analysis. The reliabilities were computed at a set of system response target values.

(a) Maximum force

(b) Minimum force

(c) Unstable equilibrium distance
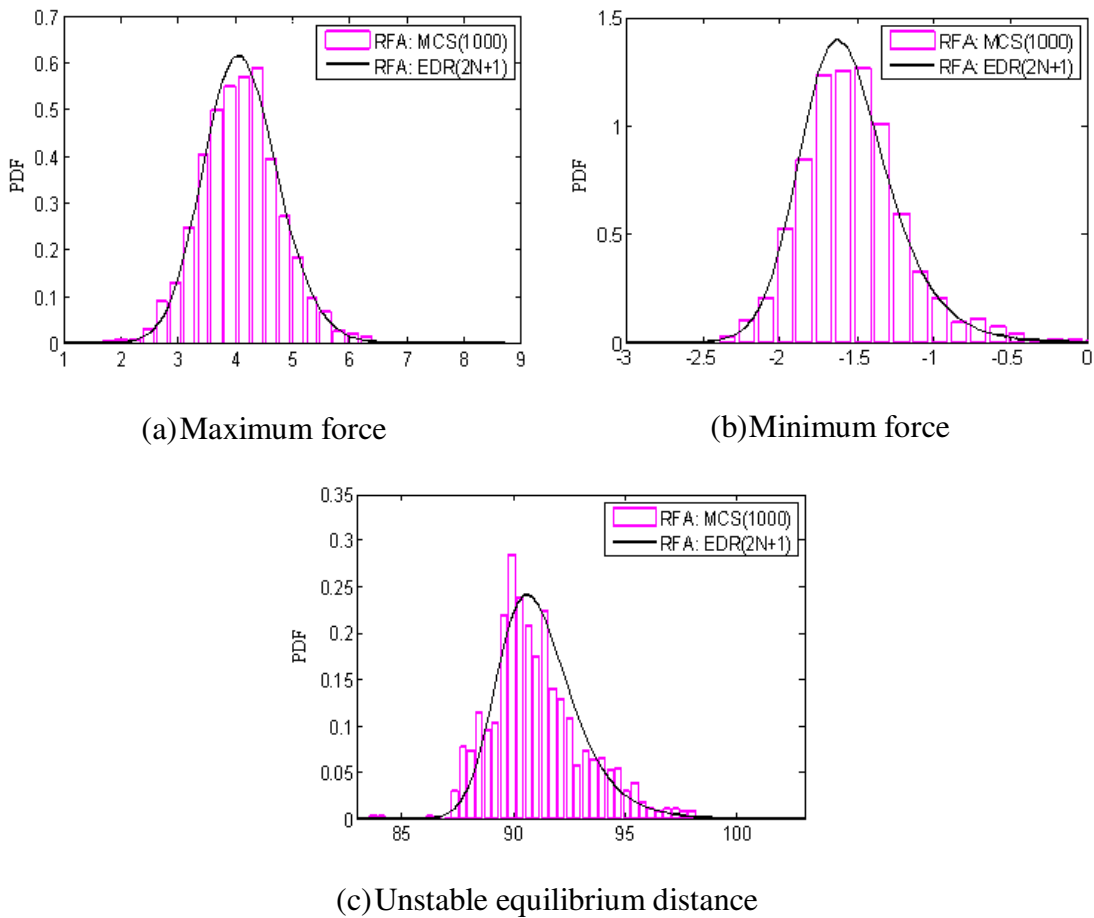
Figure 4-10: Comparison of the proposed RFA and MCS

Table 4-4: Statistical moments of *Y* using the proposed RFA and MCS

	Mean	Std	Skewness	Kurtosis	Fun. Eval.
MCS	0.3935	0.0002	0.1242	3.2262	1,000
RFA	0.3935	0.0002	0.1132	3.3143	56
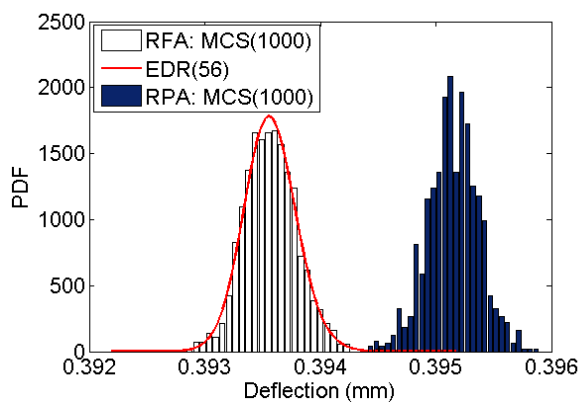
Figure 4-11: Comparison of RFA and RPA
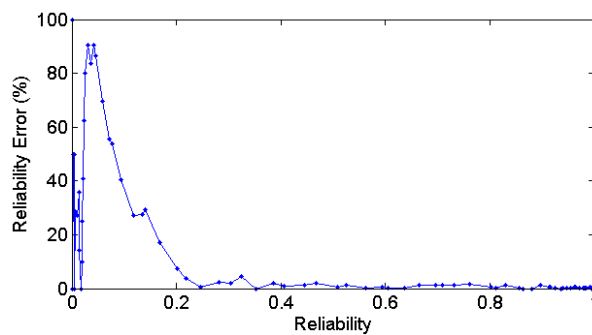
Figure 4-12: Reliability error by ignoring statistical dependence of random field

variables

4.3.2 Probability analysis with random parameter variables

Seven examples are used to show the effectiveness of the EDR method. In these examples, either 2N+1 or 4N+1 eigenvector samples are used based on the degree of response nonlinearity. A systematic selection of 2N+1 or 4N+1 is out of the scope of this study. However, it will be discussed in the future research.

4.3.2.1 Mathematical example

The following nonlinear mathematical example [Rahman and Xu 2004] is used to compare accuracy and efficiency of different probability analysis methods such as the DR method, Taylor expansion, EDR method, *etc*.

$$G = \exp\left(-\frac{1}{1+100X_1^2 + 2X_2^2 + X_1^2 X_2^2}\right) \tag{4.20}$$

where $X_j \sim Normal(0,\sigma^2)$, $j = 1, 2$ are two independent and identically normal distribution. The MCS is conducted with 100,000 samples, while the DR and EDR methods operate with 4N+1 samples (5 samples in each eigenvector direction). In addition, the DR method is performed with 6N samples (6 samples in each eigenvector direction) to illustrate the stability problem of the DR method. Additionally, the 2-nd order Taylor series and 4-th order Perturbation method (P-method) are compared. As shown in Fig. 4-13, the standard deviations of the response are displayed with different standard deviations of the inputs. The EDR method approximates the standard deviation of system response very accurately comparing with the MCS result. However, the approximated standard deviation using the DR method with 4N+1 samples is overestimated and underestimated with 6N samples when the standard deviations of the input variables increase. And the 4-th order P-method shows some degree of error in estimating the standard deviations of the

94

response except when input standard deviations are extremely small. And the 2-nd order Taylor expansion shows large error, even the input standard deviation are very small.
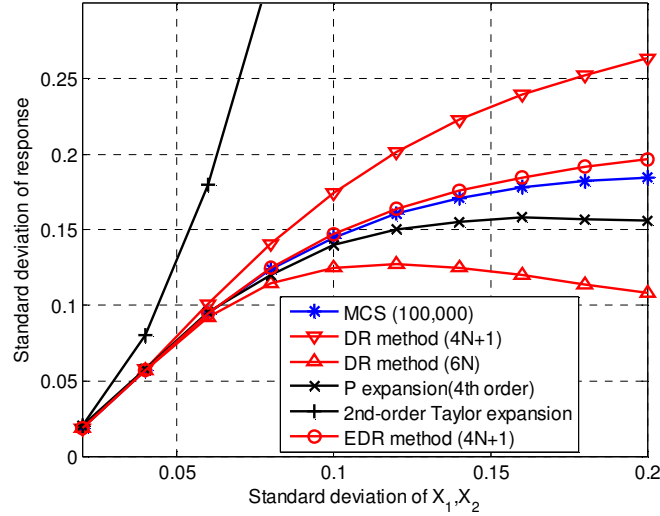
Figure 4-13: Standard deviations of response with different input standard deviations

4.3.2.2 I Beam Example

An I beam example [Huang and Du 2006] is used to demonstrate that the EDR method is capable of handling all kinds of input uncertainties such as symmetric, asymmetric, bounded and unbounded distributions. An I beam is subject to a concentrate force P with a distance a away from the fixed end as shown in Fig. 4-14. The maximum stress can be expressed as:

$$\sigma_{max} = \frac{Pa(L-a)h}{2LI} \tag{4.21}$$

where

$$I = \frac{wh^3 - (w-t_2)(h-2t_1)^3}{12}$$

The beam is safe only if the maximum stress is less than a target value S. A system response can be defined as $Y = \sigma_{max} - S$ with the safety domain $Y < 0$. The uncertainty properties of eight random variables are shown in Table 4-5. Many distribution types such as normal, lognormal, uniform, *etc.* are considered since they are commonly met in engineering problems.
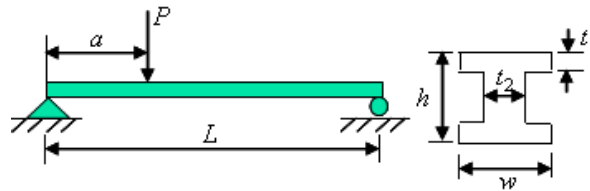
Figure 4-14: Loading condition and structure of an I beam

Table 4-5: Statistical properties of random variables in beam example

Variable	Type	Mean	Std. Dev.	Lower Bound	Upper Bound	Mode
P	Normal	6070	200	-	-	-
L	Beta	120	6	100	150	-
a	Uniform	-	-	50	80	-
S	Lognormal	170000	4760	-	-	-
h	Triangular	-	-	2.25	2.38	2.30
w	Weibull	2.9665	0.0750	-	-	-
t_1	Normal	0.1600	0.0208	-	-	-
t_2	Lognormal	0.2600	0.0208	-	-	-

$4N+1$ eigenvector samples are used to approximate the eight one-dimensional responses accurately using SMLS. Any numerical integration method can be employed to calculate the statistical moments of system response without extra computation effort except for the $4N+1$ eigenvector samples. The statistical moments

of system response achieved by the EDR method and 1,000,000 MCS are compared in Table 4-6. The percentage error of statistical moments is quite small except for the skewness because of the small value. Based on the approximated statistical moments, stabilized Pearson system is employed to approximate the PDF of system response. In Fig. 4-15, the PDF directly achieved from MCS are compared with the one constructed by the stabilized Pearson system. The reliability value calculated by the EDR method and MCS are 99.9943% and 99.9827%, respectively. The results with similar accuracy can be achieved using bivariate DR method in the reference paper [Huang and Du 2006]. However, bivariate DR method employed 277 function evaluations, which are much more than 33 function evaluations used in the EDR method.

Table 4-6: Comparison of statistical moments

	Mean	Std. Dev.	Skewness	Kurtosis
MCS(1,000,000)	-49883	12961	0.0083	3.1479
EDR($4N+1$)	-49860	12815	0.0050	2.9840
Error(%)	0.0460	1.1312	39.9880	5.2077
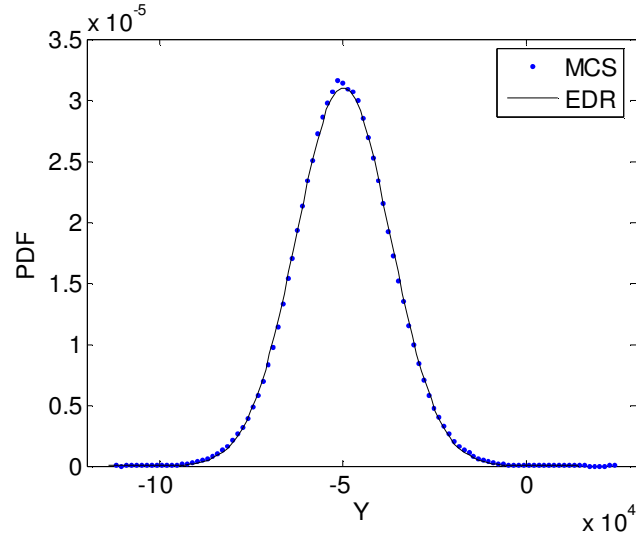
Figure 4-15: PDFs using the EDR and MCS method

4.3.2.3 Side Impact Crash Problem

Vehicle side impact [Youn et al. 2004a] responses are considered for system performances with statistical correlation. The properties of the design and random variables are shown in Table 4-7. In this example, the velocity of front door at B-pillar is studied. The system performance can be expressed as

$$Y = 16.45 - 0.489 X_3 X_7 - 0.843 X_5 X_6 + 0.0432 X_9 X_{10} - 0.0556 X_9 X_{11} - 0.000786 X_{11}^2$$

(4.22)

Table 4-7: Properties of design and random variables of vehicle side impact model

Random Variables	Distr. Type	Std Dev.	d^L	d	d^U
X_1 (B-pillar inner)	Normal	0.050	0.500	1.000	1.500
X_2 (B-pillar reinforce)	Normal	0.050	0.500	1.000	1.500
X_3 (Floor side inner)	Normal	0.050	0.500	1.000	1.500
X_4 (Cross member)	Normal	0.050	0.500	1.000	1.500
X_5 (Door beam)	Normal	0.050	0.500	1.000	1.500

98

X_6 (Door belt line)	Normal	0.050	0.500	1.000	1.500
X_7 (Roof rail)	Normal	0.050	0.500	1.000	1.500
X_8 (Mat. B-pillar inner)	Normal	0.006	0.192	0.300	0.345
X_9 (Mat. Floor side inner)	Normal	0.006	0.192	0.300	0.345
X_{10} (Barrier height)	Normal	10.0	10th and 11th random variables are		
X_{11} (Barrier hitting)	Normal	10.0	not regarded as design variables		

Two studies are performed with different set of statistical correlation. In the first study, among these input variables, $[X_3, X_7]$, $[X_5, X_6]$, and $[X_9, X_{10}]$ are assumed to have statistical correlation coefficient 0.8, 0.7, and 0.4, respectively. The EDR method employing $2N+1$ (15) analyses is carried out to approximate the first four statistical moments of system performance and construct the PDF. The MCS with 100,000 samples is also carried out for both correlated and uncorrelated cases and the PDFs are correspondingly constructed. Figure 4-16 (a) displays the results of the first case. In this case, there is only slight difference between correlated and uncorrelated cases. In the second study, since X_{10} and X_{11} are the variables having the maximum variation, they are assumed to have a statistical correlation coefficient $\rho_{X_{10}X_{11}} = 0.7$.

Unlike the previous, this case shows the significant effect of statistical correlation on the system response, as shown in Fig. 4-16 (b). In both cases, the EDR method can predict the PDF of the system response with statistical correlation very efficiently and accurately.
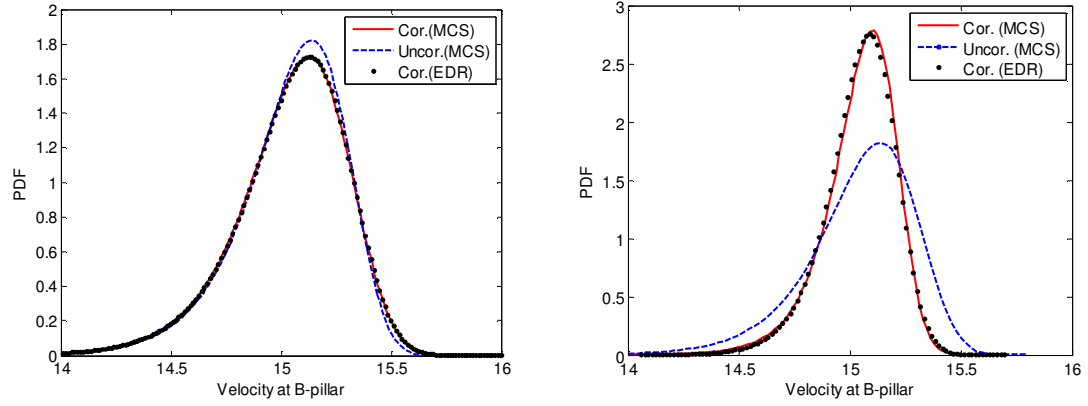
(a) PDF comparison of system response

$(\rho_{3,7}=0.8, \rho_{5,6}=0.7, \rho_{9,10}=0.4)$

(b) PDF comparison of system response

$(\rho_{10,11}=0.7)$

Figure 4-16: PDF comparison of system response with correlation

4.3.2.4 Two-dimensional statistical dependence

A mathematical example with non-normally distributed, statistically dependent random variables was employed to demonstrate the procedure of determining the best transformation sequence. The system response is expressed as

$$Y = 1 - \frac{(v_1+v_2-5)^2}{30} - \frac{(v_1-v_2-12)^2}{120} \tag{4.23}$$

where v_1 and v_2 are the statistically dependent random variables with sufficient data (say, 1,000 sampled data), as shown in Fig. 4-17. To observe the sequence effect, the total degree of deviation was calculated as 0.0279 and 0.1680 for two sequences [v_1, v_2] and [v_2, v_1], respectively, where [v_1, v_2] means the transformation of v_1 and v_2 in order. Figures 4-18 and 4-19 show the response nonlinearity after two different transformation sequences. The figures confirmed that the second sequence [v_2, v_1] produced much higher nonlinearity than the first. This study suggested using the first sequence [v_1, v_2] for probability analysis.
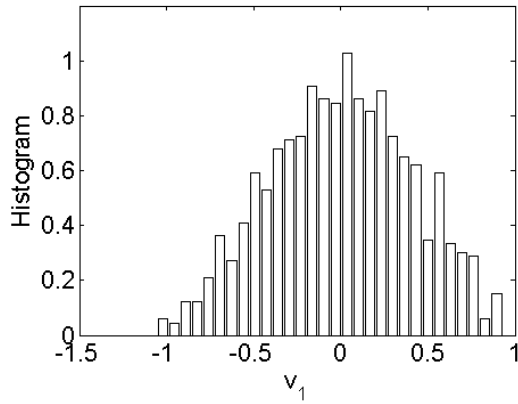
(a) Histogram of v_1
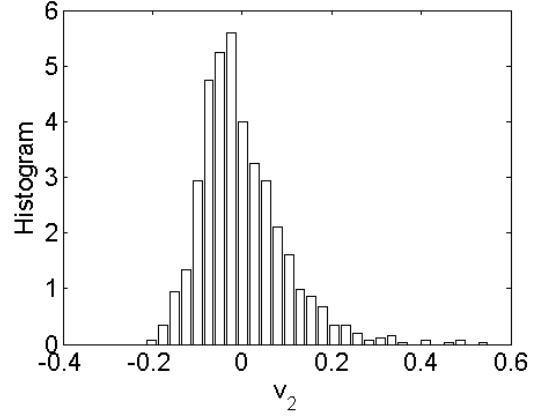
(b) Histogram of v_2
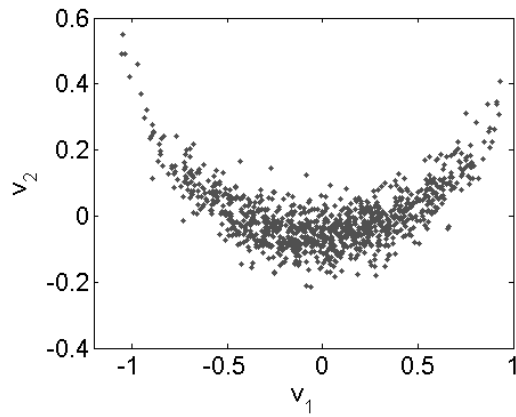
(c) Statistical dependence of v_1 and v_2

Figure 4-17: Random characteristics of two random variables, v_1 and v_2
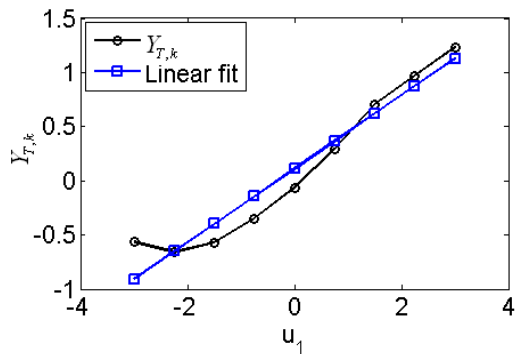
(a) Nonlinearity of $Y_{T,k}$ with respect to u_1
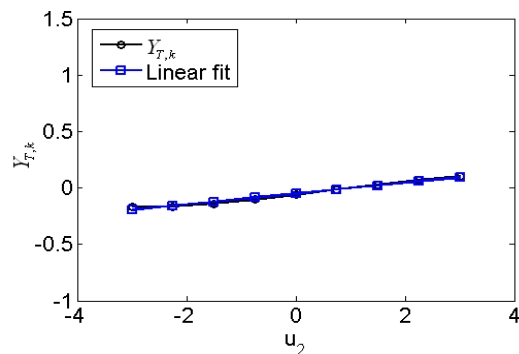
(b) Nonlinearity of $Y_{T,k}$ with respect to u_2

Figure 4-18: Nonlinearity of $Y_{T,k}$ with the transformation sequence [v_1, v_2]
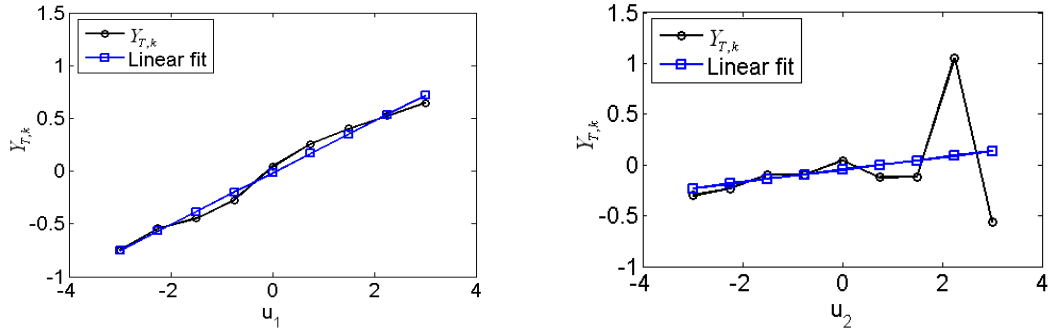
(a) Nonlinearity of $Y_{T,k}$ with respect to u_1 (b) Nonlinearity of $Y_{T,k}$ with respect to u_2

Figure 4-19: Nonlinearity of $Y_{T,k}$ with the transformation sequence [v_2, v_1]

Using the Rosenblatt transformation with the sequence [v_1, v_2], the EDR method with 4N+1 sampling scheme was employed for probability analysis of the system response subject to the non-normally distributed, statistically dependent random variables. Figure 4-20 shows the nine EDR samples mapped in V-space and the predicted PDF of the response. It was observed in Table 4-8 that the EDR method predicted the first four moments very accurately. The predicted PDF using the EDR method agrees well with the normalized histogram using MCS. It was also found in Fig. 4-21 that the EDR method using an inappropriate transformation sequence [v_2, v_1] yielded a relatively large prediction error in probability analysis.

Table 4-8: Statistical moments of Y using the EDR method and MCS

	Mean	Std	Skewness	Kurtosis	Fun. Eval.
EDR	-1.0427	0.2183	-0.0562	2.3132	9
MCS	-1.0406	0.2164	-0.0334	2.3707	1000

(a) EDR samples   (b) PDF comparison
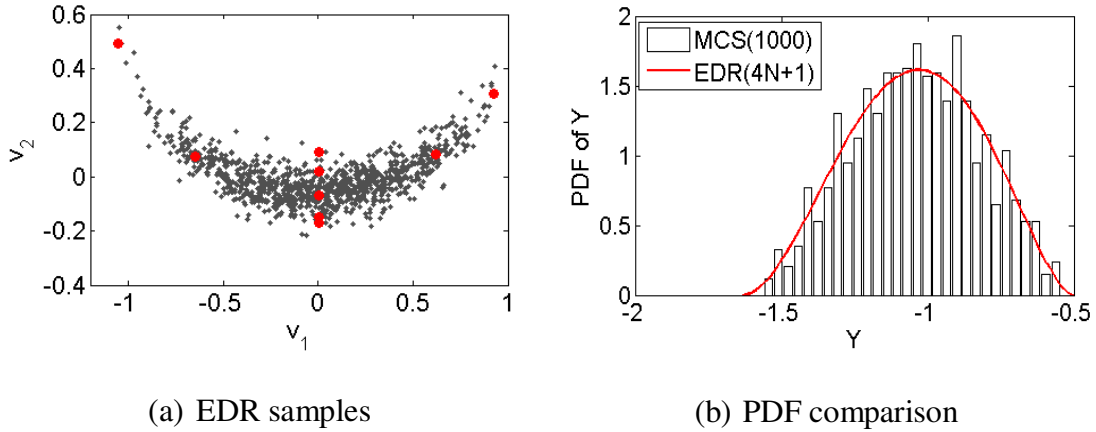
Figure 4-20: EDR results with the transformation sequence $[v_1, v_2]$

(a) EDR samples   (b) PDF comparison
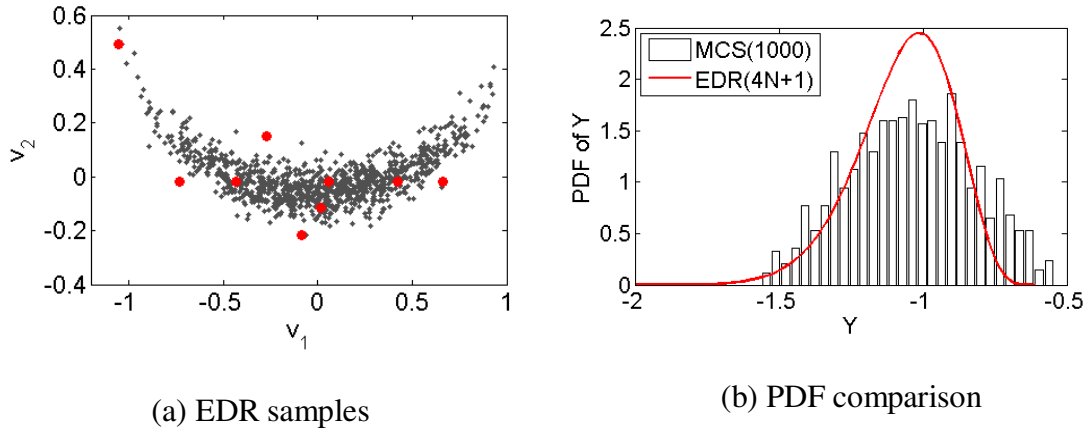
Figure 4-21: EDR results with the transformation sequence $[v_2, v_1]$

4.3.2.5 Dimension dependency study

A mathematical multi-dimension problem [Rahman and Xu 2004] is considered for the accuracy study with the increase of random variables. In this example, the standard deviation of system response is employed for the accuracy study. The input random variables are assumed to follow normal distribution as $X_k \sim Normal(0, 1)$. The multi-dimension problem is expressed as

103

$$Y = \sum_{k=1}^{N} kX_k^2 - X_k \qquad (4.24)$$

First, the analytical solution for the standard deviation of the response Y is solved for the increasing number of random variables up to 40. Then, the EDR method with $2N+1$ and MCS with 100,000 samples are separately carried out to approximate the standard deviation of response Y. Finally, their absolute errors with respect to the analytical solution are calculated, as shown in Fig. 4-22. This result clearly indicates that accuracy of EDR is independent with the number of random variables. Accuracy of MCS, however, is dependent on the random variables.
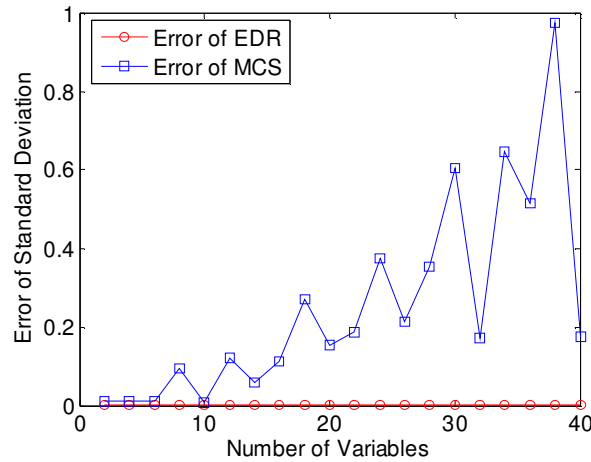
Figure 4-22: Comparison of errors using MCS and the EDR method

4.3.2.6 Plate buckling

Buckling is a very important design issue occurring in many engineering disciplines, such as mechanical, aerospace, civil, *etc*. Structural buckling often leads to catastrophic failures. Thus, it is crucial to accurately estimate the effects of uncertainties inherent in a design upon the critical buckling load. As shown in Fig. 4-23, a highly non-linear buckling example is considered with three shape design

variable: the height (*h*) and width (*w*) of the plate and the hole diameter (*d*). The statistical information regarding these variables is presented in Table 4-9. A morphing technique in the HyperWorks 7.0 software package is used to deal with the shape variables (*h*, *w* and *d*) in the FEA model. The plate is modeled using plane stress quad4 elements, consisting of 1681 nodes, 1571 elements, and 9798 DOF. A unit load is applied along the top edge of the plate, while the bottom edge of the plate remains fixed in all 6 direction. The plate is made of Aluminum 6061, where E=67.6 GPa and ν=0.3.
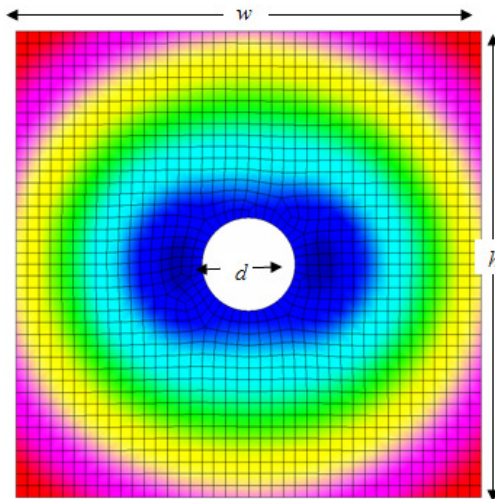
Figure 4-23: Plate FE model

Table 4-9: Random properties in plate model

Random Variable	Mean	Standard Deviation	Distribution Type
h (shape)	500.0	25.0	Normal
w (shape)	500.0	25.0	Normal
d (shape)	100.0	5.0	Normal

The 2N +1 samples (7 buckling analyses) are used for this problem. As shown in Fig. 4-24, there is a good agreement of statistical moments for the first two buckling modes between the MCS and the EDR method. As well, Table 4-10 displays the resulting statistical information of the response from the EDR method and the MCS with 100,000 samples. It is found that the EDR method performs the uncertainty propagation analysis accurately.
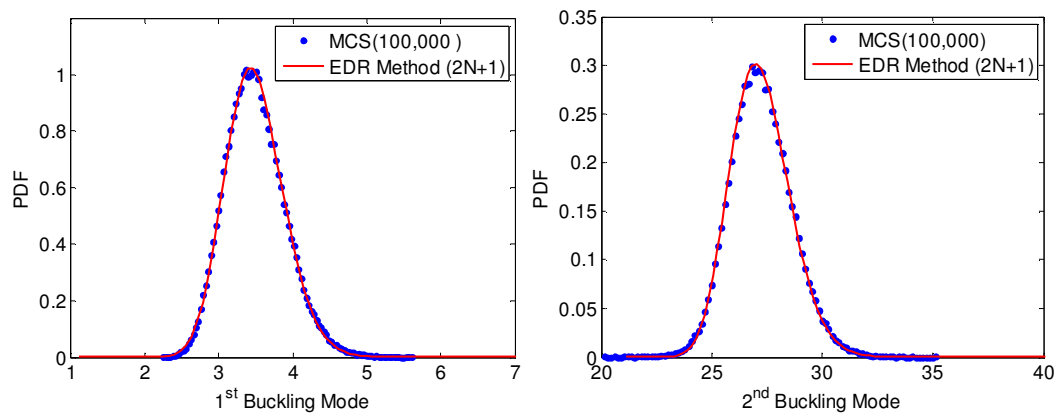
Figure 4-24: PDF of MCS and EDR method

Table 4-10: Results of buckling example

	1st Buckling Mode				2nd Buckling Mode			
Method	Mean	STD	Skew.	Kurto.	Mean	STD	Skew.	Kurto.
MCS	3.503	0.394	0.323	3.169	27.250	1.357	0.320	3.381
EDR	3.494	0.396	0.303	3.227	27.219	1.337	0.328	3.153
Error, %	0.251	0.455	6.060	1.833	0.113	1.442	2.293	6.732

4.3.2.7 Comparison of EDR, FORM and SORM for reliability

In practice, reliability is one of the important engineering metrics to determine how well a product or process is designed. The most common method for reliability

analysis is the First-Order Reliability Method (FORM) or Second-Order Reliability Method (SORM), due to their reasonable accuracy and efficiency. This study aims at comparing the EDR method with both FORM and SORM for reliability analysis. For reliability analysis and design, it will be shown that the EDR method is far more efficient than the other two, since one EDR execution takes care of reliability analyses for all constraints without requiring sensitivity of system responses.

The same example used in Section 4.3.2.3 is used here to compare reliability results from the EDR method, FORM, SORM, and MCS at the optimum design using FORM [Youn et al. 2004a]. With 90% target reliability, the optimum design point is obtained at $[d^*]^T$ = [0.500, 1.327, 0.500, 1.262, 0.623, 1.500, 0.500, 0.345, 0.192, 0.000, 0.000]^T. At the optimum design, reliabilities for ten constraints is verified using three other different methods: SORM, EDR and MCS with 100,000 samples. It is found in Table 4-11 that FORM yields large errors in reliability estimation especially for G_8 and G_{10} constraints. Although the errors can be slightly reduced to some extent using SORM, its accuracy is deficient. However, the EDR method predicts the reliability very accurately. The reason that both FORM and SORM have large error is mainly due to highly nonlinear responses, as shown in Fig.4-25. The dashed and dotted lines show the first-/second-order approximations of failure surfaces used in FORM and SORM for two active constraints G_8 and G_{10} at the optimum design. Inaccurate approximations of failure surfaces lead to the significant errors of FORM and SORM, whereas the EDR method can precisely estimate the failure domains. Nonetheless, it is found that the EDR method is far more efficient than both FORM and SORM.

(a) Failure surface for G_8 (b) Failure surface for G_{10}
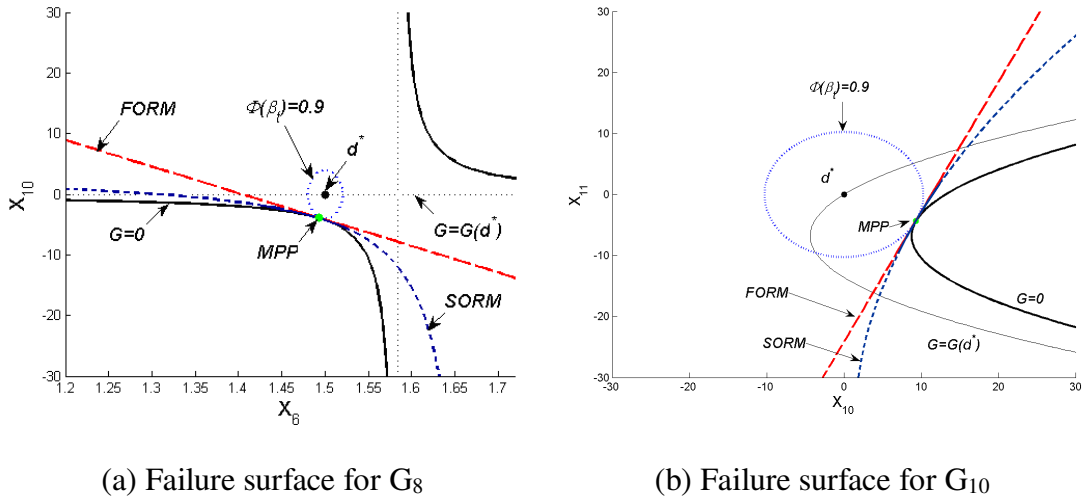
Figure 4-25: FORM and SORM reliability analysis in hyper-plane (a): G_8; (b): G_{10}

Table 4-11: Results of component reliability analysis

Reliabilities	FORM	SORM	EDR	MCS
G_1	1	1	1	1
G_2	1	1	1	1
G_3	0.9989	0.9989	0.9989	0.9989
G_4	0.9000	0.9136	0.9026	0.9026
G_5	1	1	1	1
G_6	1	1	1	1
G_7	1	1	1	1
G_8	0.9000	0.8723	0.7140	0.7067
G_9	0.9897	0.9905	0.9905	0.9900
G_{10}	0.9000	0.9025	0.9794	0.9714
Function Eval.	47	47	23	100,000
Sensitivity Eval.	47	47	0	0
Hessian Eval.	10	10	0	0

4.3.3 Probability analysis with both random parameter and field variables

This section presents probability analysis with both random parameter and field variables. The EDR method was used to perform probability analysis for engineered systems. The door misalignment example of a two-door refrigerator is used to show the effectiveness of the proposed approach. As illustrated in Section 3.5.2.2, the deformation of the front-L was represented by two random fields in both freezer and refrigerator sides and hinge variations were modeled as random parameters. Hence, the door misalignment prediction requires probability analysis with both random parameter and field variables. In this example, the problem was simplified by only considering the last assembly process. Hence, the front-L deformation after the foaming process and the hinge variation at both freezer and refrigerator sides are considered as statistical inputs for the prediction of door misalignment.

The door misalignment (Y_4) is defined as a difference between the freezer side hinge measurement (Y_{3F}) and the refrigerator side hinge measurement (Y_{3R}) as shown in Eq. (4.25).

$$Y_4 = Y_{3F} - Y_{3R} \qquad\qquad (4.25)$$

The hinge measurements (Y_{3F} and Y_{3R}) are calculated based on a rigid assembly process as shown in Fig. 4-26. The hinge measurement at freezer side (Y_{3F}) is expressed as:

$$Y_{3F} = X_{6F} \cos(\alpha(\boldsymbol{\theta}_F)) - d(\boldsymbol{\theta}_F) \qquad\qquad (4.26)$$

where X_{6F} is the hinge variation at freezer side, α and d are functions of the front-L deformation, θ_F is the front-L deformation at freezer side represented by a random field. Similarly, the hinge measurement at refrigerator side (Y_{3R}) is expressed as:

$$Y_{3R} = X_{6R} \cos(\alpha(\boldsymbol{\theta}_R)) - d(\boldsymbol{\theta}_R) \qquad (4.27)$$

Hence, the door misalignment (Y_4) is defined as:

$$Y_4 = X_{6F} \cos(\alpha(\boldsymbol{\theta}_F)) - d(\boldsymbol{\theta}_F) - X_{6R} \cos(\alpha(\boldsymbol{\theta}_R)) + d(\boldsymbol{\theta}_R) \qquad (4.28)$$

where the subscript F and R indicate freezer and refrigerator sides, respectively; $X_{6F} \sim$ Weibull (52.9525, 105.7080), and $X_{6R} \sim$ Lognormal (3.9814, 0.0097). The random fields (θ_F and θ_R) of the front-L deformation were modeled with sufficient data in Section 3.5.2.2 using the proposed approach in Section 3.3.
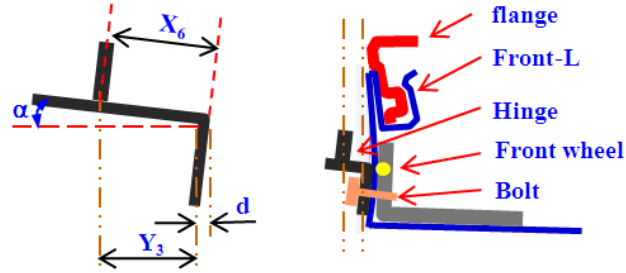
Figure 4-26: Side view of the hinge installation

Step 1: Determination of the important signatures

Using the posteriori normalized error in Eq.(3.3), six important signatures are required to approximate the random fields. Thus, the random field of the front-L deformation at freezer side can be expressed as

$$\theta_F(x) = \mu_F(x) + \sum_{i=1}^{6} V_{iF} \phi_{iF}(x) \qquad (4.29)$$

Similarly, the random field of the front-L deformation at refrigerator side can be expressed as

$$\theta_R(x) = \mu_R(x) + \sum_{i=1}^{6} V_{iR} \phi_{iR}(x) \qquad (4.30)$$

110

The use of five important signatures leads to 1.76% of the normalized error in the approximate random realization for one thousand snapshots at refrigerator side, whereas the inclusion of six most important signatures makes 0.01% error. Thus, six random field variables are necessary to define the random field at refrigerator side. Similarly, six random field variables are also required to define the random field at freezer side.

Step2: Modeling random field variables and statistical dependency

One thousand values for each random field variable can be obtained for both refrigerator and freezer sides. The Maximum Likelihood Estimation (MLE) and Chi-Square goodness-of-fit test are used to find the distributions and statistical parameters. They all follow Beta distributions with statistical properties listed in Table 4-12. It is further found that these random field variables are statistically independent.

Step 3: Probability analysis considering both random parameter and field variables

For one thousand samples, probability analyses using MCS are conducted. The EDR method with $2N+1$ eigenvector samples (29 analyses) is employed to predict the door misalignment with both random parameter and field variables. The EDR method accurately predicts the PDF of the door misalignment, which is compared with the normalized histogram from MCS, as shown in Fig. 4-27.

Table 4-12: Statistical properties of random field variables

	Mean	STD	Lower Bound	Upper Bound
V_{1R}	0	0.7537	-2.7975	4.5223
V_{2R}	0	0.4583	-2.7495	2.7495
V_{3R}	0	0.2431	-1.4584	0.9722
V_{4R}	0	0.2167	-1.3001	1.3001
V_{5R}	0	0.1377	-0.8263	0.8263
V_{6R}	0	0.0655	-0.3273	0.3927
V_{1F}	0	0.6624	-3.3121	3.3121
V_{2F}	0	0.5486	-2.7429	3.2914
V_{3F}	0	0.2473	-1.4835	1.4835
V_{4F}	0	0.2262	-1.3569	1.1308
V_{5F}	0	0.1386	-0.5545	0.6932
V_{6F}	0	0.1167	-0.7001	0.7001
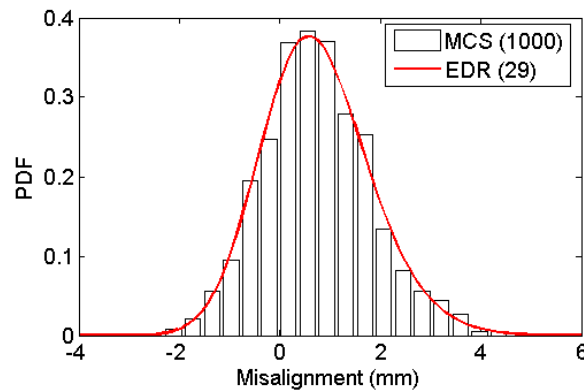
Figure 4-27: Comparison of EDR and MCS for the prediction of door misalignment

4.4 Summary

This chapter proposed the Eigenvector Dimension Reduction (EDR) method for the generic reliability analysis framework that requires no derivative information of

system responses while taking into account both random parameter and field variables. The EDR method makes a significant improvement, based upon the univariate Dimension Reduction (DR) method. In the univariate DR method, in order to improve accuracy of probability analysis, a large number of integration points must be involved. Moreover, while increasing the number of integration points, the univariate DR method may become singular and inefficient. To resolve those difficulties, the EDR method is proposed with the three new technical elements: 1) eigenvector sampling; 2) the Stepwise Moving Least Squares (SMLS) method for efficient and accurate numerical integration; and 3) a stabilized Pearson system. First, the 2N+1 and 4N+1 eigenvector sampling schemes were proposed for probability analysis to maintain high accuracy without requiring sensitivity of system performances. Second, the SMLS method was employed to accurately approximate the responses, which allow one-dimensional numerical integration with no extra cost other than simulations or experiments at the eigenvector samples. Both moment-based quadrature rule and adaptive Simpson rule can be used for numerical integration. Third, the stabilized Pearson system is proposed to eliminate a singular behavior of the original Pearson system while accurately predicting Probability Density Functions (PDFs) of engineering system performances. In summary, compared with the univariate DR method, the EDR method makes considerable improvements from the perspective of accuracy, efficiency, and stability. The EDR method outperforms the FORM and SORM in terms of the efficiency, since one EDR execution takes care of reliability analyses for all constraints without requiring sensitivity of system responses. The EDR method could be more accurate than

113

FORM and SORM for highly nonlinear limit state function or limit state function involving inflection points. The FORM and SORM maybe work better than the EDR method for problems with substantial contribution of high-order mixed terms or for problems with high reliability levels (e.g., more than 99.9%). The SORM outperforms the FORM in terms of accuracy, but it is less efficient than the FORM.

Chapter 5:   Reliability-Based Design Optimization (RBDO) with Both Random Parameter and Field Variables

This chapter proposes a generic RBDO framework that can deal with both random parameter and field variables.

5.1 Introduction

Reliability-Based Design Optimization (RBDO) is composed of two sub-problems, reliability analysis and design optimization. Reliability analysis evaluates probabilistic constraints at a given design. Design optimization seeks for an optimal design subject to the probabilistic constraints. Many efforts have been made to enhance the numerical accuracy, efficiency and stability of the RBDO through the development of three RBDO approaches: a nested double-loop, decoupled double-loop, and single-loop approach. Nested double-loop methods are structured with the inner loop for the reliability analysis and the outer loop for the design optimization. As a result, these methods are computationally expensive for most engineering design problems. Later, decoupled double-loop and single-loop methods have been developed to address the computational challenges. Despite the extensive effort made in the RBDO methods, the numerical efficiency, accuracy, and stability is still of great concern. Furthermore, the conventional RBDO approach does not consider random field variables as the system inputs.

This chapter thus proposes a very efficient and accurate approach for RBDO that can deal with both random parameter and field variables with an incorporation of the Eigenvector Dimension Reduction (EDR) method. Even if the EDR method requires no sensitivity of the responses, RBDO still requires sensitivity of reliability and

quality to find a design direction in design optimization. An effective RBDO approach with both random parameter and field variables was proposed by incorporating the EDR method. First, an approximate response surface was employed to facilitate sensitivity calculation of reliability where the response surface was constructed using the eigenvector samples. Thus, sensitivity analysis becomes very efficient and simple. Second, by taking advantage of the EDR method for reliability analysis, the proposed RBDO approach does not require an iterative process like First Order Reliability Method (FORM) or Second Order Reliability Method (SORM). Hence, the proposed RBDO methodology has a single-loop structure. Moreover, the EDR execution time can be much shorter by taking advantage of a parallel computing power and RBDO can be far more efficient. The proposed RBDO methodology could be more accurate than FORM and SORM for the problems with multiple Most Probable Points (MPPs) or highly nonlinear limit state functions. It is expected that the proposed RBDO using the EDR method can enhance numerical efficiency substantially while maintaining good accuracy. Four case studies (side impact crash, layered plate bonding process, A-Arm in HMMWV, and door misalignment) are used to demonstrate the effectiveness of the proposed RBDO method using the EDR method.

5.2 A generic RBDO framework using the EDR method

This section proposes a generic Reliability-Based Design Optimization (RBDO) framework that can deal with both random parameter and field variables. The RBDO can be formulated as

116

minimize $y(\mathbf{d}; \boldsymbol{\gamma})$

subject to $P(G_i(\mathbf{X}; \boldsymbol{\Theta}) \leq 0) = F_{G_i}(0) \geq \Phi(\beta_{t_i}), \quad i = 1, \cdots, NP$

$\mathbf{d}^{\mathrm{L}} \leq \mathbf{d} \leq \mathbf{d}^{\mathrm{U}}, \quad \mathbf{d} \in R^{ND} \text{ and } \mathbf{X} \in R^N$

$\boldsymbol{\gamma}^{\mathrm{L}} \leq \boldsymbol{\gamma} \leq \boldsymbol{\gamma}^{\mathrm{U}}, \quad \boldsymbol{\gamma} \in R^{MD} \text{ and } \boldsymbol{\Theta} \in R^M$

where $y(\mathbf{d}; \boldsymbol{\gamma})$ is the objective function, $\mathbf{d} = \boldsymbol{\mu}(\mathbf{X})$ is the design vector of random parameter variables, $\boldsymbol{\gamma} = \boldsymbol{\mu}(\boldsymbol{\Theta})$ is the design vector of random fields, $\mathbf{X}$ is the random parameter vector, $\boldsymbol{\Theta}$ is the random field vector, its prescribed reliability target β_{ti}, while NP, ND, N, MD, and M are the number of probabilistic constraints, random parameter design variables, random parameters, random field design variables, and random fields, respectively, and the probabilistic constraint, $F_{Gi}(0)$, is expressed as

$$F_{G_i}(0) = \int_{G_i(\mathbf{X}; \boldsymbol{\Theta}) \leq 0} \cdots \int f_{\mathbf{X}; \boldsymbol{\Theta}}(\mathbf{x}; \boldsymbol{\theta}) d\mathbf{x} d\boldsymbol{\theta} \qquad (5.1)$$

At a given design point, sensitivity of reliabilities with respect to a mean and a standard deviation (or variation) of a random input must be provided to perform RBDO. This is referred to as a probabilistic sensitivity analysis. In Chapter 3, the random field is represented by a set of random field variables ($\mathbf{V}$) which have the same format as the random parameter variables ($\mathbf{X}$). Hence, the procedure of the probabilistic sensitivity analysis for the random field variables is the same as for the random parameter variables. Sensitivity of reliabilities requires sensitivity analysis of system responses (e.g., fatigue, stress, etc.) at the eigenvector samples for both random parameter and field variables. The sensitivity results at the samples are obtained using the Finite Difference Method (FDM). First, perturbation of mean or standard deviation of a random input identifies new eigenvector samples. Then, the Stepwise Moving Least Square (SMLS) method is used to approximate the responses at the new eigenvector samples. Finally, the EDR method is performed to compute

117

the perturbed reliabilities with the perturbed mean or standard deviation of the random input. Using the original and perturbed values of reliabilities, the FDM computes sensitivities of quality or reliabilities.

5.2.1 Probabilistic sensitivity with respect to an input standard deviation

This section considers a probabilistic sensitivity analysis with respect to a standard deviation of a random input. As shown in Fig. 5-1, the new eigenvector sample points, $(x_{1,1'}, x_{2,0})$ and $(x_{1,2'}, x_{2,0})$, are identified with a perturbed standard deviation of the random input, X_1. A perturbation size of 0.1% is commonly used for the FDM. For $x_{i,j}$, the first subscript (i) indicates the i-th random parameter, and the second (j) indicates the j-th sample point along each random parameter.
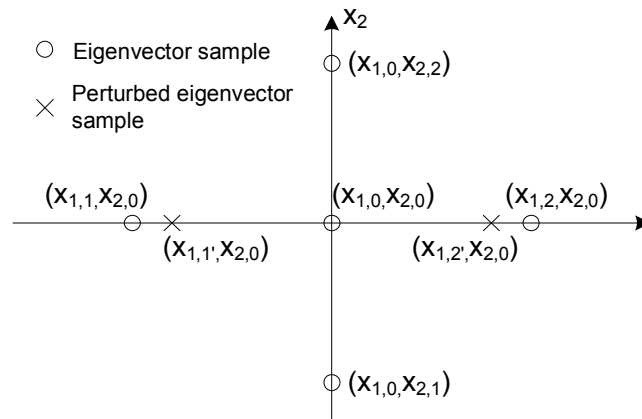
Figure 5-1: Sensitivity with respect to a standard deviation of the 1-st random input

(2N+1 eigenvector sample scheme)

The SMLS method is used to approximate the response values at the two new eigenvector sample points when the 2N+1 eigenvector sample points are employed. Finally, the EDR method is performed to compute the reliabilities (R_i) with the perturbed standard deviation of the random input. The sensitivities of reliabilities with

118

respect to the standard deviation of the i-th random variable ($i =1,…, N$) are computed using the following equations.

$$\frac{\partial R_k}{\partial \sigma_{X_i}} \approx \frac{R_k(\sigma_{X_i} + \Delta\sigma_{X_i}) - R_k(\sigma_{X_i})}{\Delta\sigma_{X_i}} \quad \text{for } k = 1,\cdots, NC \qquad (5.2)$$

where *NC* is the number of constraints for system responses.

5.2.2 Probabilistic sensitivity with respect to an input mean

This section considers a probabilistic sensitivity analysis with respect to a mean of a random input. The eigenvector samples with a perturbed mean of the random input are identified with a common perturbation size of 0.1%. The five new eigenvector samples with the perturbed mean of X_1 are identified at ($x_{1,0'}$, $x_{2,0}$), ($x_{1,1'}$, $x_{2,0}$), and ($x_{1,2'}$, $x_{2,0}$) along X_1 and ($x_{1,0'}$, $x_{2,1}$) and ($x_{1,0'}$, $x_{2,2}$) along $X_{2'}$, as shown in Fig. 5-2. The SMLS method is used to approximate the responses at the five new eigenvector sample points when the 2N+1 eigenvector sample points are employed. Finally, the EDR method is performed to compute the reliabilities (R_i) with the perturbed mean of the random input. The sensitivities of reliabilities with respect to the mean of the i-th random variable ($i =1,…, N$) are computed using the following equations.

$$\frac{\partial R_k}{\partial \mu_{X_i}} \approx \frac{R_k(\mu_{X_i} + \Delta\mu_{X_i}) - R_k(\mu_{X_i})}{\Delta\mu_{X_i}} \quad \text{for } k = 1,\cdots, NC \qquad (5.3)$$
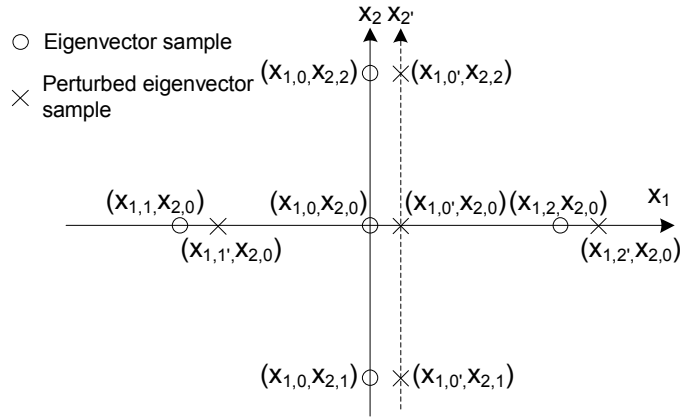
Figure 5-2: Sensitivity with respect to a mean of the 1-st random input

(2*N*+1 eigenvector sample scheme)

The response values can be accurately approximated at the perturbed eigenvector samples located along X_1 axis, since the SMLS method accurately approximates the one-dimensional response along X_1. However, it is difficult to approximate the response values at the samples, $(x_{1,0'}, x_{2,1})$ and $(x_{1,0'}, x_{2,2})$, located along the axes other than $X_{1'}$. These samples and response values are referred to as the off-axis samples and response values. A feasible approach to resolve the difficulty is to approximate the off-axis response values using the assistant points (square), as shown in Fig. 5-3. The off-axis response values can be approximated using the SMLS method after the response values at the assistant points are obtained. In doing so, hyper-assistant points (triangle) are used to approximate the responses at the assistant points. The hyper-assistant points are defined along each variable axis (e.g., X_1, X_2) and their responses can be obtained with high accuracy. Along the dotted lines in Fig.5-3, two hyper-assistant points are employed to approximate the response at one assistant point (square). It is found that the error in the response value could be relatively large when

two hyper-assistant points are directly used for off-axis response approximation. Therefore, the responses at the assistant points are employed to approximate the responses at the perturbed eigenvector samples. Such an approach is expected to reduce a numerical error in probabilistic sensitivity estimation.
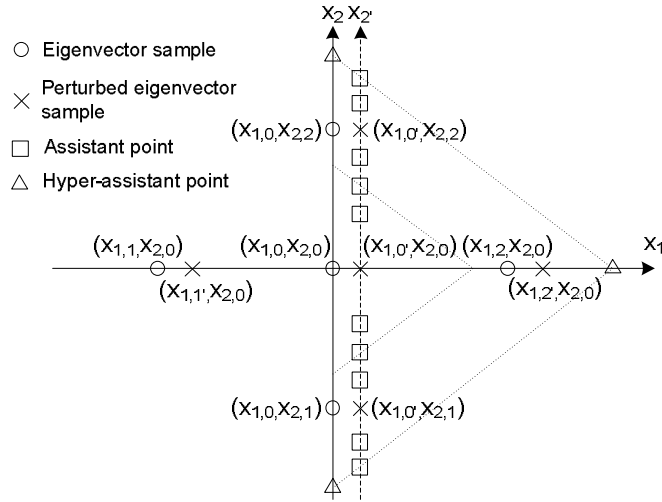
Figure 5-3: Sensitivity with respect to an input mean ($2N+1$ integration scheme)

5.3 Examples and results

In this section, four case studies (side impact crash, layered plate bonding process, A-Arm in HMMWV, and a refrigerator assembly problem) are used to demonstrate the effectiveness of the proposed Reliability-Based Design Optimization (RBDO) method considering both random parameter and field variables using the Eigenvector Dimension Reduction (EDR) method. In order to improve computational efficiency, RBDO starts with $2N+1$ and adaptively increases the sample size to $4N+1$ if a response is known to be highly nonlinear.

5.3.1 RBDO with random parameter variables

5.3.1.1 Side impact crash problem

A vehicle side impact problem is considered for RBDO with five different cases: 1) sensitivity calculation with actual function evaluation; 2) sensitivity calculation with approximated function evaluation; 3) correlated random variables; 4) non-normal random variables; and 5) standard deviation as the design parameter. The Sequential Quadratic Programming (SQP) is used in RBDO for all five cases. All the design and random variables are shown in Table 5-1 for case 1 to case 3. In this example, the quality of the abdomen load is treated as an objective function with nine reliability constraints, as defined in Table 5-2. The quality is defined as the summation of mean and standard deviation. The reliability level for all the constraints is set to 99.87%. The RBDO is formulated as

$$\text{Minimize} \quad Q = \mu_{load} + \sigma_{load}$$
$$\text{Subject to} \quad R_k = P(G_k(X) \leq 0) \leq \Phi(-\beta_{t_k}), \ k = 1, 2, \cdots, 9$$
$$0.5 \leq X_i \leq 1.5; \ i = 1, \cdots, 7; \quad 0.192 \leq X_i \leq 0.345; \ i = 8, 9$$

where μ_{load} and σ_{load} are the mean and standard deviation of abdomen load; $G_i(X)$ is the nine constraints defined in Table 5-2; and β_{ti}=3.

Table 5-1: Properties of design and random variables of vehicle side impact model

Random Variables	Distr. Type	Std Dev.	d^L	d	d^U
X_1	Normal	0.050	0.500	1.000	1.500
X_2	Normal	0.050	0.500	1.000	1.500
X_3	Normal	0.050	0.500	1.000	1.500
X_4	Normal	0.050	0.500	1.000	1.500
X_5	Normal	0.050	0.500	1.000	1.500

X_6	Normal	0.050	0.500	1.000	1.500
X_7	Normal	0.050	0.500	1.000	1.500
X_8	Normal	0.006	0.192	0.300	0.345
X_9	Normal	0.006	0.192	0.300	0.345
X_{10}	Normal	10.0	X_{10} and X_{11} are not design variables		
X_{11}	Normal	10.0			

Table 5-2: Components and safety rating criteria of vehicle side impact model

Components		Safety criteria
Objective: Quality of abdomen load (kN)		≤ 1
G_1-G_3: Rib Deflection	Upper	
	Middle	≤ 32
	Lower	
G_4 -G_6: VC (m/s)	Upper	
	Middle	≤ 0.32
	Lower	
G_7: Pubic symphysis force (kN)		≤ 4
G_8: Velocity of B-pillar		≤ 9.9
G_9: Velocity of front door at B-pillar		≤ 15.7

Case 1: sensitivity calculation with actual function evaluation

The EDR method with $2N+1$ eigenvector samples are employed to calculate the quality (objective function) and nine reliability constraints, respectively. For the sensitivity analysis of the quality and reliability, $(2N+1)M$ function evaluations must be carried out, where N and M are the number of random and design variables, respectively. Although the computation is independent upon the number of the constraint and objective function, it is still expensive. The design history is shown in Table 5-3. In each iteration, $(2N+1)(M+1)$ number of function evaluation is employed

for the calculation of the quality, reliability constraints, and their sensitivity. After four design iterations, the optimum design is obtained where the third constraint becomes active and X_2, X_3, X_4, X_8 and X_9 reach their upper bounds, as shown in Table 5-3. Using Monte Carlo Simulation (MCS) with 100,000 random samples, the reliability of G_3 at the optimum design is found to be 99.87%.

Table 5-3: Design history (Case 1)

Iteration	0	1	2	3	4	Optimum
# of analyses	230	230	230	230	230	1150
Objective	0.693	0.158	0.130	0.114	0.114	0.114
Mean	0.643	0.117	0.090	0.073	0.073	0.073
Std	0.049	0.040	0.041	0.041	0.041	0.041
X_1	1.000	1.003	1.007	1.073	1.073	1.073
X_2	1.000	1.500	1.500	1.500	1.500	1.500
X_3	1.000	1.257	1.402	1.500	1.500	1.500
X_4	1.000	1.494	1.500	1.500	1.500	1.500
X_5	1.000	1.000	1.000	1.000	1.000	1.000
X_6	1.000	1.028	1.035	1.062	1.056	1.056
X_7	1.000	1.000	1.000	1.000	1.000	1.000
X_8	0.300	0.308	0.344	0.345	0.345	0.345
X_9	0.300	0.345	0.345	0.345	0.345	0.345
G_1	-0.018	-0.377	-0.102	-0.088	-0.101	Inactive
G_2	0.459	-2.762	-3.014	-3.237	-3.237	Inactive
G_3	4.295	0.015	0.001	0.000	0.000	Active
G_4	-0.079	-0.090	-0.093	-0.097	-0.097	Inactive
G_5	-0.095	-0.093	-0.089	-0.089	-0.089	Inactive
G_6	-0.035	-0.055	-0.065	-0.067	-0.067	Inactive
G_7	0.247	-0.065	-0.108	-0.142	-0.141	Inactive
G_8	0.313	-0.441	-0.459	-0.448	-0.453	Inactive
G_9	-0.157	-0.228	-0.302	-0.370	-0.365	Inactive

Case 2: sensitivity calculation with approximated function evaluation

It is found that the case 1 turns out to be very expensive (1150 function evaluations). In the case 2, sensitivity of the quality and reliability constraints are estimated using approximate responses. The design history is shown in Table 5-4 and the reliability of G_3 (active constraint) is confirmed as 99.87% at the optimum design using MCS with 100,000 samples. The optimum design in the case 2 is slightly different from that in the case 1 due to the approximate sensitivity. However, the case 2 is far more efficient (150 function evaluations) than the case 1 (1,150 function evaluations). FORM is also employed to carry out RBDO while the FDM is used for sensitivity computation. FORM requires a total of 1,734 function evaluations in RBDO.

Table 5-4: Design history (Case 2)

Iteration	0	1	2	3	4	Optimum
# of analyses	23	23	23	23	23	
Objective	0.693	0.296	0.140	0.115	0.115	0.115
Mean	0.643	0.258	0.099	0.073	0.073	0.073
Std	0.049	0.038	0.041	0.042	0.042	0.042
X_1	1.000	1.009	1.008	1.050	1.074	1.074
X_2	1.000	1.394	1.500	1.500	1.500	1.500
X_3	1.000	1.145	1.346	1.500	1.500	1.500
X_4	1.000	1.372	1.500	1.500	1.500	1.500
X_5	1.000	1.000	1.000	1.000	1.000	1.000
X_6	1.000	1.000	0.988	0.960	0.949	0.949
X_7	1.000	1.000	1.003	1.013	0.995	0.995
X_8	0.300	0.328	0.285	0.317	0.345	0.345
X_9	0.300	0.345	0.345	0.345	0.345	0.345
G_1	-0.018	-0.621	0.012	0.005	-0.334	Inactive

G_2	0.459	-2.593	-2.110	-2.592	-3.221	Inactive
G_3	4.295	0.446	0.576	0.476	-0.001	Active
G_4	-0.079	-0.092	-0.086	-0.094	-0.100	Inactive
G_5	-0.095	-0.098	-0.089	-0.088	-0.092	Inactive
G_6	-0.035	-0.063	-0.051	-0.061	-0.067	Inactive
G_7	0.247	0.022	-0.082	-0.119	-0.116	Inactive
G_8	0.313	-0.385	-0.362	-0.428	-0.540	Inactive
G_9	-0.157	-0.153	-0.240	-0.297	-0.275	Inactive

Case 3: correlated random variables

For correlated random variables, the EDR method identifies eigenvector samples and then the correlated problem is transformed to the uncorrelated. Then the rest of the reliability analysis procedure is same as the case 2. In this example, x_2 and x_3, x_{10} and x_{11}, x_5 and x_7 are assumed correlated each other with the correlation coefficients as 0.7, 0.7, and -0.6, respectively. RBDO converges to the optimum design at the five design iterations, as shown in Table 5-5. It is found that five design variables (X_1, X_5, X_6, X_7, X_8) are different at the optimum designs of the cases 1 and 2. It indicates that the correlated random variables may have a significant impact to the reliability analysis and design. MCS with 100,000 samples verifies the reliability of G_3 as 99.88%.

Table 5-5: Design history (Case 3)

Iteration	0	1	2	3	4	5	Optimum
# of analyses	23	23	23	23	23	23	
Objective	0.694	0.149	0.126	0.118	0.118	0.118	0.118
Mean	0.643	0.101	0.080	0.073	0.073	0.073	0.073
Std	0.051	0.048	0.046	0.045	0.044	0.044	0.044

X_1	1.000	1.008	1.046	1.073	1.099	1.101	1.101
X_2	1.000	1.500	1.500	1.500	1.500	1.500	1.500
X_3	1.000	1.331	1.459	1.500	1.500	1.500	1.500
X_4	1.000	1.500	1.500	1.500	1.500	1.500	1.500
X_5	1.000	1.000	0.999	0.998	0.998	0.998	0.998
X_6	1.000	1.176	1.129	1.091	1.043	1.040	1.040
X_7	1.000	1.000	1.006	1.008	1.009	1.009	1.009
X_8	0.300	0.325	0.345	0.345	0.337	0.336	0.336
X_9	0.300	0.345	0.345	0.345	0.345	0.345	0.345
G_1	-0.088	0.031	-0.001	-0.109	-0.318	-0.335	Inactive
G_2	0.380	-2.955	-3.259	-3.347	-3.388	-3.395	Inactive
G_3	4.295	0.021	-0.008	0.000	0.003	0.000	Active
G_4	-0.062	-0.070	-0.076	-0.079	-0.081	-0.082	Inactive
G_5	-0.090	-0.082	-0.081	-0.082	-0.085	-0.085	Inactive
G_6	-0.034	-0.060	-0.068	-0.069	-0.067	-0.067	Inactive
G_7	0.272	-0.034	-0.057	-0.058	-0.045	-0.044	Inactive
G_8	0.313	-0.332	-0.391	-0.425	-0.465	-0.468	Inactive
G_9	-0.282	-0.544	-0.570	-0.561	-0.523	-0.520	Inactive

Case 4: non-normal random variables

In this case, non-normal random variables are assumed to be dominated. These random inputs are listed in Table 5-6. In the triangular distribution, the mode value is treated as design parameter unlike the mean value for all other distribution types. For the beta distribution with four parameters, the lower and upper bounds are assumed to be located at $\mu-10\sigma$ and $\mu+6\sigma$, respectively, where μ and σ indicate the mean and standard deviation, respectively. For triangular distributions, both the lower and upper bounds are assumed to be 0.018 away from the mode value. After four design iterations, an optimum design is found with an active G_3 constraint as shown in Table

5-7. The optimum design is similar to that in the case 2 except for a relatively larger standard deviation of the objective function. The mean and standard deviation of the objective function is confirmed as 0.073 and 0.064 by running MCS with 100,000 random samples. The reliability of G_3 is also confirmed as 99.87%.

Table 5-6: Properties of random input variables

Variable	Type	Mean	Std. Dev.	Lower Bound	Upper Bound	Mode
X_1	Lognormal	1.000	0.050	-	-	-
X_2	Beta	1.000	0.050	0.500	1.300	-
X_3	Beta	1.000	0.050	0.500	1.300	-
X_4	Uniform	1.000	0.0866	-	-	-
X_5	Uniform	1.000	0.0866	-	-	-
X_6	Uniform	1.000	0.0866	-	-	-
X_7	Uniform	1.000	0.0866	-	-	-
X_8	Triangular	-	-	0.282	0.318	0.300
X_9	Triangular	-	-	0.282	0.318	0.300
X_{10}	Normal	0	10.000	-	-	-
X_{11}	Normal	0	10.000	-	-	-

Table 5-7: Design history (Case 4)

Iteration	0	1	2	3	4	Optimum
# of analyses	23	23	23	23	23	
Objective	0.699	0.216	0.156	0.135	0.135	0.135
Mean	0.643	0.159	0.096	0.073	0.073	0.073
Std	0.056	0.057	0.060	0.062	0.062	0.062
X_1	1.000	1.003	1.011	1.078	1.079	1.079
X_2	1.000	1.483	1.500	1.500	1.500	1.500
X_3	1.000	1.197	1.362	1.500	1.500	1.500
X_4	1.000	1.453	1.500	1.500	1.500	1.500

X_5	1.000	1.000	1.000	1.000	1.000	1.000
X_6	1.000	0.946	0.890	0.849	0.849	0.849
X_7	1.000	1.000	1.000	1.000	1.000	1.000
X_8	0.300	0.309	0.334	0.345	0.345	0.345
X_9	0.300	0.345	0.345	0.345	0.345	0.345
G_1	0.042	-0.679	-0.476	-0.537	-0.538	Inactive
G_2	0.507	-2.767	-2.923	-3.212	-3.213	Inactive
G_3	4.317	0.001	-0.003	-0.000	-0.000	Active
G_4	-0.079	-0.091	-0.095	-0.102	-0.102	Inactive
G_5	-0.094	-0.097	-0.094	-0.094	-0.094	Inactive
G_6	-0.036	-0.054	-0.060	-0.066	-0.066	Inactive
G_7	0.254	-0.437	-0.537	-0.587	-0.587	Inactive
G_8	0.314	-0.500	-0.573	-0.624	-0.624	Inactive
G_9	-0.062	-0.048	-0.080	-0.110	-0.110	Inactive

Case 5: standard deviation as the design parameter

Generally, the mean of a random variable is regarded as a design parameter instead of the standard deviation because it is difficult to control the standard deviation rather than the mean value. Robust design attempts to minimize the standard deviation of the objective function. In this case study, the optimum design in the case 2 is defined as the initial design. Therefore, the contribution of the standard deviations of the random input variables to RBDO results can be solely investigated. The sensitivity of quality and reliability is approximated using the approach stated in section 5.2.2. The lower bound of the standard deviation (x_1 to x_9) is set as 0.001, and noise variables (x_{10} and x_{11}) are non-designable. After two design iterations, the standard deviation of the objective function is reduced from 0.042 to 0.012 as the

129

standard deviations of design variables x_2, x_3, x_4, and x_9 are reduced to the lower

bound 0.001 as shown in Table 5-8.

Table 5-8: Design history with standard deviation as the design parameter

Iteration	0	1	2	Optimum
# of analyses	23	23	23	
Objective	0.116	0.086	0.085	0.085
Mean	0.073	0.073	0.073	0.073
Std	0.042	0.013	0.012	0.012
X_1	0.050	0.050	0.050	0.050
X_2	0.050	0.001	0.001	0.001
X_3	0.050	0.017	0.001	0.001
X_4	0.050	0.001	0.001	0.001
X_5	0.050	0.050	0.050	0.050
X_6	0.050	0.050	0.050	0.050
X_7	0.050	0.050	0.050	0.050
X_8	0.006	0.006	0.006	0.006
X_9	0.006	0.001	0.001	0.001
G_1	-0.334	-0.430	-0.435	Inactive
G_2	-3.221	-3.436	-3.438	Inactive
G_3	-0.001	-0.218	-0.218	Inactive
G_4	-0.100	-0.101	-0.101	Inactive
G_5	-0.092	-0.093	-0.093	Inactive
G_6	-0.067	-0.069	-0.069	Inactive
G_7	-0.116	-0.130	-0.130	Inactive
G_8	-0.540	-0.566	-0.566	Inactive
G_9	-0.275	-0.281	-0.282	Inactive

5.3.1.2 Robust design of layered bonding plates model

The bonding process of layered plates is very popular in the manufacturing of semi-conductor or electronic display components. During this process, two layered plates are bonded together by a suitable adhesive to form laminated stacks, which can be further processed in the following 4 steps:

1) heating the two plates above the melting temperature of the adhesive;

2) applying the adhesive at each surface of the plate;

3) putting them in contact with each other;

4) cooling them down to a room temperature.

In this process, residual stress due to the mismatch of the thermal expansion coefficients of two layered plates could results in failures of the component such as crack, distortion, and interfacial delamination. Therefore, it is very important to accurately estimate the stress in order to improve the product quality. Herein, a transient thermal Finite Element (FE) analysis is used to predict the stress and deformation of plates. The model for the layered bonding plates is shown in Fig. 5-4. Considering the symmetry of the problem, a quarter of the model is used, as shown in Fig. 5-4(a). Due to the brittle property and high stress at the adherent 1, cracks and distortion could occur. To reduce such defects, weights are applied on top of the adherent 1, as shown in Fig. 5-4(a) from the beginning of the process, and are removed at the end of the cooling process. The bonded assembly is placed on a pair of supporting bars, as shown in Fig. 5-4(a). Three design variables, weight at the edge (X_1 or F_2), weight at the center (X_2 or F_1), and height of the bar (X_3 or y_0), are considered in this problem. Their statistical information is shown in Table 5-9. The

objective function is to minimize the quality (summation of mean and standard deviation) of residual stress. Two constraints are maximum stress during the process (< 130MPa) and center displacement (< 3mm).

(a) Isometric view of the quarter model   (b) FM model
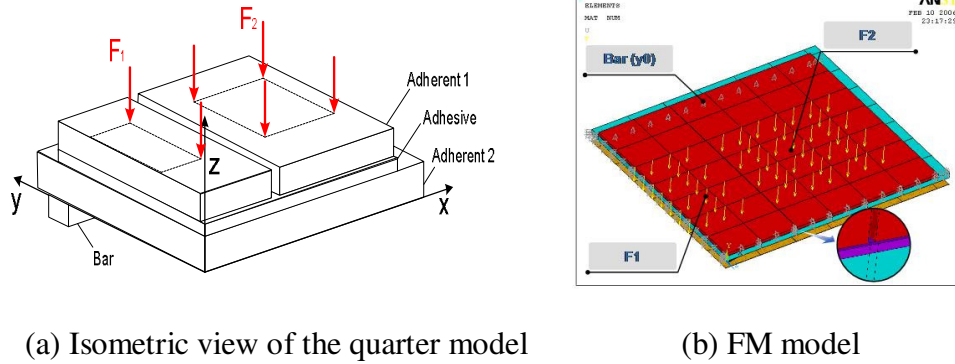
Figure 5-4: Target bonding process and FE model

Table 5-9: Design/random properties of layered plate bonding model

Design Variables	Distr.Type	Mean	Std. Dev.
X_1	Normal	4000	400
X_2	Normal	2000	200
X_3	Normal	1	0.1

The RBDO is formulated as

$$
\begin{aligned}
\text{Minimize} \quad & Q = \mu_r + \sigma_r \\
\text{Subject to} \quad & R_i = P(G_i(X) \le 0) \le \Phi(-\beta_{t_i}), \ i = 1, 2 \\
& 2000 \le X_1 \le 10000; 1000 \le X_2 \le 5000; 1 \le X_3 \le 5;
\end{aligned}
$$

where μ_r and σ_r are the mean and standard deviation of residual stress; $G_1(X)$ is the instantaneous stress; $G_2(X)$ is the edge displacement; β_{ti}=3.

The EDR method is applied to evaluate the quality (= mean + standard deviation) of residual stress and the reliabilities of two constraints. Since the

responses are highly nonlinear, the SMLS method may produce inaccurate responses with only 2N+1 eigenvector samples. Subsequently, inaccurate responses may lead to inaccurate statistical moments of the system responses. To maximize numerical accuracy and efficiency in RBDO, the sample size of the EDR method is adaptively decided. RBDO starts with the 2N+1 sample size of the EDR method to efficiently reach the neighborhood of the optimum design and then continues with the 4N+1 sample size of the EDR method to achieve accuracy of the optimum design. The transition from 2N+1 to 4N+1 is determined after satisfying a relaxed convergence criteria ($\varepsilon \leq 0.1$). This transition is found at the 4-th design iteration in Table 5-10. Although the predicted standard deviation of the residual stress is 0.075 at the 4-th design iteration, this value has relatively large error. It is confirmed by running the EDR with 4N+1 eigenvector samples at the same design. The standard deviation is found to be 0.115 instead of 0.075. The SQP is used as a design optimizer in RBDO. After eight design iterations, the optimum design is found where X_2 is close to the upper bound, as shown in Table 5-10. The EDR method requires totally 80 function evaluations for RBDO. MCS with 1000 random samples is used to confirm the EDR results at the optimum design. It is found that the results (the mean and standard deviation of the residual stress) of the EDR method are very close to those of MCS at the optimum design. The overall quality is drastically improved by 38%.

Table 5-10: Design history of layered bonding plates model

Iter.	Obj	Mean	Std. Dev.	X_1	X_2	X_3	G_1	G_2	# of analysis
0	23.322	23.020	0.302	4000.000	2000.000	1.000	-94.876	1.051	7
1	21.437	21.350	0.087	4579.841	3633.035	2.317	-85.742	0.108	7

2	21.358	21.215	0.143	4659.514	4704.467	3.356	-79.354	-0.467	7
3	21.177	21.040	0.137	4316.124	5000.000	3.734	-77.240	-0.631	7
4 (2N+1)	20.884	20.808	0.075	3121.245	5000.000	3.772	-77.371	-0.567	7
4 (4N+1)	20.976	20.862	0.115	3121.245	5000.000	3.772	-77.342	-0.563	6
5	20.909	20.802	0.110	2752.275	4996.178	3.024	-80.775	-0.207	13
6	20.900	20.798	0.102	2554.780	4998.089	2.862	-81.861	-0.122	13
7	20.898	20.795	0.103	2520.106	4998.208	2.849	-82.046	-0.114	13
Optimum	20.898	20.795	0.103	2520.106	4998.208	2.849	Inactive	Inactive	80
MCS	20.891	20.786	0.105	2520.106	4998.208	2.849	Inactive	Inactive	1000

5.3.1.3 Robust design of lower control A-arm

Vehicle suspension systems experience intense loading conditions throughout their service lives. Control arms act as the back-bone of suspension system, where the majority of these loads are transmitted through. Therefore, it is crucial that control arms be highly reliable, while minimizing its mass. For the purpose of demonstrating RBDO using the EDR method, a HMMWV lower control arm is presented as a case study.

The lower control arm is modeled with plane stress elements using 54,666 nodes, 53,589 elements, and 327,961 DOFs, where all welds are modeled using rigid beam elements. For FE and design modeling, HyperWorks 7.0 is used. The loading and boundary conditions for this case study are shown in Fig. 5-5(a), where loading is applied at the ball-joint (Point D) in three directions, and the boundary conditions are applied to simulate the bushing joints (Points A and B) and the joint with a shock absorber and spring assemble (Point C). The design variables are the thicknesses of the seven major component of the control arm, as shown in Fig. 5-5(b). The statistical information of these components is shown in Tables 5-11 and 5-12. The thicknesses

are considered as random design variables, whereas the loading condition is considered as random noise variables.
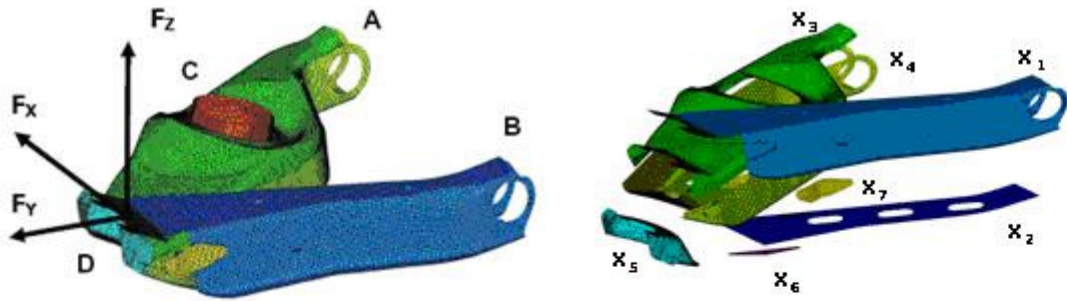
(a) Load variables (random variables)　　　(b) Thickness variables (design variables)

Figure 5-5: Three loading variables (random variables)

Table 5-11: Random properties of force for lower control A-arm model

Random Variable	Distribution
F_x	~ N(1900,95)
F_y	~ N(95,4.75)
F_z	~ (950,47.5)

Table 5-12: Design variables in lower control A-arm model

Design Variable	d_L	Initial Des.	d_U	Std. Dev.	Dist. Type
X_1	0.100	0.120	0.500	0.006	Normal
X_2	0.100	0.120	0.500	0.006	Normal
X_3	0.100	0.180	0.500	0.009	Normal
X_4	0.100	0.135	0.500	0.007	Normal
X_5	0.150	0.250	0.500	0.013	Normal
X_6	0.100	0.180	0.500	0.009	Normal
X_7	0.100	0.135	0.500	0.007	Normal

To determine the hot spots (high stress concentrations) in the model, which are used to determine the constraints, a worst case scenario analysis of the control arm is performed. For this worst case scenario, all the design variables are set at their lower bounds, and all the loads are set at their high values. From the worst case scenario, ninety-one constraints (G_1 to G_{91}) are defined on several critical regions using the von Mises stress, as shown in Fig. 5-6. In this case study, the quality function (= mean + standard deviation) of mass is treated as objective function and a target stress value for 91 stress constraints is set to 60.9 ksi. The reliability level for all the constraints is set to 99.87%.

The EDR method with $2N+1$ (=21) FE analyses is carried out to evaluate the quality of the mass, 91 reliability constraints, and their sensitivities at any design iteration, where $N=10$ (7 for random design parameters and 3 for random loads). The SQP is used for an optimizer in RBDO. At initial design, the 6-th and 80-th constraints severely violate the required reliability. After seven design iterations, the optimum design is found where the aforementioned two and 87-th constraints become active. The design variables X_1 and X_5 reach the lower bound and X_6 reaches the upper bound, as shown in Table 5-13. The EDR method requires totally 147 FE simulations for RBDO. In this example, even though RBDO begins with the severely violated initial design, the mass is slightly increased because X_6 ensures high reliability of the stress with only a small increase in the overall mass unlike other design variables. MCS with 10,000 random samples is also employed to confirm the EDR results at optimum design. The mean and standard deviation of mass are confirmed as 31.967 and 0.712. Using MCS, the reliabilities of the 6-th, 80-th, and

87-th active constraints are confirmed as 99.84%, 99.86%, and 99.89%, respectively, and all other constraints are confirmed inactive. The stress comparison at initial and optimum designs for the 6-th and 80-th constraints is shown in Fig. 5-7.
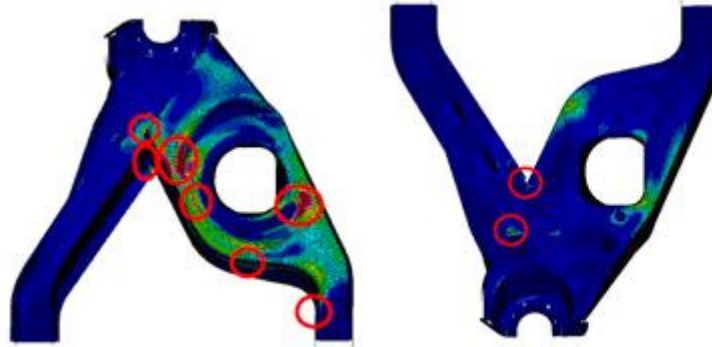
Figure 5-6: Ninety-one critical constraints of the lower control A-arm model

Table 5-13: Design history of lower control A-arm model

Iteration	0	1	2	3	4	5	6	7	Opt.
# of analyses	21	21	21	21	21	21	21	21	
Objective	31.474	32.011	32.694	32.644	32.680	32.683	32.680	32.680	32.680
Mean	30.762	31.299	31.982	31.931	31.968	31.971	31.967	31.968	31.968
Std.	0.712	0.712	0.712	0.712	0.712	0.712	0.712	0.712	0.712
X_1	0.120	0.100	0.100	0.100	0.100	0.100	0.100	0.100	0.100
X_2	0.120	0.140	0.140	0.140	0.140	0.140	0.140	0.140	0.140
X_3	0.180	0.158	0.164	0.163	0.163	0.163	0.163	0.163	0.163
X_4	0.135	0.160	0.162	0.165	0.166	0.166	0.165	0.166	0.166
X_5	0.250	0.150	0.150	0.150	0.150	0.150	0.150	0.150	0.150
X_6	0.180	0.500	0.500	0.500	0.500	0.500	0.500	0.500	0.500
X_7	0.135	0.100	0.291	0.148	0.107	0.141	0.138	0.136	0.136
G_6	1.388	0.109	-0.006	0.003	0.000	0.000	0.000	0.000	Active
G_{80}	2.804	0.365	0.006	0.029	0.009	-0.004	0.001	0.000	Active
G_{87}	-0.490	0.262	-0.021	0.003	0.000	0.000	0.000	0.000	Active

(a) G_6 at initial design   (b) G_6 at optimum design

(c) G_{80} at initial design   (d) G_{80} at optimum design
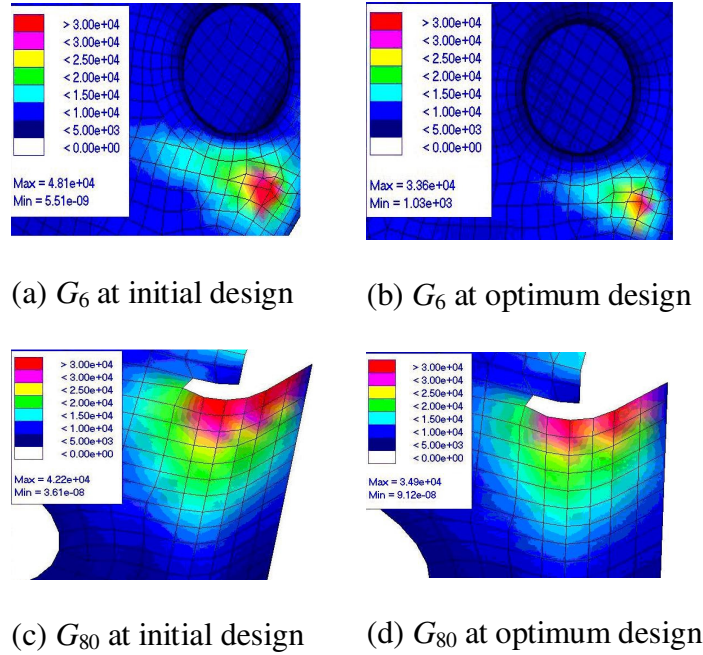
Figure 5-7: Stress comparison of initial and optimum design

5.3.2 RBDO with both random parameter and field variables

This section presents RBDO with both random parameter and field variables. The door misalignment of a two-door refrigerator is used to show the effectiveness of the proposed approach. As illustrated in Section 3.5.2.2, the door misalignment of a two-door refrigerator can be realized as a result of three assembly processes: 1) insertion process; 2) foaming process; and 3) hinge installation. The statistical inputs and outputs in three processes are shown in Fig. 5-8.

In the insertion process, a contact FE model was constructed using HyperWorks and Ansys where the insertion parts were modeled with shell elements. The edge of the inner case and the bottom of the front-L are fixed as shown in Fig. 5-9(a). The definition of the random parameter variables is shown in Fig. 5-9(b). Statistical properties of these variables at the initial design were identified for both freezer and

refrigerator sides as listed in Table 5-14. All these variables were considered as random design variables. The deformation of the front-L (Y_1) at six measurement locations (shown in Fig. 3-23) is the system response which is represented by a random field.
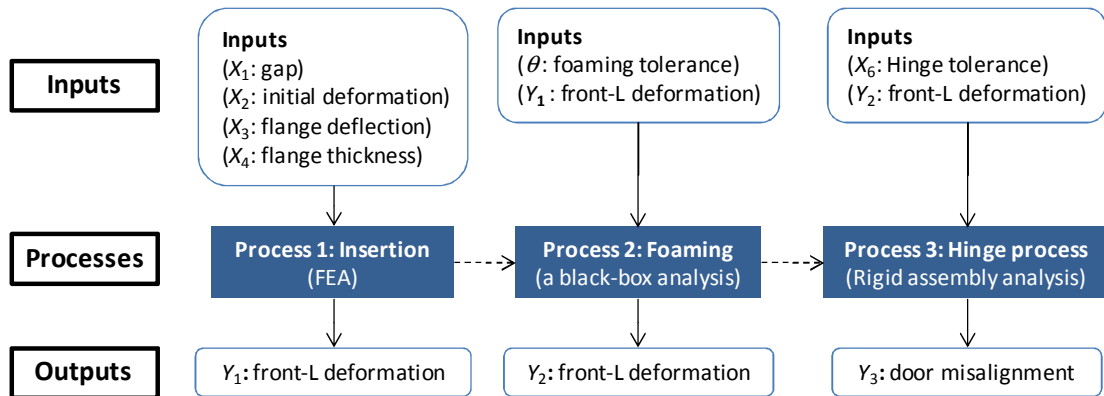
Figure 5-8: Process flowchart of a two-door refrigerator assembly

(a) FE model   (b) Parameter definition
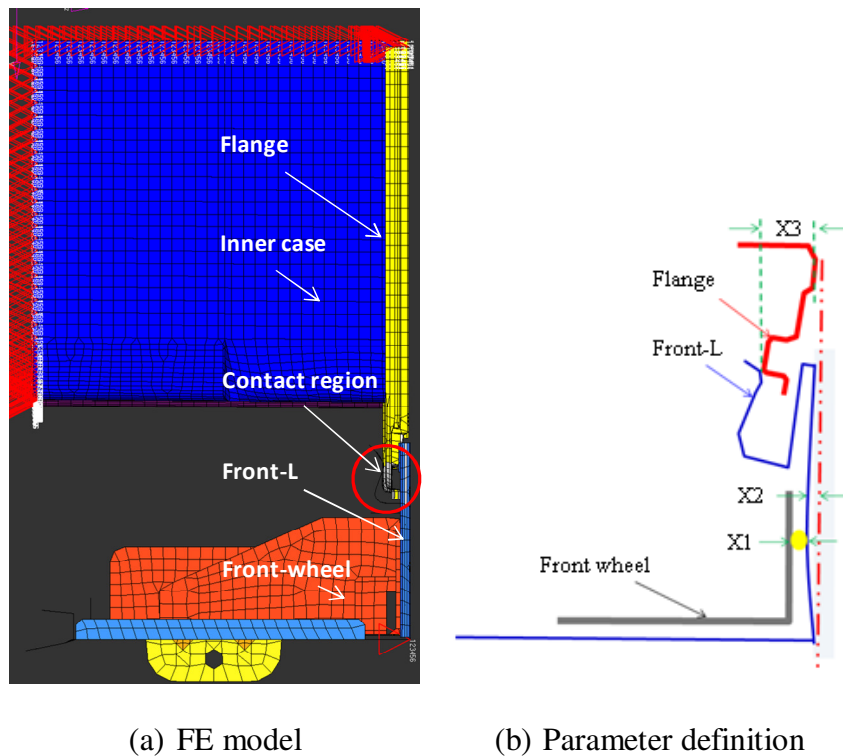
Figure 5-9: FE model and input parameters in the insertion process

Table 5-14: Properties of random input variables in insertion process

Variable	Type	Mean	Std. Dev.
X_{1R}	Gamma	0.383	0.260
X_{2R}	Lognormal	0.321	0.387
X_{3R}	Beta	0.631	0.431
X_{4R}	Weibull	2.000	0.300
X_{1F}	Gamma	0.222	0.431
X_{2F}	Beta	0.467	0.398
X_{3F}	Beta	0.433	0.375
X_{4F}	Lognormal	1.897	0.290

In the 2-nd assembly process, the deformation of the front-L (Y_1) was further changed after the foaming process to increase the stiffness of the main frame of the refrigerator. The foaming tolerance (θ) was modeled as a random field for both freezer and refrigerator sides as shown in Fig. 5-11. Each random field is characterized with six random field variables and their statistical properties are shown in Table 5-15. These variables are considered as random design variables to affect the mean and variation of the foaming tolerance. The deformation of the front-L (Y_2) after the foaming process is calculated using Eq. (5.4).

$$Y_2 = Y_1 + \theta \tag{5.4}$$

In the last process, the hinge is installed to the deformed front-L at both freezer and refrigerator sides where a rigid assembly process is considered. The door misalignment caused by the uneven deformation of the front-L (Y_2) and the hinge tolerance (X_6) and can be calculated using Eq. (4.28) in Section 4.3.3.

(a)   (b)
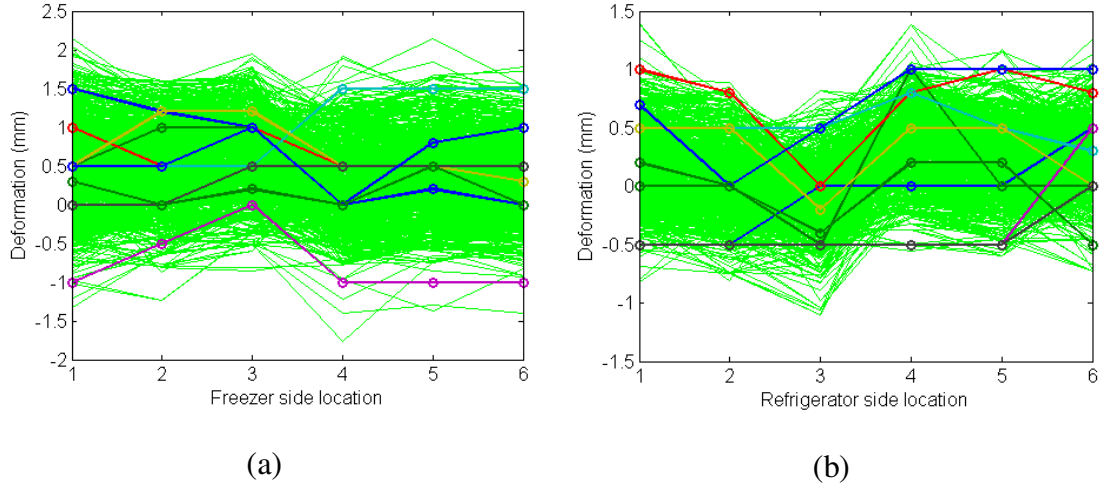
Figure 5-11: Foaming tolerance at both freezer and refrigerator sides

Table 5-15: Statistical properties of random field variables

	Distribution	Mean	STD	Lower Bound	Upper Bound
V_{1R}	Beta	0	0.4608	-1.5408	1.3915
V_{2R}	Beta	0	0.4030	-1.2139	1.2191
V_{3R}	Beta	0	0.3029	-0.9185	1.1227
V_{4R}	Beta	0	0.2527	-0.6938	0.8990
V_{5R}	Beta	0	0.1728	-0.7114	0.6856
V_{6R}	Beta	0	0.1387	-0.5360	0.5357
V_{1F}	Beta	0	0.9400	-3.5811	2.7251
V_{2F}	Beta	0	0.7504	-2.3523	2.2264
V_{3F}	Beta	0	0.3312	-0.9784	1.0110
V_{4F}	Beta	0	0.2333	-0.8149	0.8382
V_{5F}	Beta	0	0.1905	-0.5951	0.5284
V_{6F}	Beta	0	0.1291	-0.3810	0.4736

A Robust Design Optimization (RDO) problem is formulated to minimize the door misalignment (Y_3) subject to a design cost ($30,000) by changing the mean and standard deviation of the random design variables.

$$\text{minimize } \mu_{y3}(\boldsymbol{\mu_X},\boldsymbol{\sigma_X},\boldsymbol{\mu_\Theta},\boldsymbol{\sigma_\Theta})+6\sigma_{y3}(\boldsymbol{\mu_X},\boldsymbol{\sigma_X},\boldsymbol{\mu_\Theta},\boldsymbol{\sigma_\Theta})$$
$$\text{subject to } G(\boldsymbol{\mu_X},\boldsymbol{\sigma_X},\boldsymbol{\mu_\Theta},\boldsymbol{\sigma_\Theta}) \leq 30,000$$
$$\boldsymbol{\mu_X}^L \leq \boldsymbol{\mu_X} \leq \boldsymbol{\mu_X}^U, \boldsymbol{\sigma_X}^L \leq \boldsymbol{\sigma_X} \leq \boldsymbol{\sigma_X}^U$$
$$\boldsymbol{\mu_\Theta}^L \leq \boldsymbol{\mu_\Theta} \leq \boldsymbol{\mu_\Theta}^U, \boldsymbol{\sigma_\Theta}^L \leq \boldsymbol{\sigma_\Theta} \leq \boldsymbol{\sigma_\Theta}^U$$

A cost function G is defined as the summation of the cost for changing the mean and standard deviation of each random design variable as shown in Eq. (5.5).

$$G(\boldsymbol{\mu_X},\boldsymbol{\sigma_X},\boldsymbol{\mu_\Theta},\boldsymbol{\sigma_\Theta}) = G_1(\boldsymbol{\mu_X})+G_2(\boldsymbol{\mu_\Theta})+G_3(\boldsymbol{\sigma_X})+G_4(\boldsymbol{\sigma_\Theta}) \tag{5.5}$$

A constant cost is assigned for the change of each mean, whereas a linear cost function is defined for the change of the standard deviation as shown in Eqs.(5.6) and (5.7).

$$G_3(\boldsymbol{\sigma_X}) = \sum_i k_i \left(\sigma_{X_i,0} / \sigma_{X_i,1} -1 \right) \tag{5.6}$$

$$G_4(\boldsymbol{\sigma_\Theta}) = \sum_j k_j \left(\sigma_{\Theta_j,0} / \sigma_{\Theta_j,1} -1 \right) \tag{5.7}$$

where $\sigma_{X_i,0}$ and $\sigma_{X_i,1}$ denote the i-th initial and new standard deviation of the random parameter variable, respectively; $\sigma_{\Theta_j,0}$ and $\sigma_{\Theta_j,0}$ stand for the j-th initial and new standard deviation of the random field, respectively; k_i (=$2,000) and k_j (=$6,000) are the cost coefficients. For this problem, $1,000 and $3,000 are demanded to change each mean of a random parameter variable and a random field, respectively.

The EDR method with $2N+1$ (=45) analyses was carried out to evaluate the mean and standard deviation of the door misalignment, the cost for design changes,

and their sensitivities at any design iteration, where $N=22$ (10 for random parameter variables and 12 for random field variables). The SQP was used for an optimizer in RDO. The objective function was reduced from 9.84 *mm* to 3.28 *mm* within a $30,000 budget limit after eleven design iterations. The PDF comparison of the door misalignment is shown in Fig. 5-12 between the initial and optimal design.
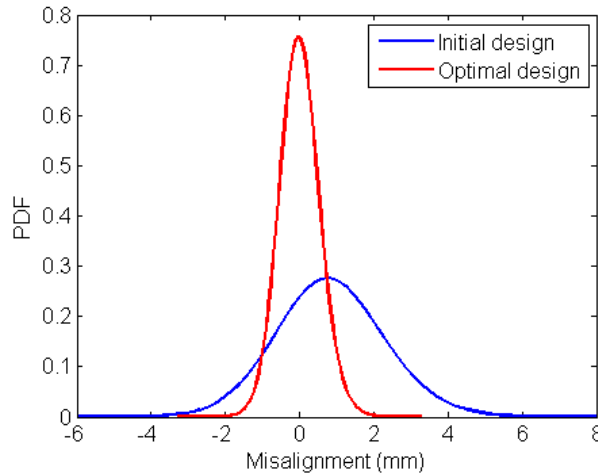
Figure 5-12: PDF comparison of the door misalignment at initial and optimal design

5.4 Summary

This chapter proposed an effective approach for Reliability-Based Design Optimization (RBDO) considering both random parameter and field variables by incorporating the Eigenvector Dimension Reduction (EDR) method. It has been shown that the use of the EDR method provides three benefits to RBDO. First, an approximate response surface facilitates sensitivity calculation of reliability and quality where the response surface is constructed using the eigenvector samples. Thus, sensitivity analysis becomes very efficient and simple. Second, one EDR execution evaluates a set of quality (objective) and reliability (constraint) functions.

In general, the EDR requires $2N+1$ or $4N+1$ simulation runs where N is the total number of random variables. Unlike First Order Reliability Method (FORM) or Second Order Reliability Method (SORM), the EDR execution does not require an iterative process, so the proposed RBDO methodology has a single-loop structure. Moreover, the EDR execution time can be much shorter by taking advantage of a parallel computing power and RBDO can be far more efficient. Third, the EDR method allows solving problems with statistical dependent and non-normally distributed random inputs. As demonstrated with four case studies (side impact crash, layered plate bonding process, A-Arm in HMMWV, and door misalignment), it is expected that the proposed RBDO using the EDR method can enhance numerical efficiency substantially while maintaining good accuracy. Even though the EDR method provided many desirable features to RBDO, the use of the EDR method must be carefully considered when system responses have high-order interaction terms or when high target reliability (e.g., greater than 99.9%) is required.

Chapter 6: Conclusion

6.1 Principle contributions and significances

This dissertation presented a generic reliability analysis and design framework, which enabled the use of random parameter, field, and process variables for reliability prediction and design improvement even with a dearth of data. The significant contributions of this dissertation are as follows.

Contribution 1: An effective random field characterization approach capable of projecting the random field onto a set of important field signatures (or random field variables).

The conventional random field characterization approach, such as the Proper Orthogonal Decomposition (POD) method, demands an infinite number of field signatures to represent the actual random field. It can also be employed to approximate the actual random field with a few important field signatures. However, the number of signatures is subjectively determined by the weight of a few eigenvalues compared to the sum of all the eigenvalues. Furthermore, the definition of the random field variable is unclear since the POD method is not typically applied for reliability analysis and design of engineered systems. These technical issues were resolved in this dissertation. First, an adaptive approximation scheme was developed to find the minimum number of important field signatures while preserving prescribed approximation accuracy. The approximation accuracy was determined by a defined posteriori normalized error. Then, random field variables were defined from the coefficients of the field signatures, and their statistical properties were identified using the Chi-Square

goodness-of-fit test. The proposed random field characterization approach is very accurate and efficient, as demonstrated by three examples in Section 3.5.1.

Contribution 2: A Rosenblatt transformation with an optimal transformation sequence to transform statistically dependent random variables into statistically independent random variables.

Statistical dependence has been given little attention in reliability analysis and design because of the lack of an effective tool to model the statistical dependence and perform reliability analysis. This dissertation highlighted the importance of considering the statistical dependence in reliability analysis and design, since it is often observed in the random field variables. Ignoring the statistical dependence could cause unreliable and risky design. An effective approach was proposed to transform statistically dependent random variables into statistically independent random variables. Rosenblatt's transformation was employed for the transformation. However, the number of the transformation sequences exponentially increases as the number of random variables becomes large. It was found that improper selection of a transformation sequence among many may introduce high nonlinearity into system responses, which may result in inaccuracy for reliability analysis and design. Hence, a novel procedure was proposed to determine an optimal sequence of the Rosenblatt transformation that introduces the least degree of nonlinearity into the system response. Any probability analysis method can be employed for reliability analysis and design with the statistically dependent random variables using the proposed approach.

Contribution 3: A Bayesian approach with copula dependence models to characterize the random field with the lack of field data sets.

Conventional random field characterization demands sufficient field data sets, which is not practical for many engineered systems. There is thus a need for an effective tool to characterize the random field with insufficient field data sets. This technical challenge must be resolved to make a reliable design of the engineered system subject to the unknown field variability. A Bayesian approach with Bayesian copula dependence modeling was proposed to characterize the random field with a lack of field data sets. First, a Bayesian updating approach using the Markov Chain Monte Carlo (MCMC) method was employed to update the random field with insufficient and evolving data sets. Second, a Bayesian copula dependence modeling approach was proposed to model the statistical dependence among random field realizations at different measurement locations. Hence, sufficient random field data sets can be generated based on the proposed approach. The random field characterization with insufficient field data sets is thus transformed into one with sufficient field data sets.

Contribution 4: A generic reliability analysis framework to accurately assess system reliability in the presence of both random field and parameter variables.

Many advanced methods for reliability analysis have been focused on the enhancement of numerical efficiency, accuracy and stability. Despite these advances, no generic reliability analysis framework currently exists to accurately assess system reliability in the presence of both random parameter and field variables. Furthermore, statistical dependence has been little considered in

147

reliability analysis and design. The Eigenvector Dimension Reduction (EDR) method was proposed for reliability analysis and design with both random parameter and field variables while considering the statistical dependence. The EDR method makes a significant improvement, based upon the univariate Dimension Reduction (DR) method, with three new technical elements. First, the $2N+1$ and $4N+1$ eigenvector sampling schemes were proposed for probability analysis to maintain high accuracy without requiring sensitivity of system performances. Second, the Stepwise Moving Least Square (SMLS) method was developed to accurately approximate the responses, which allow one-dimensional numerical integration with no extra cost other than simulations or experiments at the eigenvector samples. Third, the stabilized Pearson system was proposed to eliminate a singular behavior of the original Pearson system while accurately predicting the Probability Density Functions (PDFs) of engineering system performances. Compared with the univariate DR method, the EDR method makes considerable improvements in accuracy, efficiency, and stability. The EDR method is far more efficient than traditional probability analysis methods, such as the First Order Reliability Method (FORM) and Second Order Reliability Method (SORM), since one EDR execution takes care of reliability analyses for all constraints without requiring sensitivity of system responses. The EDR method could be more accurate than FORM and SORM for highly nonlinear limit state functions or limit state functions involving inflection points. However, the EDR method may not be good for problems with substantial contribution of

high-order mixed terms. In addition, the EDR method may be less accurate than FORM/SORM for high probability levels (e.g., more than 99.9%).

Contribution 5: A generic Reliability-Based Design Optimization (RBDO) framework to solve engineering design problems with both random parameter and field variables.

Despite extensive efforts made in the RBDO methods, no generic RBDO framework currently exists to solve engineering design problems with both random parameter and field variables. Furthermore, the numerical efficiency, accuracy, and stability of RBDO methods is still of great concern. In this dissertation, a generic RBDO framework was proposed by incorporating the EDR method to effectively analyze probabilistic system responses with both random parameter and field variables. It has been shown that the proposed RBDO has three benefits. First, an approximate response surface facilitates sensitivity calculation of reliability and quality where the response surface is constructed using the eigenvector samples. Thus, sensitivity analysis becomes very efficient and simple for the design optimization. Second, the proposed RBDO methodology has a single-loop structure since there is no iterative process for reliability analysis. Thus, the RBDO is very efficient. Third, the proposed RBDO allows solving problems with statistical dependent and non-normally distributed random inputs. As demonstrated with four case studies (side impact crash, layered-plate bonding process, A-Arm in HMMWV, and door misalignment), it is expected that the proposed RBDO using the EDR method will enhance numerical efficiency substantially while maintaining good accuracy.

6.2 Recommended future research

In this section, several possible directions for future research are discussed. Based on the approaches described in the previous chapters, these directions can be applied to overcome the shortcomings of the proposed approaches or to extend the applicability of these approaches.

- Random field characterization with inconsistent and variable numbers of measurement locations

  Two conditions must be satisfied to characterize a discrete random field in the proposed approach presented in Chapter 3. First, the number of measurement locations must be the same for each random field snapshot. Second, the measurement location must be the same for each random field snapshot. These two conditions are required to build a discrete covariance matrix Σ that is used for the random field characterization. However, these two conditions cannot be guaranteed in the real discrete process of the random field. In this situation, the proposed approach cannot be applied to random field characterization. A rigorous approach needs to be developed to deal with inconsistent and variable numbers of measurement locations.

- Investigation of the fundamental reason for statistically dependent random field variables

  The Proper Orthogonal Decomposition (POD) method uses the covariance matrix to find the orthogonal signature of the random field data. Random field variables defined from the coefficients of the orthogonal signature are statistically uncorrelated but could be statistically dependent. To address the challenge of

probability analysis and design considering the statistically dependent random field variables, this dissertation proposed an effective approach to transform the statistically dependent random variables into statistically independent random variables. However, the fundamental reason for the statistical dependence is not clear. A thorough investigation should be conducted to determine why the statistical dependence appears and to develop a feasible approach to avoid the statistical dependence. This study could bring significant contributions to the random field characterization.

- Adaptive eigenvector samples for the Eigenvector Dimension Reduction (EDR) method for effective reliability analysis

  The EDR method demands either $2N+1$ or $4N+1$ eigenvector samples for constructing one-dimensional response approximation using the Stepwise Moving Least Square (SMLS) method, where N is the number of random variables. For problems with less nonlinearity, the EDR method with $2N+1$ eigenvector samples can accurately predict the variability of the system response with high efficiency. For problems with high nonlinearity, the EDR method with $4N+1$ eigenvector samples is necessary to improve the prediction accuracy of the system response. However, the selection of the sampling scheme is dependent on the engineering justification. An adaptive sampling scheme should be developed to determine the optimal eigenvector samples with high accuracy and efficiency for reliability analysis and design.

- Comparative study of the Probability Density Function (PDF) approximation methods for reliability analysis

The PDF approximation methods first approximate the PDF of the system response from the estimated statistical moments, and then reliability analysis based on the approximate PDF is performed. The stabilized Pearson system, as one of the PDF approximation methods, was proposed for reliability analysis in the EDR method. In recent years, a number of other methods have been proposed to approximate the PDF of the system response, such as the saddlepoint approximation, the Maximum Entropy Principle (MEP), and the Johnson system. Systematic performance evaluations and comparative analyses of these methods have not yet been performed. A comparative study of these PDF approximation methods could give insightful guidance for selecting the most appropriate PDF approximation method for reliability analysis.

References

1. Ba-abbad, M.A., Nikolaidis, E., and Kapania, R.K., 2006, "New Approach for System Reliability-Based Design Optimization", *AIAA Journal*, Vol. 44(5), pp: 1087 – 1096.

2. Berg, B.A., 2004, "Markov Chain Monte Carlo Simulations and Their Statistical Analysis", World Scientific Publishing Co. Pte. Ltd. ISBN, 981-238-935-0.

3. Berkooz, G., Holmes, P., and Lumley, J.L., 1996, "Turbulence, Coherent Structuress, Dynamical Systems and Symmetry." Cambridge University Press: Cambridge Monographs on Mechanics.

4. Bjerager P, 1988, "Probability Integration by Directional Simulation", *Journal of Engineering Mechanics*, Vol. 114, pp: 1285–1302.

5. Bucher, C. G., 1988, "Adaptive Sampling – an Iterative Fast Monte Carlo Procedure", *Structural Safety*, Vol. 5, pp: 119-126.

6. Buckland, T. B., 1984, "Monte Carlo Confidence Intervals", *Biometrics*, Vol. 40(3), pp: 811-817.

7. Chen, S., Chen, W., and Lee, S., 2010, "Level Set Based Robust Shape and Topology Optimization Under Random Field Uncertainties", *Structural and Multidisciplinary Optimization*, Vol. 41(4), pp: 507-524.

8. Chen, X. and Fan,Y., 2005. "Pseudo-likelihood Ratio Tests for Semiparametric Multivariate Copula Model Selection", *La Revue Canadienne de Statistique*, Vol. 33(3), pp: 389–414.

9. Chen, X., and Hasselman, T. K., 1997, "Reliability Based Structural Design Optimization for Practical Applications", 38th AIAA/ASME/ASCE/AHS/ASC Structures, Structural Dynamics and Materials Conference, Kissimmee, Florida.

10. Choi, S.K., Canfield, R.A., and Grandhi, R.V., 2006, "Estimation of Structural Reliability for Gaussian Random Fields", *Structure and Infrastructure Engineering*, Vol. 2, pp: 161-173.

11. Clarke, S. M., Griebsch, J. H., and Simpson, T. W., 2005, "Analysis of Support Vector Regression for Approximation of Complex Engineering Analysis", *Journal of Mechanical Design*, Vol. 127, pp: 1077-1087.

12. Cressie, N., 1988, "Spatial Prediction and Ordinary Kriging", *Mathematical Geology*, Vol. 20(4), pp: 405-421.

13. Der Kiureghian, A. and Ke, J.B., 1988, "The Stochastic Finite Element Method in Structural Reliability," *Probabilistic Engineering Mechanics,* Vol. 3(2), pp: 83-91.

14. Du, X., and Chen, W., 2004, "Sequential Optimization and Reliability Assessment Method for Efficient Probabilistic Design", *Journal of Mechanical Design*, Vol. 126(2), pp: 225-233.

15. Du, X. and Chen, W., 2005, "Collaborative Reliability Analysis under the Framework of Multidisciplinary Systems Design," *Journal of Optimization & Engineering,* Vol. 6(1), pp: 63-84.

16. Dyn, N., Levin, D., and Rippa, S., 1986, "Numerical Procedures for Surface Fitting of Scattered Data by Radial Basis Functions", *SIAM Journal on Scientific and Statistical Computing*, Vol. 7(2), pp: 639–659.

17. Efron B., 1982, "The Jackknife, the Bootstrap, and Other Re-sampling Plans", SIAM, monograph #38, CMNS-NSF.

18. Engelund S, and Rackwitz R., 1993, "A Benchmark Study on Importance Sampling Techniques in Structural Reliability", *Structural Safety*, Vol. 12, pp: 255–276.

19. Fang, H., and Horstemeyer, M.F., 2006, "Global Response Approximation with Radial Basis Functions", *Engineering Optimization*, Vol. 38(4), pp: 407–424.

20. Fermanian, J.D., 2005. "Goodness-of-Fit Tests for Copulas", *J. Multivariate Anal.* Vol. 95, pp: 119–152.

21. Friedman, J. H., 1991, "Multivariate Adaptive Regression Splines", *The Annals of Statistics*, Vol. 19(1), pp: 1–67.

22. Fukunaga, K., 1990, "Introduction to Statistical Recognition," NewYork: Academic Press.

23. Gerstner, T., and Griebel, M., 1998, "Numerical Integration Using Sparse Grids," *Numerical Algorithms*, Vol 18(3), pp: 209–232.

24. Ghanem, R.G., and Spanos, P.D. 1991, "Spectral Stochastic Finite Element Formulation for Reliability Analysis", *Journal of Engineering Mechanics*, Vol. 117(10), pp: 2351-2373.

25. Ghanem R.G., and Spanos P.D., 1991, "Stochastic Finite Elements: A Spectral Approach," Springer: New York, NY.

26. Golly, C., Bacher, W., Bustgens, B., Maas, D., Menz, W, and Schomburg, W.K., 1996, "Microvalves with Bistable Buckled Polymer Diaphragms," *J. Micromech. Microeng*. Vol. 6, pp: 77–79.

27. Hasofer, A.M., and Lind, N.C., 1974, "Exact and Invariant Second-Moment Code Format", *Journal of the Engineering Mechanics*, Vol. 100, pp: 111-121.

28. Haykin, S., 1999, "Neural Networks: A Comprehensive Foundation", 2nd Edition, Prentice Hall, Upper Saddle River, NJ.

29. Hoffmann, M., Kopka, P., and Voges, E., 1999, "Bistable Micromechanical Fiber-Optic Switches on Silicon with Thermal Actuators", *Sensors and Actuators* Vol. 78, pp: 28-35.

30. Hu, C. and Youn, B.D. 2009, "Adaptive-Sparse Polynomial Chaos Expansion for Reliability Analysis and Design of Complex Engineering Systems", ASME 2009 IDETC-CIE, San Diego, California, USA.

31. Huang B, and Du X, 2006, "Uncertainty Analysis by Dimension Reduction Integration and Saddlepoint Approximations," *Journal of Mechanical Design*, Vol. 128, pp. 26-33.

32. Huard, D., Evin, G. and Favre, A.C., 2006, "Bayesian Copula Selection", *Computational Statistics & Data Analysis*, Vol. 51(2), pp: 809 – 822.

33. Jaynes, E.T. and Bretthorst, G.L., 2003, "Probability Theory: The Logic of Science", Cambridge University Press, Cambridge, UK, NewYork.

34. Jin, R., Chen, W., and Simpson, T.W., 2001, "Comparative Studies of Metamodeling Techniques under Multiple Modeling Criteria", *Structural and Multidisciplinary Optimization*, Vol. 23(1), pp: 1–13.

35. Johnson NL, Kotz S, and Balakrishnan N., 1995, "Continuous Univariate Distributions", New York: Wiley.

36. Kleiber, M., and Hien T.D., 1992, "The Stochastic Finite Element Method", New York, NY, Wiley.

37. Le Maître, O.P., Reagan, M., Najm, H.N., Ghanem, R.G., and Knio, O.M., 2002, "A Stochastic Projection Method for Fluid Flow: II. Random Process," *Journal of Computational Physics*, Vol 181(1), pp: 9–44.

38. Lee, S.H. and Chen, W., 2009, "A comparative study of uncertainty propagation methods for black-box type problems", *Structural and Multidisciplinary Optimization*, Vol. 37(3), pp: 239-253.

39. Lin, C. Y., Huang, W. H., Jeng, M. C., and Doong, J. L., 1997, "Study of An Assembly Tolerance Allocation Model Based on Monte Carlo simulation", *Journal of Materials Processing Technology*, Vol. 70, pp: 9–16.

40. Liu, P. L. and Der Kiureghian A., 1991, "Finite Element Reliability of Geometrically Nonlinear Uncertain Structures," *Journal of Engineering Mechanics*, Vol. 117(8), pp: 1806-1825.

41. Liu, P. and Liu, K., 1993, "Selection of Random Field Mesh in Finite Element Reliability Analysis", *Journal of Engineering Mechanics*, Vol. 119(4), pp: 667-680.

42. Liu, W. K., Belytschko, T., and Mani, A. 1986, "Random Field Finite Elements," *Int. J. of Numerical Methods in Engrg.,* Vol. 23(10), pp: 1831-1845.

43. Maute, K.; Frangopol, D.M., 2003, "Reliability-based Design of MEMS Mechanisms by Topology Optimization," *Computers & Structures*, Vol. 81, pp: 813-824.

44. Melchers, R. E., 1989, "Importance Sampling in Structural Systems", *Structural Safety*, Vol. 6, pp: 6-10.

45. Missoum. S., 2008, "Probabilistic Optimal Design in the Presence of Random Fields," *Structural and Multidisciplinary Optimization*, Vol. 35, pp: 523-530.

46. Mullur, A. A., and Messac, A., 2005, "Extended Radial Basis Functions: More Flexible and Effective Metamodeling", *AIAA Journal*, Vol. 43(6), pp: 1306–1315.

47. Myers, R. H., and Montgomery, D. C., 1995, "Response Surface Methodology: Process and Product Optimization Using Designed Experiments", Wiley, New York.

48. Niederreiter H, and Spanier J, 2000, "Monte Carlo and Quasi-Monte Carlo Methods", Berlin: Springer.

49. Panchenko, V., 2005, "Goodness-of-Fit Test for Copulas", *Physica A: Statistical Mechanics and its Applications*, Vol. 355(1), pp: 176 – 182.

50. Penmetsa, R., and Grandhi, R. V., 2002, "Structural System Reliability Quantification Using Multi-Point Function Approximations," *AIAA Journal*, Vol. 40(12), pp: 2526-2531.

51. Picheny, V., Kim, N.H., and Haftka, R.T., 2010, "Application of Bootstrap Method in Conservative Estimation of Reliability with Limited Samples", *Structural and Multidisciplinary Optimization*, Vol. 41(2), pp: 205 – 217.

52. Qiu, J., Lang, J.H., Slocum, A.H., and Strumpler, R., 2003, "A High-Current Electrothermal Bistable MEMS Relay," Micro Electro Mechanical Systems, MEMS-03 Kyoto, pp: 64- 67.

53. Qiu, J., Lang, J.H. and Slocum, A.H., 2004, "A Curved-Beam Bistable Mechanism," *Journal of microelectromechanical systems*, Vol. 13, pp: 137-146.

54. Qu, X., and Haftka, R.T., 2004, "Reliability-Based Design Optimization Using Probability Sufficiency Factor," *Structural and Multidisciplinary Optimization*, Vol. 27(5), pp: 314-325.

55. Rabitz, H. and Alis, O. F., 1999, "General Foundations of High-Dimensional Model Representations," *Journal of Mathematical Chemistry*, Vol. 25, pp: 197-233.

56. Rabitz, H., Alis, O. F., Shorter, J., and Shim, K., 1999, "Efficient Input-Output Model Representations," *Computer Physics Communications*, Vol. 117, pp: 11-20.

57. Rahman, S., and Rao, B.N., 2001, "A Perturbation Method for Stochastic Meshless Analysis in Elastostatics", *International Journal for Numerical Methods in Engineering*, Vol. 50, pp: 1961-1991.

58. Rahman, S. and Xu, H., 2004, "A Univariate Dimension-Reduction Method for Multi-Dimensional Integration in Stochastic Mechanics," *Probabilistic Engineering Mechanics*, Vol. 19, pp: 393-408.

59. Rajaee, M., Karlsson, S.K.F., and Sirorich, L., 1994, "Low-Dimensional Description of Free-Shear-Flow Coherent Structures and Their Dynamical Behavior," *Journal of Fluid Mechanics* Vol. 258, pp: 1-29.

60. Roser B.N., 1999, "An Introduction to Copulas", Springer, New York.

61. Shan, S. and Wang, G.G., 2008, "Reliable Design Space and Complete Single-Loop Reliability-Based Design Optimization", *Reliability Engineering and System Safety*, Vol. 93, pp: 1218 – 1230.

62. Simpson, T. W., Mauery, T. M., Korte, J. J., and Mistree, F., 2001, "Kriging Metamodels for Global Approximation in Simulation-based Multidisciplinary Design Optimization", *AIAA Journal*, Vol. 39(12), pp: 2233–2241.

63. Sklar, A., 1959. "Fonctions de répartition à *n* dimensions et leurs marges", Publications de l'Institut de Statistique de l'Université de Paris 8, pp. 229–231.

64. Smith, N., and S. Mahadevan, 2005, "Probabilistic Design of Aerospace Vehicles: Coupling Global and Local Requirements," *Journal of Spacecraft and Rockets*, Vol. 42(4), pp: 752-760.

65. Sobol IM, 1998, "On Quasi-Monte Carlo Integrations", *Mathematics and computers in simulation*, Vol. 47, pp: 103–112.

66. Sudret, B. and Der Kiureghian A., 2000, "Stochastic Finite Element Methods and Reliability: A State-Of-The-Art Report," Technical Report UCB/SEMM-2000/08, Department of Civil & Environmental Engineering, University of California, Berkeley, CA.

67. Tamura, Y., Suganuma, S., Kikuchi, H., and Hibi, K., 1999, "Proper Orthogonal Decomposition of Random Wind Pressure Field," *Journal of Fluids and Structures* Vol. 13, pp: 1069-1095.

68. Thanedar, P. B., and Kodiyalam, S., 1992, "Structural Optimization Using Probabilistic Constraints", *Journal of Structural Optimization*, Vol. 4, pp. 236–240.

69. Tu, J., Choi, K.K., and Park, Y.H., 1999, "New Study on Reliability-Based Design Optimization", *Journal of Mechanical Design*, Vol. 121(4), pp: 557-564.

70. Tu, J., Choi, K.K., and Park, Y.H., 2001, "Design Potential Method for Robust System Parameter Design", *AIAA Journal*, Vol. 39(4), pp: 667-677.

71. Turk, M., and Pentland, A., 1991. "Eigenfaces for Recognition". *Journal of Cognitive Neuroscience,* Vol. 3(1), pp: 71–86.

72. Varghese, P., Braswell, R.N., Wang, B., and Zhang, C., 1996, "Statistical Tolerance Analysis Using FRPDF and Numerical Convolution", *Computer-Aided Design*, Vol. 28(9), pp: 723-732.

73. Vanmarcke, E. H. and Grigoriu, M. 1983, "Stochastic Finite Element Analysis of Simple Beams," *J. Engrg. Mech.,* ASCE, Vol. 109(5), pp: 1203-1214.

74. Wang, G.G., Shan, S., 2007, "Review of Metamodeling Techniques in Support of Engineering Design Optimization", *Journal of Mechanical Design*, Vol. 129(4), pp: 370-380.

75. Wang, L., and Kodiyalam, S., 2002, "An Efficient Method for Probabilistic and Robust Design with Non-normal Distributions", 43rd AIAA Structures, Structural Dynamics, and Materials Conference.

76. Wang, P., Youn, B.D., Xi Z., and Kloess, A., 2009, "Bayesian Reliability Analysis with Subjective, Insufficient, and Evolving Data Sets," *Journal of Mechanical Design*, Vol. 131(11), pp: 111008(11).

77. Wu, Y.T., 1994, "Computational Methods for Efficient Structural Reliability and Reliability Sensitivity Analysis", *AIAA Journal*, Vol. 32(8), pp: 1717-1723.

78. Wu, Y.T., Shin, Y., Sues, R., and Cesare, M., 2001, "Safety-Factor Based Approach for Probability-Based Design Optimization," AIAA Paper 2001-1522.

79. Xiu D., and Karniadakis G.E., 2003, "The Wiener–Askey Polynomial Chaos for Stochastic Differential Equations", *SIAM Journal on Scientific Computing*, Vol.187, pp: 137–167.

80. Xu, H., and Rahman, S., 2004, "A Generalized Dimension-Reduction Method for Multidimensional Integration in Stochastic Mechanics", *International Journal for Numerical Method in Engineering*, Vol. 61, pp: 1992-2019.

81. Yamazaki, F., and Shinozuka, M., 1988, "Neumann Expansion for Stochastic Finite Element Analysis", *Journal of Engineering Mechanics*, Vol. 114, pp: 1335-1354.

82. Yamazaki, F. and Shinozuka, M., 1990, "Simulation of Stochastic Fields by Statistical Preconditioning", *Journal of Engineering Mechanics*, Vol. 116(2), pp: 268-287.

83. Yin, X. and Chen, W., 2006, "Enhanced Sequential Optimization and Reliability Assessment Method", *Structure and Infrastructure Engineering,* Vol. 2(3), pp: 261-275.

84. Youn, B.D., Choi, K.K., and Park, Y.H., 2003, "Hybrid Analysis Method for Reliability-Based Design Optimization", *Journal of Mechanical Design*, Vol. 125, pp: 221 – 232.

85. Youn B.D. and Choi K.K., 2004a, "An Investigation of Nonlinearity of Reliability-Based Design Optimization," *Journal of Mechanical Design,* Vol. 126(3), pp: 403-411.

86. Youn, B.D., and Choi, K.K., 2004b "A New Response Surface Methodology for Reliability-Based Design Optimization," *Computers and Structures*, Vol. 82, pp. 241-256.

87. Youn, B.D., Choi, K.K., Gu, L., and Yang, Ren-Jye, 2004a, "Reliability-Based Design Optimization for Crashworthiness of Side Impact," *Structural and Multidisciplinary Optimization*, Vol. 26(3-4), pp: 272-283.

88. Youn, B.D., Choi, K.K., and Du, L., 2004b, "Adaptive Probability Analysis Using an Enhanced Hybrid Mean Value (HMV+) Method", *Structural and Multidisciplinary Optimization*, Vol. 28(4), pp: 319-333.

89. Youn, B.D., Choi, K.K., and Tang, J., 2005, "Structural Durability Design Optimization and Its Reliability Assessment," *International Journal of Product Development*, Vol. 1(3-4), pp: 383-401.

90. Youn B.D., Xi, Z., and Wang, P., 2008, "Eigenvector Dimension Reduction (EDR) Method for Sensitivity-free Probability Analysis", *Structural and Multidisciplinary Optimization*, Vol. 37(1), pp: 13-28.

91. Zhang, J. and Ellingwood, B., 1994, "Orthogonal Series Expansions of Random Fields in Reliability Analysis," *Journal of Engineering Mechanics*, Vol. 120(12), pp: 2660-2677.

92. Zou, T., and Mahadevan, S., 2006, "A Direct Decoupling Approach for Efficient Reliability-Based Design Optimization", *Structural and Multidisciplinary Optimization*, Vol. 31(3), pp: 190-200.

93. Zou, T., Mahadevan, S., Mourelatos, Z., and Meernik, P., 2002, "Reliability Analysis of Automotive Body-Door Subsystem," *Reliability Engineering and System Safety*, Vol. 78(3), pp: 315-324.